Abstracts

University of Michigan International Workshop on Arterial Spin Labeling MRI: Technical Updates and Clinical Experience

March 9-10, 2019
Kahn Auditorium, Biomedical Sciences Research Building
University of Michigan
Ann Arbor, MI, USA

FUNCTIONAL MRI LABORATORY
UNIVERSITY OF MICHIGAN

ESMRMB
European Society for Magnetic Resonance in Medicine and Biology

Table of Contents

Title: Metabolic and vascular risk factors are associated with widespread alterations in cerebral blood flow: ASL data from the CARDIA study

Authors: Bradley J MacIntosh[1,2,3], Zahra Shirzadi[1,2,3], Sarah Atwi[1,2,3], John A Detre[5,6,7], Sudipto Dolui[5,6,7], R Nick Bryan[4], Lenore J Launer[8], Walter Swardfager[2,3,9]

[1]Department of Medical Biophysics, University of Toronto; [2]Heart and Stroke Foundation, Canadian Partnership for Stroke Recovery, Sunnybrook Research Institute, University of Toronto, Toronto; [3]Hurvitz Brain Sciences, Sunnybrook Research Institute, University of Toronto, Toronto; [4]Department of Diagnostic Medicine, University of Texas, Austin, Austin, TX; [5]Department of Radiology, [6]Department of Neurology, [7]Center for Functional Neuroimaging, University of Pennsylvania, Philadelphia, Pennsylvania; [8]Laboratory of Epidemiology and Population Science, National Institute on Aging, Bethesda, Maryland; [9]Department of Pharmacology and Toxicology, University of Toronto

Introduction: Vascular dysregulation and cerebral blood flow (CBF) deficits appear to be early harbingers of dementia, including Alzheimer's disease [1]. In this study, we hypothesize that regional grey matter CBF will be associated with mid-life vascular risk factors that make up metabolic syndrome, namely: obesity, dyslipidemia, dysregulated glucose homeostasis and hypertension, which studies suggest play a role in neurodegeneration [2].
Methods: Data are from a sub-sample of black and white men and women who participated in year-25 of the community-based Coronary Artery Risk Development in Young Adults (CARDIA) study [3]. CARDIA is a longitudinal study of the development and determinants of cardiovascular disease. This abstract focuses on the sub-sample of participants (N=451) that underwent a 3 T brain MRI, including T1-weighted (for brain region segmentation), phase contrast angiography of the internal carotid and vertebral arteries (used to compute ASL labeling efficiency) [4], and pseudo-continuous ASL with 2D echo planar imaging. Body mass index was not associated with global CBF estimates (i.e. ASL to phase contrast angiography, t=-0.67, p=0.50). We employ a multivariate partial least squares (PLS) analysis, an approach designed to handle highly collinear variables [5].
Results: Ten vascular risk factors used in the PLS model had a high degree of collinearity (Fig. 1). We identified one significant PLS latent variable ($p<0.001$, 80% explained variance) that consisted of measures of obesity (body mass index and waist circumference), dysregulated glucose homeostasis (fasting glucose, oral glucose tolerance level, and insulin level), low high-density lipoprotein, and high triglycerides. Among the participants, (50.3 ± 3.5 years, 220 male / 231 female), we observed 60 out of the 93 pre-defined grey matter CBF regions significantly contributed to the PLS latent variable. **Discussion:** Components of metabolic syndrome are associated with widespread alterations in regional CBF, as revealed by an analysis approach that accounts for the high degree of overlap seen in both inter-regional CBF and among the vascular risk factors. In particular, obesity, dyslipidemia, dysregulated glucose homeostasis were associated with decreased CBF, whereas blood pressure was not. Decreased CBF may explain lower memory performance, as revealed by a second PLS that included a verbal learning cognitive test (data not shown). Longitudinal analysis will help pinpoint the decade(s) most critical in maintaining cerebrovascular health.

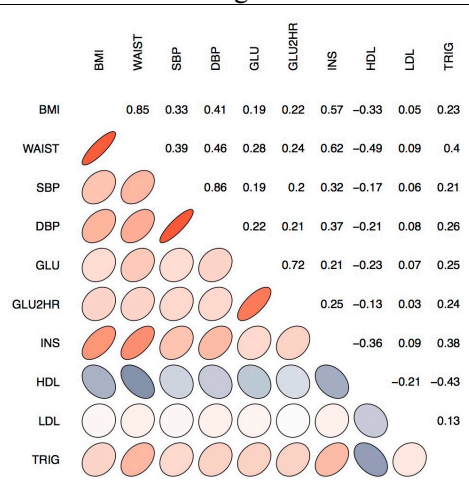

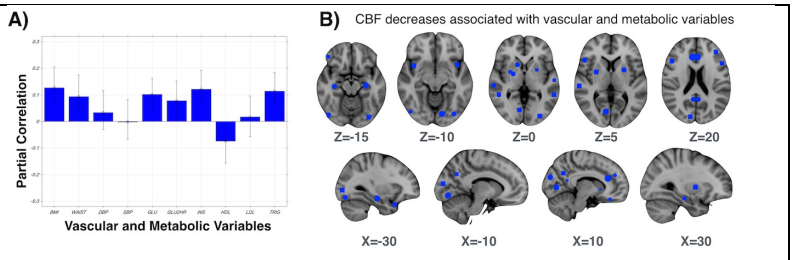

Left: Bivariate correlations between each of the vascular risk factors are shown both as colored ellipses and numerically. **Above:** The partial least squares identified the regions in blue where cerebral blood flow is altered in relation to the metabolic syndrome factor.

References:

1. Iturria-Medina Y, et al. *Nat Commun*. 2016;7:11934. doi:10.1038/ncomms11934.
2. Whitmer RA, et al. *BMJ*. 2005;330(7504):1360. doi:10.1136/bmj.38446.466238.E0.
3. Friedman GD, et al. *J Clin Epidemiol*. 1988;41(11):1105-1116.
4. Dolui S, et al. *J Cereb Blood Flow Metab*. 2016;36(7):1244-1256.
5. McIntosh AR, et al. *Neuroimage*. 1996;3(3 Pt 1):143-157.

White matter oxygen delivery is impaired in both sickle and non sickle anemia syndromes

[1]Yaqiong Chai, [2]Adam Bush, [2]Chau Vu, [1]Natasha Lepore, [3]Thomas Coates and [4]John C Wood
[1]Department of Radiology and Nuclear Medicine, Children's Hospital Los Angeles, CA, [2]Department of Radiology, Stanford University, Palo Alto, CA, [3]Section of Hematology, Children's Hospital Los Angeles, CA, [4]Division of Cardiology, Children's Hospital Los Angeles, CA

Introduction:Patients with thalassemia intermedia, beta thalassemia major and sickle cell disease have a higher risk of cerebrovascular disease and stroke[1]. We have previously demonstrated that patients with chronic anemia syndromes have increased total cerebral blood flow to compensate for their decreased oxygen carrying capacity such that global oxygen delivery is preserved[2]. Using arterial spin labeling, we observed that while global and grey matter (GM) oxygen (O_2) delivery was normal in patients with sickle cell anemia, white matter (WM) O_2 delivery was 35% lower than control subjects and declined monotonically with age[3]. In this study, we compared regional O_2 delivery in patients with sickle cell and non-sickle cell anemia syndromes to determine whether the effect could be solely attributed to low hemoglobin levels.

Methods: The study included 20 patients with anemic syndromes (ACTL), 32 patients with sickle cell disease (SCD) and 25 healthy control patients (CTL) that were recruited from the Children's Hospital Los Angeles. Brain MRI was performed on a Philips Achieva 3 Tesla scanner with an 8-channel head coil. Imaging protocol consisted to 3D T1w, 3D T2w, 3D MRA, and 3D PCASL scans[4].

CBF quantification was calculated using a two-compartment kinetic quantification model reported by Wang et. al[5]. Sickle cell specific quantification parameters were previously described[4]. The CBF maps were converted into cerebral O_2 delivery maps to correct for hemoglobin and O_2 saturation in anemic groups. The equations show the relationship of hemoglobin, O_2 content and O_2 delivery:

$$\text{Oxygen Delivery} = \text{CBF} \times \text{Oxygen Content} \quad (1)$$

$$\text{Oxygen Content} = 1.34 \times \text{Hemoglobin} \times SpO_2 + 0.003 \times pO_2 \quad (2)$$

where S_pO_2 is the arterial oxygen saturation and pO_2 is the partial pressure of oxygen (~100 torr in room air). The preprocessing and registration pipeline of CBF to standard atlas was previously published in Chai et. al.[6]. Predictors of global, GM and WM were identified using univariate and stepwise multivariate regression (JMP Pro, SAS, Cary NC).

Results: Patients' demographics have been summarized in previous work[2,3]. There was no significance difference in age and sex between three groups and hemoglobin levels were well balanced in SCD and ACTL groups. All anemic subjects were mildly desaturated compared to CTL group and exhibited higher circulating cell-free hemoglobin due to ineffective erythropoiesis. Thirteen of the 23 non-sickle anemic subjects and 8 out of 32 sickle cell patients were receiving transfusion therapy every three weeks; these patients were studied at their hemoglobin nadir to better match non-transfused subjects. MRA images were screened by a licensed neuroradiologist and were normal for all participants.

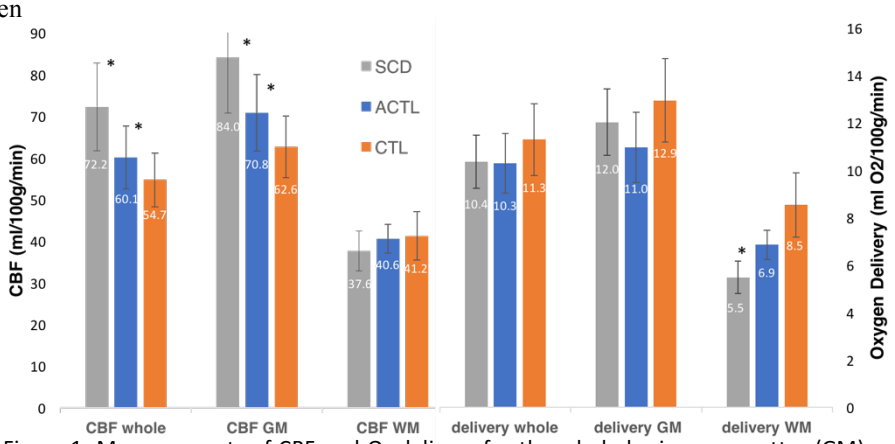

Figure 1: Measurements of CBF and O_2 delivery for the whole brain, grey matter (GM) and white matter (WM). SCD= sickle cell disease, CTL = healthy controls, ACTL = anemic control subjects. Asterisk indicates significant group difference ($p<0.05$), compared to CTL. Error bar shows standard deviation.

Figure 1 illustrates group comparison of CBF and O_2 delivery in GM, WM and whole brain. Whole brain and GM CBF in both anemic groups were significantly higher than CTL but WM CBF was not. CBF was inversely correlated with oxygen content, similar to phase contrast studies[7]. O_2 delivery in whole brain and GM was equivalent in all three groups, but WM O_2 delivery was 35% lower in SCD subjects ($p<0.0001$), and 20% lower in ACTL patients ($p=0.07$). O_2 delivery was inversely correlated with age, with p-values of 0.0043, 0.0036 and 0.1 for global, GM and WM, respectively.

Discussion: Chronically anemic subjects appear to maintain normal GM oxygen delivery by increasing cerebral blood flow. However, deep WM structures do not experience comparable hyperemia with anemia, making WM O_2 delivery hematocrit dependent. This observation may explain the high prevalence of WM injury observed in sickle cell and thalassemia intermedia subjects. The present data also suggests that the nature of the anemia, in addition to its severity, may also contribute to WM health. Although the SCD and ACTL cohorts were relatively balanced for hemoglobin levels, SCD patients had significantly worse WM oxygen delivery. Larger studies are necessary to determine whether resting oxygen delivery predicts WM stroke risk and whether chronic transfusion or hydroxyurea therapy improves WM perfusion.

Reference:

1. Musallam KM, et. al., Cerebral infarction in β-thalassemia intermedia: Breaking the silence. *Thromb Res*. 2012;130(5):695-702.
2. Chai Y, et al. Chronic anemic patients have impaired cerebral oxygen delivery using PCASL MRI, submitted to: ISMRM 2019
3. Chai et al, White Matter has Impaired Resting Oxygen Delivery in Sickle Cell Patients. Am J Hematol, under revision.
4. Bush AM, et al. PCASL quantification in anemic subjects with hyperemic cerebral blood flow. *Magn Reson Imaging*. 2018;47
5. Wang J, et al. Comparison of quantitative perfusion imaging using ASL at 1.5 and 4.0 Tesla. *Magn Reson Med*. 2002;48
6. Chai et al. Regional Cerebral Blood Flow Measurement in Patients with Sickle Cell Disease Using PCASL. EMBC: 2016
7. Bush AM, et al. Determinants of resting cerebral blood flow in sickle cell disease. *Am J Hematol*. 2016;

Voxelwise correlation between vascular parameters obtained with ASL and DSC as predictor of IDH-mutation status in non-enhancing glioma

E.A.H. Warnert[1], F. Incekara[1,2], A.J.P.E. Vincent[2], J.W.Schouten[2], M.J. van den Bent[3], P.J. French[3], H.J. Dubbink[4], J.M. Kros[4], J.A. Hernandez-Tamames[1], Marion Smits[1]

[1] Department of Radiology & Nuclear Medicine, Erasmus MC, Rotterdam, The Netherlands, [2] Department of Neurosurgery, Erasmus MC, Rotterdam, The Netherlands,[3] Department of Neurology, Erasmus MC, Rotterdam, The Netherlands, [4] Department of Pathology, Erasmus MC, Rotterdam, The Netherlands

Introduction Dynamic susceptibility contrast (DSC) based measurement of cerebral blood volume (CBV) can be used as predictor of glioma grade and progression-free and overall survival[1]. Arterial spin labelling (ASL) allows for measurements of cerebral blood flow (CBF) without the use of exogenous contrast agents. Previous studies have shown good correlation between ASL and DSC vascular measurements as predictors of glioma grade[2], indicating an option to omit DSC imaging in light of the recent finding of gadolinium deposition in the brain. However, the majority of these comparative studies were conducted before the introduction of the recently updated World Health Organisation classification of brain tumours[3], in which molecular diagnosis has become pertinent for glioma classification. One such classification factor is whether or not there is a mutation in the isocitrate dehydrogenase (IDH) encoding gene, which has recently been shown related to the vascular phenotype of glioma with more angiogenic profiles corresponding to more aggressive IDH-wildtype glioma[4]. Here we investigate the effect of IDH-mutation status on the correlation between ASL and DSC-based perfusion measurements.

Methods Sixteen patients with non-enhancing glioma and confirmed IDH-mutation status (next generation sequencing, 6 IDH-wildtype and 10 IDH-mutated) are included within this study. Patients underwent 3T MRI scanning (GE, Milwaukee, WI, USA) with a standardised brain tumour imaging protocol extended with advanced imaging. Image acquisition included 3D sagittal CUBE FLAIR (0.8x0.8 mm^2 in plane resolution, slice thickness 1.6mm, TR/TE/TI= 6.1ms/2.1ms/1897ms), 3D spiral pseudocontinuous ASL with time-encoded labelling (7 effective label delays from 0.8 to 2 s, reconstruction matrix 128x128x42, resolution 1.9x1.9x3.5 mm^3), and 2D DSC imaging (122 TRs, TR/TE 1500m/18.6ms, 15 slices, voxel size: 1.875 x 1.875 x 4 mm^3) in which a bolus of 7.5ml of gadolinium-based contrast agent (Gadovist, Bayer, Leverkussen, GE) was injected. A pre-load bolus of equal size was given approximately 5 minutes prior to DSC imaging.

DSC images were motion corrected (mcflirt in FSL, version 5.0.9, Oxford, UK) and linearly registered to the FLAIR images (flirt in FSL). Relative CBV (rCBV) maps were calculated via previously described methods[5]. In addition, relative CBF (rCBF) maps were calculated with verbena in FSL, which uses a Bayesian framework for fitting rCBF[6]. Transit time corrected CBF maps were calculated from the pCASL imaging series, based on previously described methods[7] and linearly registered to the FLAIR images.

The glioma region of interest (ROI) was determined via manual segmentation of the hyperintense FLAIR region. Normalised histograms were calculated across the ROI to investigate differences in ASL-CBF, DSC-rCBV, and DSC-rCBF between IDH-mutated and IDH-wildtype tumours. Voxel-wise Pearson's linear correlation coefficients (ρ) within this ROI were calculated between ASL-CBF and DSC-rCBV, and between ASL-CBF and DSC-rCBF.

Results The normalised histograms (Figure 1) indicate that IDH-wildtype glioma has higher values for ASL-CBF, DSC-rCBV, and DSC-rCBF than IDH-mutated glioma. IDH-wildtype glioma has a significantly lower $\rho_{ASL\text{-}CBF\ vs\ DSC\text{-}rCBV}$ and $\rho_{ASL\text{-}CBF\ vs\ DSC\text{-}rCBF}$ than IDH-mutated glioma (0.14 ± 0.21 and 0.15 ± 0.19 compared to 0.39 ± 0.11 and 0.38 ± 0.11, respectively, two-sample t-tests $p < 0.005$, Figures 2 & 3).

Discussion To the best of our knowledge this study is the first to indicate that IDH-mutation status of non-enhancing glioma may affect the correlation between ASL-CBF and DSC-rCBF/rCBV. The decreased correlation between ASL and DSC-based vascular parameters in IDH-wildtype gliomas may be due to the more angiogenic phenotype in these more aggressive tumours, including irregular vasculature such as larger and leaky vessels[8]. This in turn can lead to arteriovenous shunting of blood, which will result in overestimation of perfusion in ASL due to presence of labelled water in the venous vasculature[9].

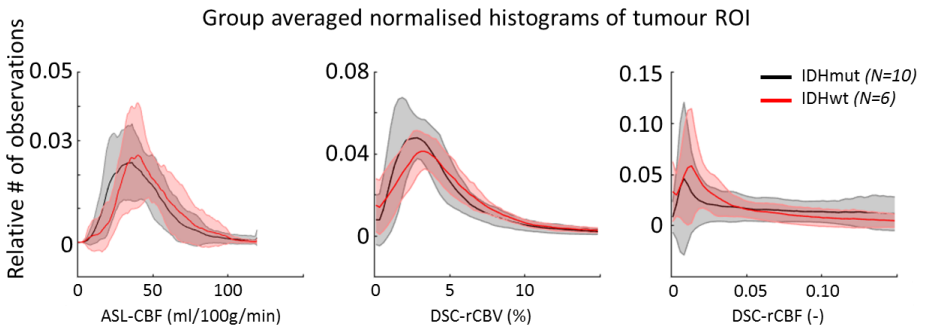

Figure 1. Group averaged normalised histograms across the tumour ROI for IDH-mutated (black lines) and IDH-wildtype (red lines) non-enhancing gliomas. The shaded errorbars indcate the standard deviation across the groups. Note that IDH-wildtype histograms indicate that on average ASL-CBF, DSC-rCBV, and DSC-rCBF are higher than for the IDH-mutated histograms.

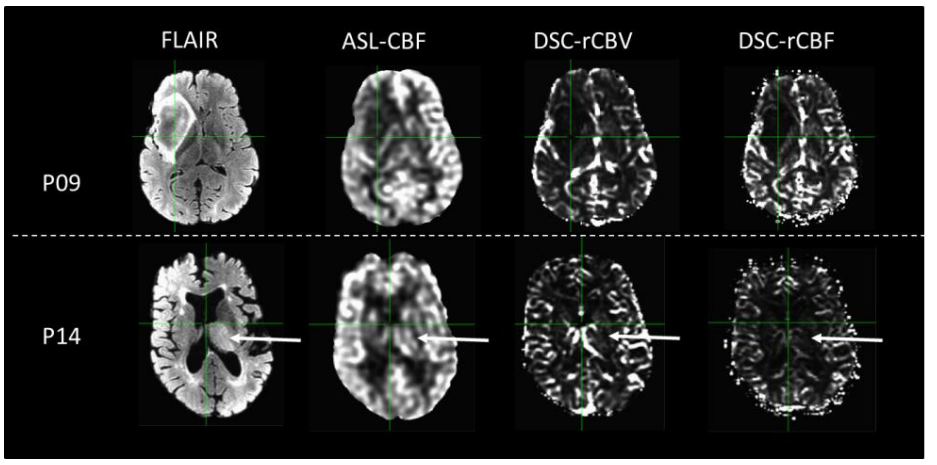

Figure 2. Example MR images of an IDH-mutated (P09) and an IDH-wildtype glioma (P14). The white arrows indicate the IDH-wildtype glioma locations.

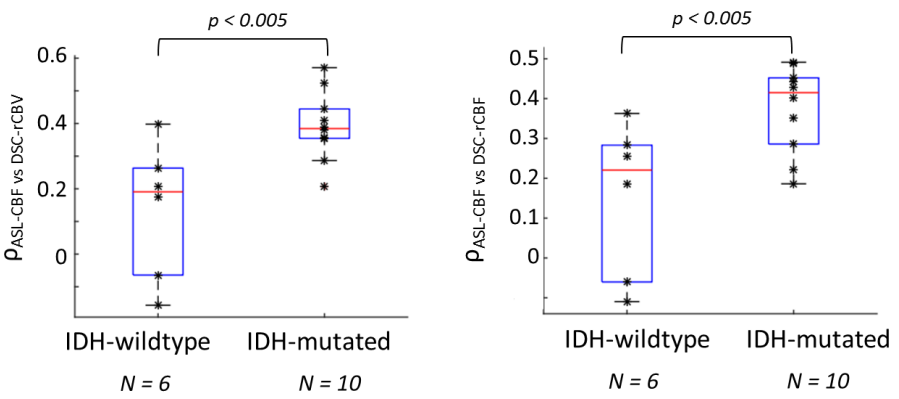

Figure 3. Voxelwise correlation coefficients between ASL-CBF and DSC-rCBV (left) and DSC-rCBF (right) within non-enhancing gliomas. The spatial correlation between ASL-CBF and DSC-rCBF and DSC-rCBV are lower for the IDH-wildtype tumours (two-sample t-tests, $p < 0.005$).

This works shows the potential of voxelwise correlations of ASL-CBF and DSC-rCBF/DSC-rCBV as predictor of IDH-mutation status in non-enhancing glioma and highlights that IDH-mutation status should not be neglected when performing comparative studies of ASL and DSC perfusion parameters in glioma. Future work includes expansion of the current patient cohort (part of the ongoing iGENE study) and matching the MRI vascular parameters with their histological counterparts in targeted biopsies of glioma tissue.

References **1**. Law M et al. Radiology. 2008; **2**. Grade M et al. Neuroradiology. 2015. **3**. Louis DN et al. Vol. 131, Acta Neuropathologica. 2016. p. 803–20. **4**. Zhang L et al. Neuro Oncol. 2018; **5**. Kellner E et al. J Magn Reson Imaging. 2015;42(4):1117–25. **6**. Chappell MA et al. Magn Reson Med. 2015;74(1):280–90. **7**. Dai W et al. Magn Reson Med. 2013;69(4):1014–22. **8**. Conroy S et al. J Neurooncol. 2017; **9**. Wolf RL et al. Am J Neuroradiol. 2008;29(4):681–7.

Variable-density FSE with Compressed-Sensing for high-resolution multi-organ volumetric ASL perfusion

Manuel Taso[1], Li Zhao[2], Arnaud Guidon[3], Daniel V. Litwiller[3], David C. Alsop[1]

[1]MRI research division, Radiology, Beth Israel Deaconess Medical Center, Harvard Medical School, Boston, MA ; [2]Diagnostic Imaging and Radiology, Children's National Medical Center, Washington, DC ; [3]Global MR Applications and Workflow, GE Healthcare

Introduction: While brain volumetric ASL is now routinely feasible, especially using Stack-of-Spirals Fast-Spin-Echo (FSE) or Gradient-Spin-Echo (GRASE) imaging readouts as stated in the ASL consensus paper for neurological application[1], the translation of 3D imaging to abdominal organs is challenging due to the presence of strong inhomogeneities in the body, limiting coverage to single or a few slices. Additionally, they suffer from loss of resolution either from blurring or off-resonance. Therefore, FSE using Cartesian encoding would be desirable, but its slowness is a major handicap. We report the development of a volumetric ASL sequence using Cartesian FSE encoding and Compressed-Sensing acceleration and present applications for brain and abdominal organs.

Methods: We modified a commercially available segmented 3D-FSE sequence[2] with variable refocusing flip-angles with a background-suppressed pCASL magnetization preparation and variable-density Poisson-disk sampling for k-space undersampling. This variable-density sampling combined a fully sampled 6x6 central region and variable outer k-space sampling. Furthermore, since multiple averages are usually collected to increase SNR, we took advantage of the temporal dimension to vary the outer k-space sampling across averages. We repeated 4 times an individual R=14.7 accelerated acquisition with the variable temporal sampling leading to an equivalent acceleration of R=4.3. We scanned 4 healthy volunteers for brain and 3 for abdomen (kidneys) on a 3T GE Discovery MR750 with 32-ch head and body array coils. Common brain/abdomen parameters were: TR/TE=6200/10ms, 128x128 matrix, 64 coronal slices, bandwidth 31.25 kHz, separate acquisition of a reference PD-w scan without ASL preparation and solely parallel-imaging acceleration. All abdominal scans were performed using a timed-breathing approach to mitigate motion and compared to a single-slice single-shot FSE. For the brain, we compared the VD-3D-FSE with a standard Stack-of-Spirals FSE (512 points, 8 arms, 3.6x3.6x4mm^3 nominal resolution, same acquisition time).

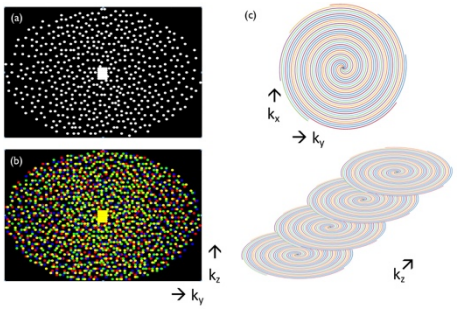

The CS reconstructions relied on the BART toolbox[3]. We estimated the coil-sensitivities for the PI-CS reconstruction using the ESPIRiT method[4] on the reference acquisition (calibration region 32^3, cluster size k=6^3, σ^2_{cutoff}=0.01 and threshold=0.8). Then, we performed a complex k-space subtraction of the control and label ASL data, followed by PI-CS reconstruction of that subtracted volume *m* with *k*-t sparsity enforcement of the data *y* by minimizing the L_1-norm of spatial wavelets (Ψ) and L_1-TV (λ_1=0.001, λ_2=0.05) using the ADMM algorithm (max. 100 iterations): $m(x,y,z,t) = argmin\|DFSm(x,y,z,t) - y(x,y,z,t)\|_2^2 + \lambda_1\|\Psi m(x,y,z)\|_1 + \lambda_2\|\mathrm{TV}m(t)\|_1$ with *D* a sampling, *F* Fourier-transform and *S* ESPIRiT operators.

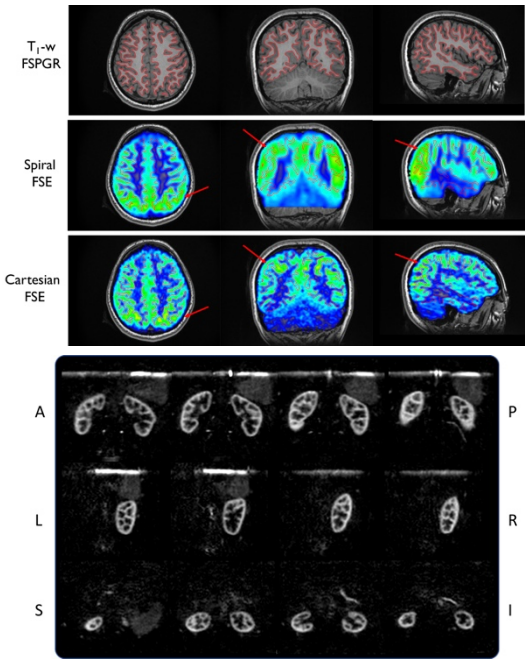

Results: Brain imaging using the Cartesian VD-FSE provided high-quality images with minimal blurring compared to SoS-FSE. This can be seen when looking at the projection of cortical surfaces estimated on a T_1-w volume on the ASL data, and confirmed by quantitative blurring analysis (data not shown). In the abdomen, we were also able to collect artifact-free, close to isotropic perfusion volumes covering the entire kidneys, allowing high-resolution multi-planar reformats that could not be obtained before.

Discussion and conclusion: We successfully implemented a CS-accelerated volumetric ASL sequence using Cartesian imaging. This sequence presents significant advantages over more widely-used non-Cartesian or GRE-based sequences, especially for high-resolution imaging with minimal blurring as seen in our brain experiments.

For abdominal imaging, the variable density sampling in combination with 4D-CS reconstruction allowed collecting high-quality whole kidney perfusion images in a clinical compatible time of ≈4 min. Future developments should be focused on tackling the respiratory motion issue in abdominal imaging but also to add additional dimension undersampling (e.g. PLD) to allow fast and robust multiparametric perfusion imaging (blood-flow, transit-time) across different organs.

References:

1. Alsop, D. C. *et al. Magn. Reson. Med.* **73**, 102–116 (2015). 2.Busse, R. F. *et al. Magn. Reson. Med.* **55**, 1030–1037 (2006). 3. Uecker, M. *et al. Proc. Intl. Soc. Mag. Reson. Med* 2486 (2015). 4. Uecker, M. *et al. Magn. Reson. Med.* **71**, 990–1001 (2014).

A Pipeline for ASL Quantification and Analysis using Inter-regional Differences and Support Vector Machine Learning: Application to Young Onset Alzheimer's Disease

Jack Highton (UCL), Dr Enrico De Vita (KCL), Dr Jonathan Schott (UCL), David Thomas (UCL)

INTRODUCTION Arterial Spin Labelling (ASL) is a non-invasive MRI method to measure cerebral blood flow (CBF) with great potential to assist in early dementia diagnosis – which may allow emerging therapies to be administered earlier with greater effect. However, difficulties in quantitative consistency frustrate the development of robust ASL biomarkers. Here, ASL data acquired from patients with Young Onset Alzheimer's Disease (YOAD) was analysed with an optimized processing pipeline, using both a novel region based statistical approach and voxel based machine learning. This is the first study to analyse ASL data from patients with Posterior Cortical Atrophy using machine learning, and the statistically significant results from both analysis approaches agree with previous perfusion studies, despite the limited cohort size.

METHODS Following manual removal of motion corrupted data, the YOAD study cohort (age 51-70) consisted of: 22 healthy controls, 23 patients diagnosed with typical AD (tAD), and 10 with Posterior Cortical Atrophy (PCA). Structural T1 weighted images were acquired (MPRAGE, 1.1mm isotropic resolution, TR 2.2s, TI 0.9ms). Five ASL image pairs were acquired per subject (8-shot 3D GRASE, FAIR Q2 TIPS, 3.8×3.8×4.0mm, TI 2s, bolus length 0.8s). Using the same acquisition scheme, saturation recovery (SR) images were acquired with recovery times of 1, 2 and 5s, to fit M0 maps for calibration of the ASL data. After group-wise registration using the NiftyReg toolbox [1] CBF was quantified using Oxford ASL [2]. Separate CBF maps were calculated for grey matter (GM) and white matter (WM) using linear regression partial volume correction (PVC) [3]. The GM and WM CBF maps were normalised to remove inter-individual global perfusion differences. The MPRAGE images were parcellated into 8 ROIs using GIF [4] (see figure 1) which were transferred to the normalized GM perfusion images for analysis. Mean CBF values were computed for each anatomical region, with voxels containing a volume fraction of different regions handled in a similar manner to the PVC approach. In a simple comparison of regional CBF, significant differences between ROIs in control and dementia subject CBF maps are identified using a t-test (figure 1). In the novel approach proposed here, within-subject inter-regional perfusion differences are compared between control and dementia subjects (figure 3), using an inhomogeneous variance t-test [5]. As a second analysis, the PRoNTo toolbox [6] was used to train a classifier for each dementia type to predict whether a perfusion map belongs to that group or the control group. Via a binary soft support vector machine, this produced a weights map which reveals perfusion increases/decreases in a voxel linked to the disease.

RESULTS The results (figure 1) show significant hypoperfusion linked to tAD in the external cortical lobes and hippocampus, as expected [7][8]. In PCA patients, hypoperfusion was observed in the temporal lobes, parietal lobes and hippocampus, agreeing with previous studies [9].The inter-regional analysis (figure 1) yielded significant results only for the tAD subjects, with the parietal lobe identified as a useful reference region. The machine learning analysis showed hippocampal and occipital lobe hypoperfusion linked to tAD (figure 2), and occipital lobe hypoperfusion linked to PCA (figure 2).

DISCUSSION Overall, this study demonstrated that statistically significant regional changes in perfusion can be discerned in small groups of patients with young onset AD, with both traditional statistical methods and also with a machine learning algorithm usually applied to large datasets. The novel inter-regional analysis suggested the parietal lobe is the most useful benchmark region, to separate region specific hypoperfusion associated with tAD from global perfusion changes.

CONCLUSION ASL is increasingly used as a secondary diagnostic for dementia, and a quantitative biomarker which can distinguish between different dementia types is desirable. This study confirms the perfusion patterns linked with two types of AD seen in previous work, and suggests pattern recognition and inter-regional comparison of perfusion changes as more robust biomarkers to individual variation.

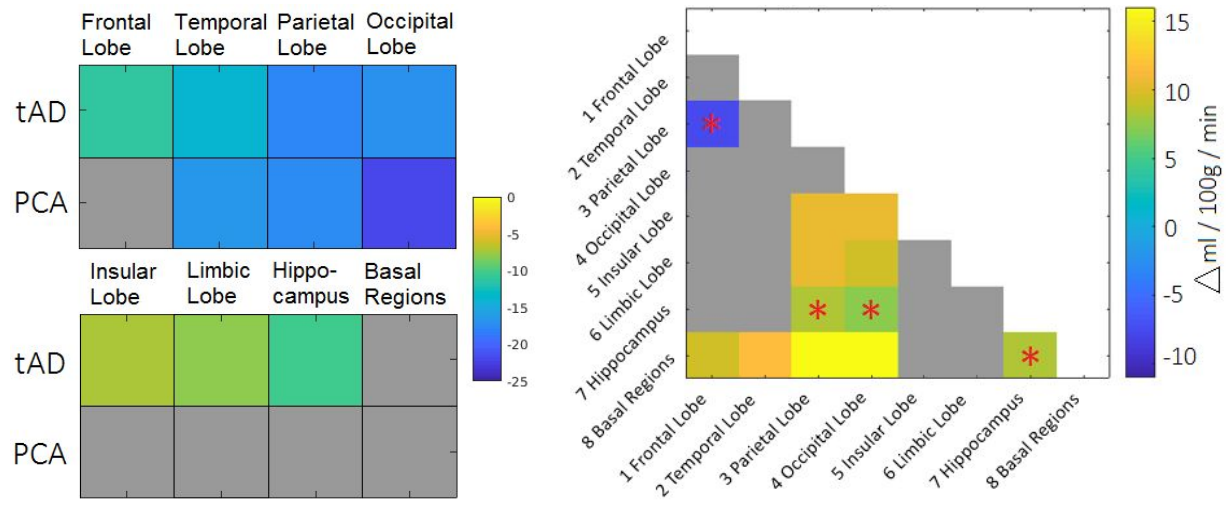

Figure 1 - Left: Basic regional statistical analysis. The colour scale represents the magnitude of statistically significant changes where the confidence interval was above 0.95, or 0.9 where there is an asterix. Right: A novel inter-regional statistical analysis, in which regional perfusion changes between control and dementia subjects are calculated, then statistically significant inter-regional differences in these values are sought. E.g. the difference in tAD linked CBF change between the insular and parietal lobe was positive (i.e. more hypoperfusion in the parietal lobe) was significant, with a confidence level of 0.97.

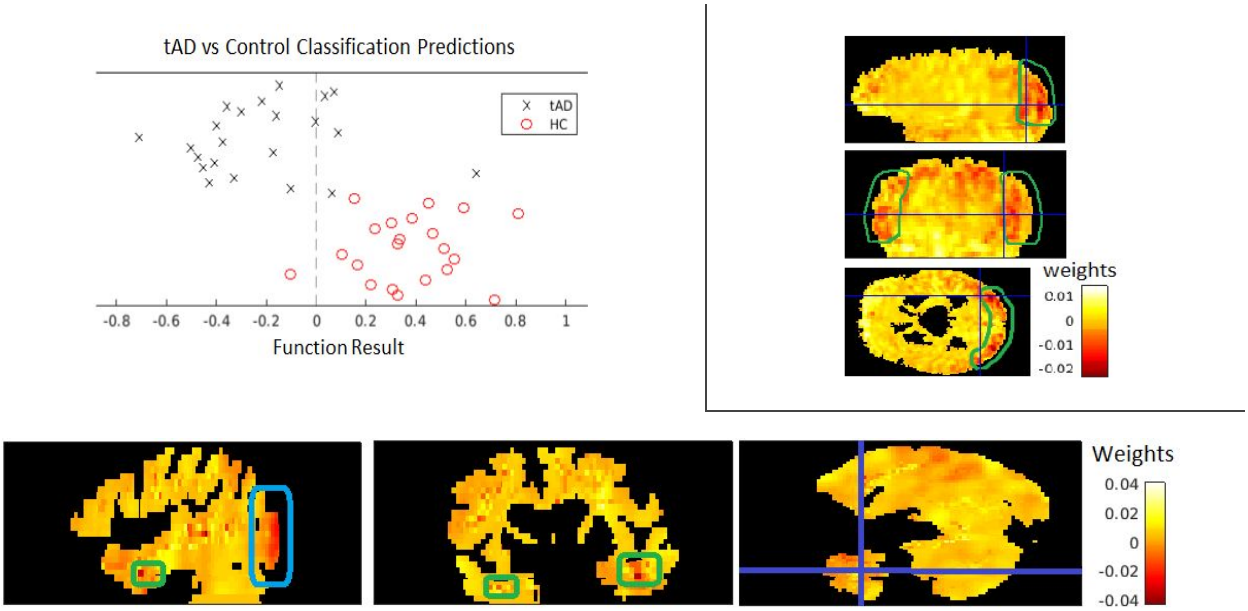

Figure 4 - Top left: classifier result yielding 86% accuracy. Bottom: the weights map from the tAD classifier training, showing the statistical importance of hypoperfusion in the hippocampus (area outlined green) and occipital lobe (blue). Top right: the PCA classifier weights map, showing the statistical importance of hypoperfusion in the occipital lobe.

REFERENCES

[1] Modat M, Cash DM, Daga P, Winston GP, Duncan JS, Ourselin S. Global image registration using a symmetric block-matching approach. J Med Imaging (Bellingham). 2014;1(2):024003.

[2] Chappell MA, et al. Variational Bayesian Inference for a Nonlinear Forward Model. IEEE TRANSACTIONS ON SIGNAL PROCESSING. 2009;57(1):223–236.

[3] Asllani I, Borogovac A, Brown TR. Regression algorithm correcting for partial volume effects in arterial spin labeling MRI. Magn Reson Med. 2008;60(6):1362-71.

Beyond the consensus: is sacrificing part of the PCASL scan time for measurement of labeling efficiency and T1 of blood beneficial?

Piet Bladt[1], **Matthias J.P. van Osch**[2,3], **Eric Achten**[4], **Arnold J. den Dekker**[1,5], **Jan Sijbers**[1]

[1]imec Vision Lab, University of Antwerp, Belgium [2]Department of Radiology, Leiden University Medical Center, The Netherlands
[3]Leiden Institute of Brain and Cognition, Leiden University, The Netherlands [4]Department of Radiology and Nuclear Medicine, Ghent University, Ghent, Belgium [5]Delft Center for Systems and Control, Delft University of Technology, The Netherlands

Introduction: In 2015, the ISMRM perfusion study group and the European consortium for ASL in dementia delineated a recommended implementation of arterial spin labeling (ASL) MRI for clinical application[1]. While this has pushed ASL towards clinical adoption, several potential quantification confounders remain, such as variations in labeling efficiency (α), longitudinal relaxation time of blood (T_{1b}) and arterial transit times (Δt)[2]. These parameters can be estimated from additional experiments (α and T_{1b})[3,4] or by a modified acquisition of ASL data (Δt)[5]. However, both the ASL scan as the supporting measurements come with limited SNR posing the question how to distribute scan time in say a five-minute protocol between averaging of ASL data and acquiring supporting measurements. In this work, this trade-off is studied by means of simulations.

Methods: The simulation experiment consisted of three parts (Fig.1). First, a physiological state associated with a perfusion process was defined by a set of parameters $\boldsymbol{\theta}_i$ drawn randomly from a population distribution $p(\boldsymbol{\theta})$ (see Table 1) and by the cerebral blood flow (CBF), which was kept constant at 50mL/100g/min. With these parameters, pseudocontinuous ASL (PCASL) data can be simulated accurately by a convolution of a rectangular arterial input function[6] and a single-pass approximation (SPA) impulse residue function[7]. In the second step, a five-minute experiment was simulated in which the scan time is divided between the ASL acquisition and support-scans to estimate α_i and $T_{1b,i}$. Three options were considered for the ASL acquisition: single-post-labeling-delay PCASL (single-PLD PCASL) with labeling duration $\tau = 1.8$s and PLD $= 1.8$s, time-encoded free-lunch PCASL[5] (te-FL PCASL) with the duration of block one 1.8s followed by ten blocks of 175ms and a 50ms shortest PLD, and multi-PLD PCASL with $\tau = 1.8$s and PLDs $= 0.2, 0.4, ..., 2.0$s. Number of averages of the ASL acquisition was set based upon the available scan time. Estimates of α_i and $T_{1b,i}$ were simulated by a random draw from normal distributions $\mathcal{N}(\alpha_i, \sigma_\alpha)$ and $\mathcal{N}(T_{1b,i}, \sigma_{T_{1b}})$, with σ_α and $\sigma_{T_{1b}}$ scaled inversely by the square root of the respective assigned scan time to reflect averaging. Realistic values for the temporal SNR of ASL data, and σ_α and $\sigma_{T_{1b}}$ for certain reported scan times were adopted from literature[3,4,8]. Thirdly, the single-compartment model was used to quantify CBF.[1,6] For te-FL and multi-PLD PCASL, Δt is estimated alongside the CBF. This entire protocol was repeated on three levels: 1) varying distributions of the five-minute scan time 2) for each scan time distribution, 10000 physiological conditions ($i = 1, ..., 10000$) were simulated, and 3) for each of these, 1000 noise realizations of the PCASL data and α and T_{1b} measurements were generated ($j = 1, ..., 1000$).

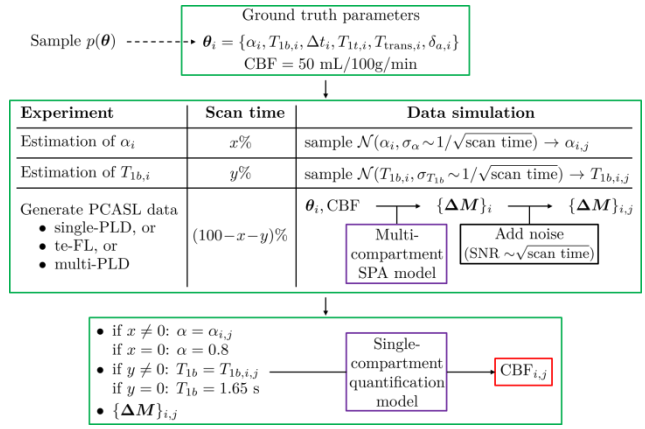

Figure 1: Flowchart of the simulation experiment.

Table 1: The prior distribution $p(\boldsymbol{\theta})$ of the model parameters $\boldsymbol{\theta}$ in gray matter in the general population. A normal distribution is described as $\mathcal{N}(\mu, \sigma)$ with μ the mean and σ the standard deviation; a uniform distribution is described as $\mathcal{U}(l, u)$ with l and u the lower and upper bound, respectively.

	$p(\theta)$	
labeling efficiency α [ ]	$\mathcal{N}(0.80, 0.06)$	9
longitudinal relaxation time of blood T_{1b} [s]	$\mathcal{N}(1.65, 0.12)$	4
arterial transit time Δt [s]	$\mathcal{N}(0.82, 0.15)$	10
longitudinal relaxation time of tissue T_{1t} [s]	$\mathcal{N}(1.45, 0.14)$	11
arterial microvascular transit time δ_a [s]	$[0.30, 1.00]$	12
blood-to-tissue water transit time T_{trans} [s]	$[0.30, 3.60]$	13

Results: For every considered five-minute experiment, the standard deviation of the set of estimates $\{\text{CBF}_{ij}\}_{i=1,j=1}^{N,M}$ is a measure of reproducibility (Fig.2). According to this metric, the optimal distribution of scan time between ASL, α and T_{1b} is 62%-16%-22%, 71%-16%-13% and 60%-27%-13% for single-PLD, te-FL and multi-PLD PCASL, respectively. Compared to the consensus-statement single-PLD experiment, the optimal configurations show a gain in precision of 20%, 19% and 42%, respectively (Fig.3). The same comparison is shown in Fig.4 for a repetition of the entire simulation with longer Δt values ($p(\Delta t) = \mathcal{N}(1.60, 0.15)$s). In this case, scan time is optimally divided as 59%-19%-22%, 77%-10%-13% and 68%-19%-13% with a precision-gain of 45%, 48% and 39% for single-PLD, te-FL and multi-PLD PCASL, respectively.

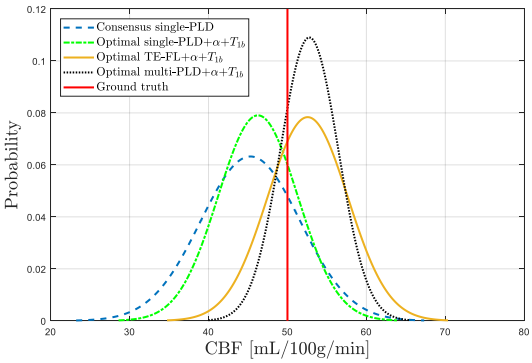

Figure 3: Distributions of CBF estimates $\{\text{CBF}_{ij}\}_{i=1,j=1}^{N,M}$ j for the experiments highlighted with black and red ellipses in Fig.2.

Discussion and conclusions: Splitting scan time between acquisition of ASL data and estimating α and T_{1b} drastically improves the CBF estimation reproducibility in the general population compared to the consensus-statement ASL experiment. Sacrificing ASL scan time for estimating α and T_{1b} increases the noise level in the ASL data, yet it captures the underlying physiological state more accurately. On a population level, the latter clearly outweighs the former (Fig.3). For the parameter distributions in Table 1, combining multi-PLD PCASL with estimating α and T_{1b} proves most reliable (Fig.3). For the assumed Δt distribution, a large amount of signal is lost in single-PLD and te-FL PCASL, impeding their performance. The fact that they outperform multi-PLD PCASL for longer Δt values (Fig.4) shows the dependence of this simulation on the chosen distribution of Δt values and might point to the necessity of including dispersion effects in simulation studies to capture a more realistic spread of arrival times. The results from any simulation experiment depend on the parameter distributions used to generate data. The benefit of sacrificing ASL scan time for α and T_{1b} estimation is directly related to the assumed uncertainties for both. Confidence in the conclusions drawn from this experiment can be attributed to the reported distributions being representative for the general population and the use of an accurate data-generation model. In the future, dispersion will be included to further increase the accuracy of the signal generation process of PCASL.

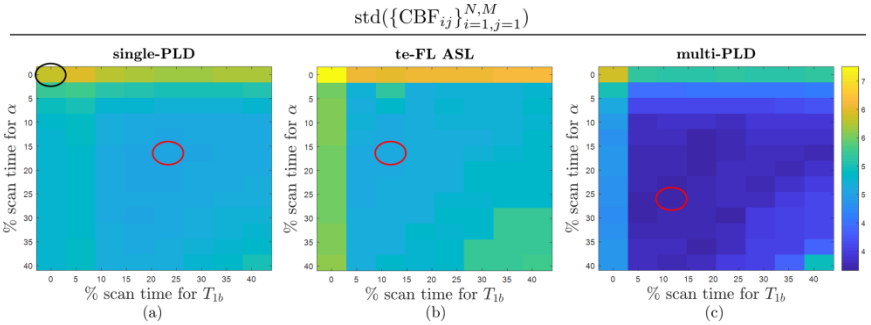

Figure 2: : The standard deviation of the set of estimates $\{\text{CBF}_{ij}\}_{i=1,j=1}^{N,M}$ for combinations of a (a) single-PLD (b) te-FL and (c) multi-PLD PCASL experiment with α and T_{1b} measurements. The red ellipses correspond to the five-minute experiment with the most peaked distribution of $\{\text{CBF}_{ij}\}_{i=1,j=1}^{N,M}$ per type of ASL experiment. The black ellipse highlights the result for the single-PLD experiment corresponding to the consensus statement.

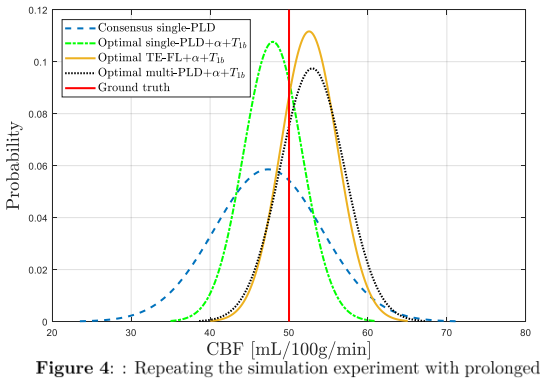

Figure 4: : Repeating the simulation experiment with prolonged Δt results in the following CBF estimate distributions for the consensus-statement experiment and the optimal experiment combinations.

References [1]Alsop D, et al. MRM, 2015;73:102:116. [2]van Osch MJP, et al. J Cereb Blood Flow Metab, 2018;38:1461-1480. [3]Chen Z, et al. MRM, 2017;77:1841-1853. [4]Li W, et al. MRM, 2016;77:2296-2302. [5]Teeuwisse WM, et al. MRM, 2014;72:1712-1722. [6]Buxton R, et al. MRM, 1998;40:383-396. [7]St Lawrence K, et al. MRM, 2000;44:440-449. [8]Vidorreta M, et al. NeuroImage, 2013;66:662-671. [9]Jung Y, et al. MRM, 2010;64:799-810. [10]Petersen ET, et al. NeuroImage, 2010;49:104-113. [11]Bojorquez JZ, et al. MRM, 2017;35:69-80. [12]Li KL, et al. MRM, 2005;53:511-518. [13]Gregori J, et al. JMRI, 2013;37:332-342.

A novel technique to improve the reliability of pseudo continuous arterial spin labeling

Matthias Günther[1,2,3], Praveen Iyyappan Valsala[1]

[1]Fraunhofer MEVIS, Bremen, Germany, [2]University of Bremen, Germany, [3]mediri GmbH, Heidelberg, Germany

Synopsis: Labeling performance of pseudo continuous arterial spin labeling (pCASL) is susceptible to the off-resonances introduced by B_0 inhomogeneity and eddy current effects. Here, a short calibration approach using the recently presented ASL-IF (arterial spin labeling – input function) method [1] is used to maximize the labeling efficiency. Vessel-specific optimization can be achieved. Further optimizations like RF power deposition are possible, but typically not needed. This new calibration approach could pave the way for robust and reliable pCASL measurements in a clinical setup.

Introduction: PCASL is the recommended labeling scheme for its high SNR [2]. However, off-resonance induced phase evolution of the transverse magnetization in-between the excitation pulses lead to reduction in the labeling efficiency. Also, inter-scan variability of the labeling efficiency influences reproducibility and reliability of the perfusion quantification. The earlier proposed methods involve long repetitive measurements to probe the phase offset of the system. Later, the measured phase offset is compensated in post processing by model fitting [3] or corrected in the future measurements by altering the RF phase or gradients [4,5]. In this study, we propose a quick calibration protocol which can measure and compensate the phase offset at higher precision within 10 seconds.

Materials and Method: The capability of ASLIF method to sample the arterial input function (AIF) during the labeling process is utilized in this study. The arterial input function is modulated by phase offset of the labeling pulse and measured at the readout slice downstream to the labeling slice. In order to measure the labelling efficiency of several phase offset in a single experiment, the continuous labeling block is split into several short measurement blocks (see figure 1). In addition to the phase of the labeling pulse, this method gives the possibility to optimize other protocol parameters like readout slice position, labeling and readout pulse power.

Data Acquisition: Experiments were performed on a clinical 3T MR-scanner (Magnetom Skyra, Siemens Healthineers, Erlangen, Germany). A perfusion phantom (Gold Standard Phantoms, London, UK) and three healthy male volunteers (age 26-35) were scanned to validate the method. An informed consent according the ethical standards of the university is signed by all the volunteers. The flow rate of phantom is set to 350 ml/min. An extended labeling duration of 6000 ms was used to cover the offset range of 320° with a resolution of 20°.

Processing: The AIF signal is integrated over the time in each offset block. The measurement block with maximum AIF signal is considered corresponds to the optimal parameter. The data processing pipeline is implemented in the scanner to reconstruct the AIF readout data and automatically predict the optimal parameter in real time.

Results: Figure 2 presents the results of the experiment on a perfusion phantom. The labeled bolus before and after optimizing the labeling pulse phase and the corresponding perfusion images are shown.

Discussion: Typically, the labeled bolus reaches the readout slice in less than a few hundred milliseconds and it is measured in real time. Therefore, the time consuming elements like post labeling delay (PLD) and image acquisition during repetitive methods are avoided in this prescan routine. Furthermore, there is no model assumed and the combined effect of all the off-resonance sources are measured. Also, the dispersion of the signal due to the flowing spins at different velocities and the transit delay effects are minimal at the readout slice. This makes the method more reliable. A 10 s calibration scan is sufficient to optimize the phase offset of the labeling process. Further repetitions of the calibration scan (each lasting 10 seconds) may be performed to reduce SAR or to optimize other parameters of ASL-IF method.

Conclusions: To conclude, the phase offset correction method proposed using the ASLIF technique is significantly faster and robust compared to earlier methods. The fully automatic implementation can be easily integrated into a clinical setup for reliable ASL measurement.

References:

1. Günther, M. in *Proc.ISMRM. 26* 0305 (2018),
2. Alsop, D. C. et al. Magn. Reson. Med. 73, 102–116 (2015),
3. Jung, Y. et al. Magn. Reson. Med. 64, 799–810 (2010),
4. Luh, W.-M. et al. Magn. Reson. Med. 69, 402–410 (2013),
5. Jahanian, H. et al. NMR Biomed. 24, 1202–1209 (2011).

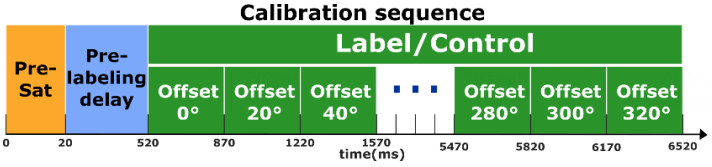

Figure 1 The scheme of the calibration sequence is shown. In this illustration, the phase of labeling pulse is varied across the measurement block.

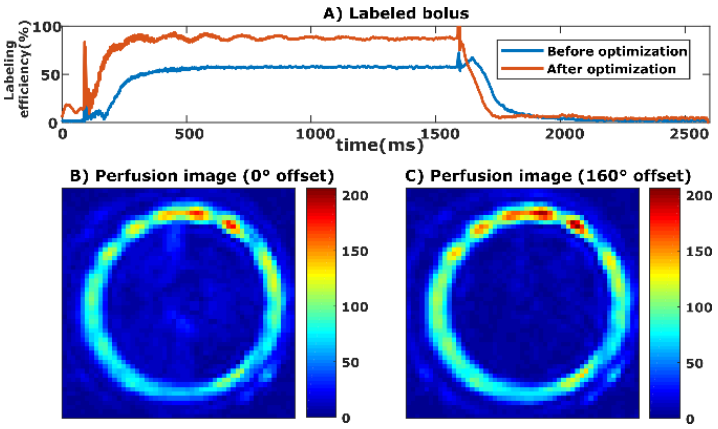

Figure 2 The labeled bolus before and after optimizing the labeling pulse phase is plotted in the graph A. The signal axis is scaled by the labeling signal achieved by a hyperbolic secant pulse (Assumed as 100%). The subfigures B and C show the perfusion images at sub-optimal offset (0^0) and optimal phase offset (160^0) predicted by the calibration scan respectively. The time shift of the optimized bolus is due to translation of the labeling slab towards the readout slice. The spikes in the boli are the result of signal separation error at the beginning and end of labeling.

Comparison of optimized pseudo-continuous arterial spin labeling protocols for cerebral blood flow measurements

Joseph G. Woods[1], Michael A. Chappell[1,2], Thomas W. Okell[1]

[1]Wellcome Centre for Integrative Neuroimaging, FMRIB, NDCN, University of Oxford, UK, [2]Institute of Biomedical Engineering, University of Oxford, UK. Correspondence to jwoods@fmrib.ox.ac.uk

Introduction There have been many different techniques proposed for estimating cerebral blood flow (CBF) using pseudo-continuous Arterial Spin Labeling (PCASL). However, it is still unclear which can yield the most accurate CBF estimates in a typical scan duration because previous studies have not rigorously optimized each technique and have only compared a limited selection of techniques.[1-3] Here, we optimize a wide range of existing techniques (Fig. 1) for CBF accuracy using a recently developed framework[4] and compare them using simulations and in vivo data. We also propose a new hybrid technique which benefits from the averaging of Hadamard-encoding while also being able to use longer label durations (LDs). We demonstrate that the commonly held view that single-delay CBF estimates are more robust in a typical scan duration is not necessarily true.

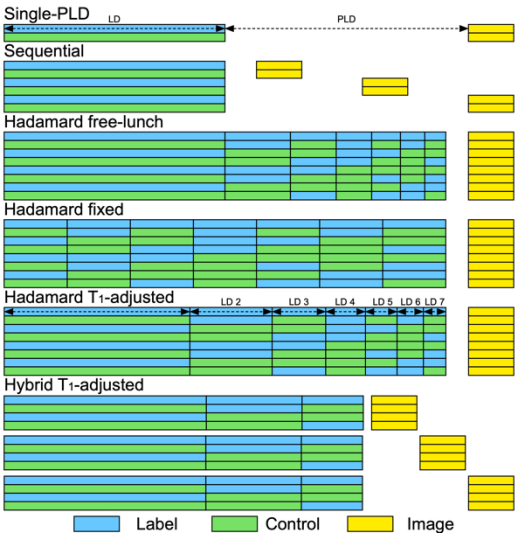

***Fig. 1**: Schematic of the protocols compared.*

Theory It is often argued that acquiring data at an appropriate single post-labeling delay (PLD) will result in the most robust and reproducible estimates, because many averages can be acquired to improve SNR. This SNR improvement is expected to outweigh the potential errors from simplifications to the physiological model.[5]

A more complex approach is to acquire data at multiple PLDs (and/or LDs) and to estimate both arterial transit time (ATT) and CBF at the same time by fitting a dynamic signal model to the data. This reduces the ambiguity of when the label reaches the tissue and starts to decay with tissue T_1, but fewer averages at each PLD can be acquired. The PLDs can either be sequentially varied for each acquisition or the LDs and PLDs can be encoded into the PCASL pulse train using a Hadamard encoding scheme.[6,7] The latter technique has been suggested to be more efficient, but it is not clear if the shorter LDs available in Hadamard-encoded techniques limits CBF accuracy.

Methods We optimized the LDs and PLDs of the protocols in Fig. 1 across an ATT range of 0.5 - 2 s using the Cramér-Rao lower bound (CRLB) framework in [4]. The framework aims to minimize the expected estimation variance (uncertainty) of CBF estimates by adjusting the protocol timings. Scan time 5 min, maximum LD 1.8 s, number of PLDs <10, variable-TR. The single-PLD protocol was LD 1.8 s, PLD 2 s. Monte Carlo (MC) simulations and in vivo experiments (10 healthy volunteers, background suppressed single-shot 3D GRASE) were performed. Gray matter data was fit for CBF and ATT using a variational Bayesian framework[8] with noninformative priors. Single-PLD fitting assumed an ATT of 1.3 s. Tissue T_1=1.445 s, blood T_1=1.65 s. The CBF and ATT posterior probability standard-deviations (SD) were used as a measure of uncertainty. Voxel-wise test-retest comparisons were performed by fitting the first and last half of each scan and calculating the root-mean-squared errors (RMSE) between these. Ground truth estimates were generated by fitting the combined data from all scans.

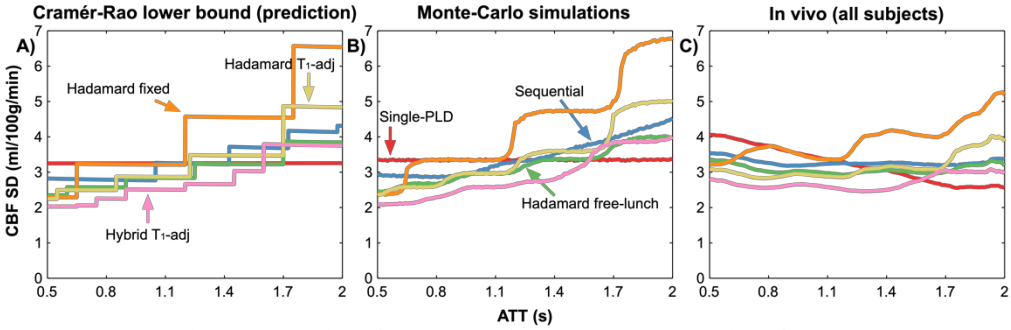

***Fig. 2** CBF SDs: A) CRLB SD, B) median MC simulations posterior SD, C) median in vivo posterior SD. The in vivo data was plotted against the ground truth ATT estimates using a sliding window.*

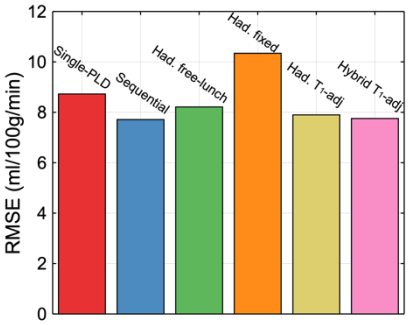

***Fig. 3**: Test-retest CBF RMSE between each 2.5 min scan for each protocol.*

Results and Discussion The posterior SDs for each protocol are shown in Fig. 2. The MC simulation SDs agree extremely well with the CRLB SDs, while similar trends can be seen in vivo. The Hadamard fixed protocol has the highest uncertainty while the Hybrid T_1-adj protocol maintains the lowest average uncertainty across ATTs. The free-lunch and T_1-adj Hadamard protocols performed similarly well to the sequential protocol. The in vivo test-retest RMSEs are shown in Fig. 3. All of the multi-PLD protocols except Hadamard fixed have lower RMSEs than the single-PLD protocol, demonstrating their improved reproducibility. All of the Hadamard protocols produced more accurate ATT estimates than the sequential protocol (not shown).

Conclusions We have shown that by appropriately designing and optimizing multi-PLD protocols, it is possible to produce similar or more robust and repeatable CBF estimates than a typical single-PLD protocol, while also providing ATT maps. We have also demonstrated that the short LDs and design rigidity in typical Hadamard protocols greatly diminishes the signal averaging benefit. The hybrid method is a promising alternative because it is able to take advantage of longer LDs, has more flexible timings, and has moderate Hadamard averaging. Using fewer encodes should also improve robustness to image corruption.

References [1] Dai et al. MRM 2013; [2] Johnston et al. IEEE Trans. Med. Imag. 2015; [3] Guo et al. JMRI 2018; [4] Woods et al. MRM 2018; [5] Alsop et al. MRM 2015; [6] Günther ISMRM 2007; [7] Teeuwisse et al. MRM 2014; [8] Chappell et al. IEEE Trans. Sig. Proc. 2009.

Perfusion Measurement in Brain Gliomas Using Velocity-Selective Arterial Spin Labelling: Comparison with Pseudo-Continuous Arterial Spin Labelling and Dynamic Susceptibility Contrast Perfusion

Yaoming Qu[1], Doris D. Lin[2], Dapeng Liu[2,3], Wenbo Li[2,3], Peter C. van Zijl[2,3], Zhibo Wen[1], Qin Qin[2,3]

1. Department of Radiology, Zhujiang Hospital, Southern Medical University, Guangzhou, Guangdong Province, China;
2. Department of Radiology; Johns Hopkins University School of Medicine, Baltimore, Maryland, USA;
3. F.M. Kirby Research Center for Functional Brain Imaging, Kennedy Krieger Institute, Baltimore, Maryland, USA;

Introduction: Pseudo-continuous arterial spin labeling (PCASL) [1] has been shown to be an effective alternative to dynamic susceptibility contrast-enhanced perfusion weighted imaging (DSC-MRI) for evaluating vascularity in brain tumors [2-4]. Velocity-selective arterial spin labeling (VSASL) employing Fourier-transform based velocity-selective pulse trains is an emerging perfusion imaging method [5] with high sensitivity to perfusion signal. The purpose of this work is to evaluate the performance of VSASL on preoperative patients with gliomas by comparing with PCASL and DSC-PWI.

Methods: This prospective study was approved by the local IRB. Patients with newly diagnosed brain tumors were recruited to undergo preoperative MRI between Nov. 2017 and Dec. 2018 using a 3T Philips Ingenia scanner. In additional to conventional anatomic sequences, each MRI consists of DWI (b=0, 1000s/mm²) and 3 perfusion sequences including VSASL, PCASL and DSC-PWI. Both ASL and DSC-PWI were acquired with echo planar imaging (EPI). VSASL and PCASL had post labeling delays of 1.5s and 2.0s, as described in [5] and [6], respectively. Both ASL methods were acquired with 10 slices and a resolution of 3.3x3.0x4.4mm^3 (4.8min). DSC-PWI was acquired with 24 slices and a resolution of 2.2x2.0x4.4mm^3 (2.5min).

The voxel-wise CBF quantification of ASL data was processed in Matlab using standard equations [5][6]. The CBF maps of DSC-PWI were obtained using the software Olea Sphere (Olea Medical, France). Three representative 3×3 pixel regions of interest (ROIs) were manually chosen from tumor regions showing the maximal perfusion signal on CBF maps. For each method and each patient, the ratio of tumor blood flow (TBF) and contralateral normal-appearing grey matter blood flow (CBF_{GM}) were compared.

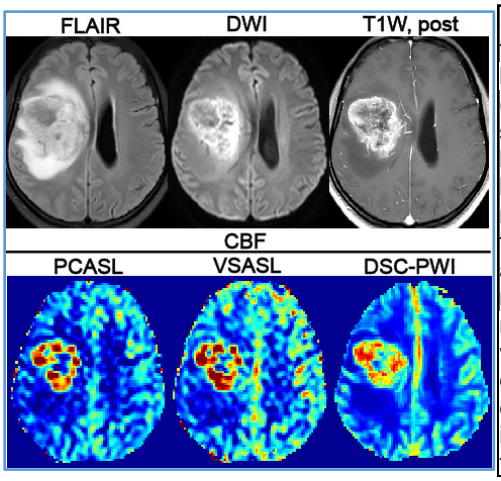

Fig.1: A 34-year-old female with right frontal lobe glioblastoma (WHO Grade IV) showing DWI hyperintensity reflecting hypercellularity. CBF maps are comparable for PCASL, VSASL, and DSC-PWI, all revealing a thickened rim of increased vascularity around central necrosis, corresponding to the irregularly enhancing tumor.

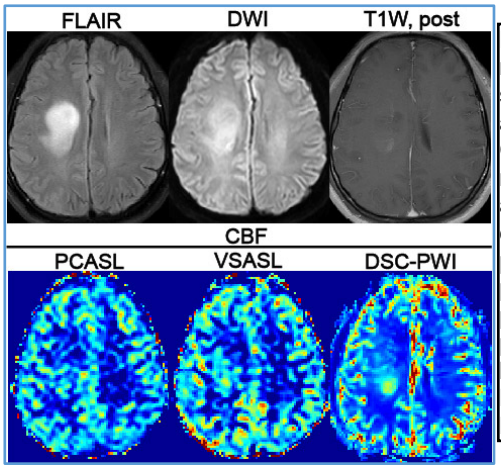

Fig.2: A 48-year-old male with right centrum semiovale diffuse astrocytoma (WHO Grade II) that shows mild DWI hyperintensity associated with minimal contrast enhancement posteriorly. Higher perfusion signal, particularly within the posterior portion of the lesion, is depicted by PCASL, VSASL, and DSC-PWI.

Results: 45 patients (Grade IV, N=15, 53±13yo; Grade III, N=6, 51±6yo; Grade II, N=24, 40±12yo) with a histopathological diagnosis of primary gliomas based on the 2007 WHO brain tumor classification were included in this analysis.

Figs.1,2 show representative images with high and low glioma grades of FLAIR, DWI, and post-Gadolinium contrast T1w. CBF maps derived from VSASL, PCASL and DSC-PWI were largely comparable on visual inspection.

Fig.3 shows linear regression and Bland-Altman analyses of the ratios of TBF over CBF_{GM}, between PCASL, VSASL with DSC-PWI, respectively. Compared to PCASL (a,b), VSASL (c,d) demonstrated better correlation (R^2=0.79 vs 0.52) and agreement with DSC-PWI. Both methods show good separation between low grade (grade II) and high grade (grade III & IV) tumors based on differences in tumor perfusion.

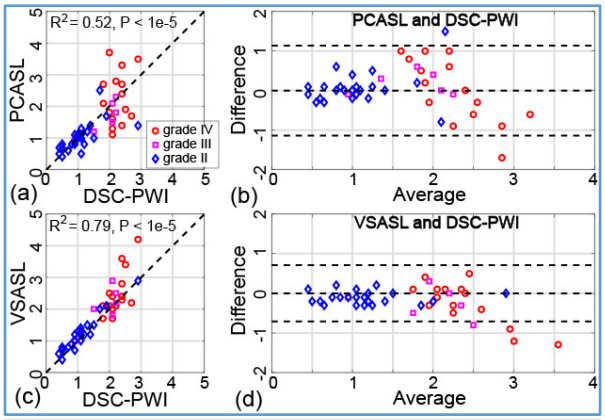

Fig. 3: Correlation (a,c) and agreement (b,d) of TBF-CBF_{GM} ratios measured between PCASL (a,b) or VSASL (c,d) and DSC-PWI.

Conclusion: VSASL shows great promise for accurate, noninvasive quantification of CBF in patients with glioma. With the advantages of insensitivity to transit delay and no need of prescribing a labeling plane, VSASL could potentially improve the diagnostic performance of ASL in preoperative grading of gliomas.

References:

[1] Dai, W, et al. MRM, 2008 60: p1488;
[2] Järnum, H, et al. Neuroradiology 2010 52: p307;
[3] Roy, B, et al. J Comput Assist Tomogr, 2013 37: p321;
[4] Zeng, Q, et al. AJNR, 2017 38: p1876;
[5] Qin, Q, et al. MRM, 2016 76: p1136; [6] Alsop, D, et al. MRM, 2015 73: p102;

Non-contrast assessment of blood-brain-barrier permeability with water-extraction-with-phase-contrast-arterial-spin-tagging (WEPCAST) MRI

Zixuan Lin[1], Yang Li[1], Sandeepa Sur[1], Jinsoo Uh[2], Peiying Liu[1], Pan Su[1], Eboni Lance[3], Matthias van Osch[4], and Hanzhang Lu[1]
[1]Department of Radiology, Johns Hopkins School of Medicine, Baltimore, MD, [2]Department of Radiation Oncology, St. Jude Children's Research Hospital, Memphis, TN, [3]Kennedy Krieger Institute, Baltimore, MD, [4]Department of Radiology, Leiden University Medical Center, Leiden, the Netherlands

INTRODUCTION: Disruption of blood-brain barrier (BBB) permeability has been associated with numerous brain diseases. Conventional MRI approaches to image BBB permeability require the use of Gd contrast agent, which limits its clinical application. In this study we developed a new sequence, water-extraction-with-phase-contrast-arterial-spin-tagging (WEPCAST) MRI, to assess BBB permeability to water by selectively measuring venous ASL signal. The work presented in this abstract includes sequence design, validation with contrast-based method, and applications in mild cognitive impairment (MCI) and sickle cell disease (SCD).

THEORY: BBB permeability can be characterized by permeability-surface-area product (PS): $PS = -\ln(1-E)\cdot f$, where E is the extraction fraction of water in its first-pass and f is cerebral-blood-flow (CBF)[1]. To measure E, we can use pCASL to label the water molecules in arterial blood. At capillary-tissue interface, most labeled spins are extracted to tissue (Fig.1, red), whereas non-extracted spins are drained directly to venous system (blue). Additionally, a small amount of labeled spins that are extracted to tissue will re-exchange back into venous system (yellow). Then ASL signal at superior-sagittal-sinus (SSS) can be written as $\Delta M = \Delta M_1 + \Delta M_2$, where $\Delta M_1 = 2\alpha(1-E)M_{0,blood}\exp(-\delta_v/T_{1,blood})c(t)$ represents non-extracted spins and $\Delta M_2 = 2\alpha f/\lambda E M_{0,blood}\exp(-\delta_v/T_{1,blood})c(t)\otimes[r(t)m(t)]$ represents extracted spins that were re-exchanged into vessel. λ is blood-brain partition coefficient, α is labeling efficiency, δ_v is bolus arrival time (BAT) to SSS, $c(t)$ is arterial input function, $r(t) = e^{-ft/\lambda}$ is residue function and $m(t) = e^{-t/T_{1,tissue}}$ represents T_1 relaxation.

METHODS: *Study I WEPCAST MRI sequence:* To reduce the confounding contribution of tissue perfusion signal, we devised a new sequence, WEPCAST MRI, by adding a phase-contrast velocity-encoding gradient during acquisition of pCASL sequence. Images were acquired in mid-sagittal plane (N=6, 23±3yrs, 3F) with four long post-labeling-delays (PLD): 3000, 3500, 4000, 4500ms and encoding velocity of 15cm/s. *Study II Acceleration:* To expedite the acquisition, a background-suppressed Look-Locker readout was applied (LL-WEPCAST) in coronal plane, allowing 8-PLD acquisitions in one TR (N=6, 28±8yrs, 3F). Results were compared with those from sequence in study I. *Study III Validation:* We sought to validate WEPCAST MRI by comparing its results with those from Gd-based MRI. WEPCAST MRI was performed (N=6, 34±15yrs, 5F), followed by a dynamic contrast-agent scan, in which 30 T_1-weighted images (multi-echo VASO MRI sequence[2]) were acquired with Gd injection at the beginning of the 4th dynamic. *Study IV Application in MCI*: WEPCAST MRI was applied on 27 MCI patients (68±7yrs) and 20 controls (69±6yrs). PS of patients and controls were compared. Relationship between PS and cognitive test results and CSF biomarkers were examined. *Study V Application in SCD:* WEPCAST MRI was applied in SCD children (N=8, 10±1yrs), PS of whom were compared with adult controls. Association between PS and silent cerebral infarct (SCI) and neuropsychological scores were examined.

RESULTS: *Study I:* Fig.2 shows representative control, label, and difference images of WEPCAST MRI at PLD=4000ms. Venous signal can be seen at SSS and tissue signal is well suppressed. Quantitative analysis of posterior SSS revealed an average E of 95.5±1.1% and PS of 188.9±13.4mL/100g/min, consistent with previous literatures[3-5]. *Study II:* Fig.3a shows images acquired with LL-WEPCAST. Averaged signal curves from two methods showed similar intensities and temporal characteristics. PS from two methods was in good agreement (R^2=0.85). *Study III:* Fig.4 shows a scatter plot between $PS_{WEPCAST}$ and PS_{Gd}. WEPCAST MRI showed a strong correlation with Gd-based BBB method (R^2=0.75 and p=0.025). *Study IV:* Fig 5a shows representative WEPCAST images in a MCI patient and a control subject. The patient revealed much less signal compared with the control. Statistical analysis showed that the MCI group had a significantly higher PS (i.e. leaky BBB) than controls (Fig.5b, p=0.04). Regression analysis also suggested that individuals with a higher PS tend to have a lower MoCA scores (poorer overall cognition, p=0.04), poorer episodic memory (p=0.005) and poorer language function (p=0.01). Higher PS was also associated with higher CSF Tau level (p=0.04) and lower Aβ42 level (p=0.09). *Study V:* Fig.6a shows representative WEPCAST images for a SCD child. Compared with healthy adult, SCD child revealed significant higher signal in SSS (p<0.001), lower extraction fraction (p<0.001) and slightly higher PS (p=0.50). Among SCD patients, higher PS was correlated with significantly lower hematocrit level (Fig.6b, p=0.02) and lower hemoglobin (p=0.02). Higher PS was also associated with a greater risk of SCI (Fig.6c, p=0.002) and attention deficits (p=0.003).

CONCLUSION: In this study, we developed a new sequence, WEPCAST MRI, for assessment of BBB permeability to water without using exogenous contrast agent. The technique was applied to MCI and SCD patients to demonstrate its potential clinical utility.

REFERENCES: 1. Crone, Acta Physio Scan, 1963. 2. Uh et al, MRM, 2009. 3. St. Lawrence et al, MRM, 2012. 4. Gregori et al, JMRI, 2013. 5. Herscovitch et al, JCBFM, 1987.

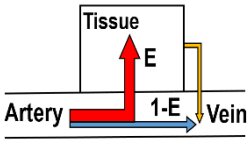

Fig.1 Model of water extraction across BBB.

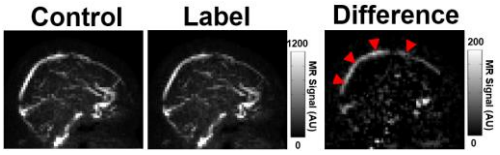

Fig.2 WEPCAST results. (a) Representative control, label and difference images. (b) SSS signal time course at different PLDs.

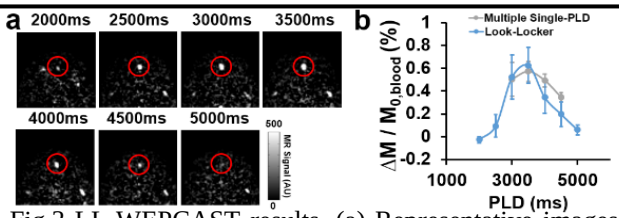

Fig.3 LL-WEPCAST results. (a) Representative images. (b) SSS signal time course from two methods.

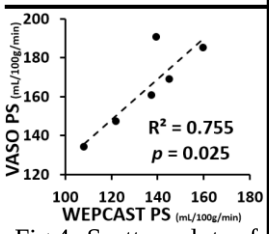

Fig.4 Scatter plot of PS from WEPCAST and VASO methods.

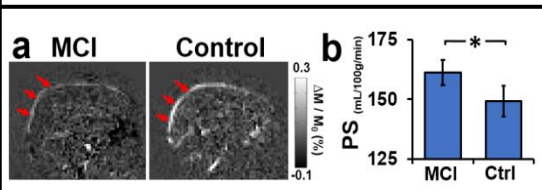

Fig.5 WEPCAST in MCI. (a) WEPCAST images of a MCI patient and a control. (b) Bar plot of PS for MCI and control groups.

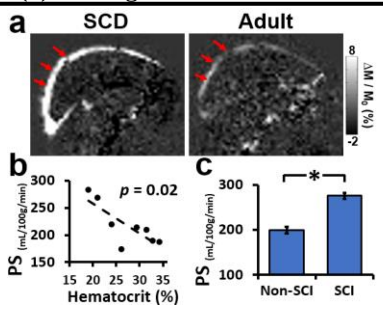

Fig.6 WEPCAST in SCD. (a) WEPCAST images of a SCD children and an adult control. (b) Association between PS and hematocrit in SCD. (c) PS of patients with and without silent cerebral infarct.

Quantification of CBF in glioblastoma multiforme; challenges of ASL calibration in the presence of oedema.

Paula L.Croal[1,2], Flora Kennedy-McConnell[1,2], Benjamin Harris[4,5], Ruichong Ma[4], Stasya M. Ng[5], Puneet Plaha[4,6] Simon Lord[4,5] Nicola R. Sibson[3]Michael Chappell[1,2]

[1]Institute of Biomedical Engineering, University of Oxford [2]Wellcome Centre for Integrative Neuroscience, University of Oxford, [3]Oxford Institute for Radiation Oncology, University of Oxford, [4]Oxford University Hospitals NHS Trust, [5]Department of Oncology, University of Oxford, [6]Nuffield Department of Clinical Neuroscience, University of Oxford.

Introduction: The 'ASL white paper' has been instrumental in reaching a consensus for both acquisition and analysis in the clinical setting[1]. However, as ASL continues to gain clinical traction, particularly within cancer imaging[2-4], it is important to question whether the current recommended analysis pipeline is appropriate in patients with gross pathology. Here we assess the impact of calibration method in patients with glioblastoma multiforme (GBM); hypothesising that voxelwise calibration, as proposed in the White paper[1], may confound results in the presence of oedema.

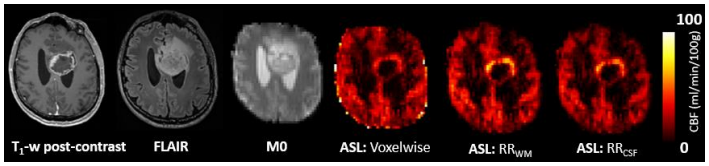

Figure 1) GBM shown in a representative patient. Quantitative CBF maps are shown for voxelwise, white matter (RR_{WM}) and CSF (RR_{CSF}) calibration, with hyperperfusion evident in the tumour rim.

Methods: Seven patients (4/3F, 59.7±12.6 years) with primary occurrence of GBM were imaged at 3T (Siemens Verio) prior to surgical resection, as part of the ongoing IMAGO trial, with institutional ethics approval. *Acquisition:* Whole-head T_1-weighted MPRAGE (with/without Gadolinium (Gd-HP-DO3A, Prohance™) TR/TE=1900/3.17ms, 0.7×0.7×1mm), and FLAIR (TR/TE=5000/495ms, 1.0×1.0×1.0mm) were acquired for tumour visualisation, and PCASL MRI (5 PLD:400-2000ms, TR/TE=5484/14ms, 26 slices, 3.4×3.4×5mm), including calibration (M_0) image with matched parameters, minus labeling/background suppression. *Analysis:* ASL data were motion corrected[5], and pairwise subtraction performed to create perfusion-weighted images, which were averaged across PLDs. A Bayesian nonlinear fit to the general kinetic model[6] was used for voxelwise CBF quantification[7], assuming α=0.85, and T_1=1.3/1.65s for tissue/blood. Signal calibration was performed, both by voxelwise division of M_{0a} (M_0 of arterial blood, defined as M_0/λ), and using a reference M_{0a} value, assuming λ=0.9/0.82/1.15 for whole-brain/WM/CSF, and correcting for T_2 differences between tissue types (T_2=50/750/150ms for WM/CSF/Blood). We compared three calibration approaches: voxelwise (VW) calibration in line with the White paper[1], mean M_{0a} from a WM reference region (RR_{WM}), and mean M_{0a} from a CSF reference region (RR_{CSF}). Tumour ROIs, were manually defined[8] on enhancing post-Gd MPRAGE, with enhancing regions included only. Contralateral normal appearing GM and WM (NAGM, NAWM) ROIs were extracted using FAST segmentation of pre-Gd MPRAGE[9] (partial-volume thresholded at 0.8 and 0.9 respectively). CSF ROIs were manually defined from the ventricles on the M_0 image to ensure pure CSF voxels. ROIs were transformed via linear registration to M_0 and FLAIR images[5], and mean CBF, M_0 and FLAIR signal intensity calculated for each ROI. *Statistics:* Within-subject comparisons were made using a paired *t*-test, and multiple-comparisons controlled for using Bonferroni correction.

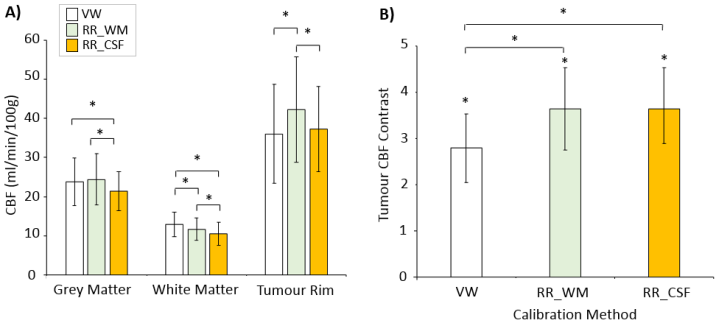

Figure 2 (A) Absolute CBF in grey matter, white matter and tumour rim for both voxelwise (VW), WM calibration (RR_{WM}) and CSF calibration (RR_{CSF}). (B) Tumour CBF Contrast is significantly higher for both RR_{WM} and RR_{CSF} than for voxelwise. Data shown as mean across subjects ± SD,

Results: FLAIR and M_0 signal intensities were significantly elevated in tumour ROIs in comparison to NAWM (p=0.004, p=0.002 respectively, *Fig.1*), with tumour contrast correlated between the sequences (r=0.78, p=0.039). Significant tumour CBF contrast (Tumour/NAWM) was observed for all calibration methods (*Figs.1-2*), with contrast significantly greater for both RR_{WM} and RR_{CSF}. Absolute CBF_{tumour} was significantly higher with RR_{WM} calibration in comparison to both VW (32.29±20.8%, p=0.03*)* and RR_{CSF} (13.1±8.7%, p = 0.049) calibration (*Fig.2*). CBF_{NAWM} was significantly lower with RR_{WM} in comparison to VW calibration (9.1±2.5%, p<0.001), while CBF_{NAGM} did not differ (*Fig.2B*). Both CBF_{NAGM} and CBF_{NAWM} were significantly lower with RR_{CSF} in comparison to VW calibration (9.0±5.3%, p=0.02, and 19.1±8.2%, p=0.004, respectively).

Discussion: Calibration method significantly affected absolute CBF; a significant loss of CBF contrast in tumours was evident when using voxelwise calibration, whilst the impact on absolute CBF was more variable. Results suggest voxelwise calibration is suboptimal due to reduced tumour contrast. However, it is less apparent whether CSF or WM is the appropriate alternative, whilst CSF calibration is likely more susceptible to coil sensitivity errors, recent findings suggest that NAWM may not be truly 'normal', with observed alterations in T_2[10]. From a clinical perspective, reduced sensitivity to tumour CBF in[13]. From a technical perspective, reference region calibration involves additional processing steps in comparison to voxelwise, however, these steps can be automated as part of existing pipelines[14,15]. the presence of oedema may negatively impact both grading, and assessment of peritumoural pathophysiology associated with tumour invasion and recurrence[11-

References: [1] Alsop et al., *MRM*, 2016 [2] Kim et al., *Neuroadiology*, 2017 [3] Dangouloff-Ros et al., *Radiology*, 2016 [4] Brendle et al., *Clin. Neuroradiol.*, 2018 [5] Jenkinson et al., *NIMG*, 2002 [6] Buxton et al., *MRM*, 1998 [7] Chappell et al., *IEEE Trans Signal Process*, 2009 [8] Yushkevich et al., *NIMG*, 2006 [9] Zhang et al., *IEEE Trans Med Imag*., 2001 [10] Mehrabian et al., *Proc. ISMRM*, 2018 [11] Jarnum et al., *Neuroradiol.*, 2010 [12] Delgado et al., *Neuro-Oncol.* [13] Lu et al., *Clin. Radiol.*, 2018 [14] www.quantiphyse.org [15] https://fsl.fmrib.ox.ac.uk/fsl/fslwiki/BASIL

System conditioning effects on temporal SNR and perfusion when computing GRAPPA reconstruction coefficients for accelerated EPI-based PASL imaging

W. Scott Hoge[1,2], and Jonathan R. Polimeni[2,3]

[1]*Brigham and Women's Hospital, Boston, MA,* [2]*Athinoula A. Martinos Center for Biomedical Imaging, Massachusetts General Hospital, Charlestown, MA,* [3]*Harvard-MIT Health Sciences and Technology, Massachusetts Institute of Technology, Cambridge, MA*

Introduction: Accelerated parallel MR imaging (pMRI) can increase MRI temporal efficiency. With accelerated echo planar imaging (EPI), pMRI can also reduce geometric distortions and image blurring due to T2* decay. Both of these improvements improve spatial accuracy, but at the cost of non-uniform SNR loss due to *g-factor* effects that depend the geometric layout of the receive coil array and acceleration rate. To date, mitigation of SNR loss in pMRI have focused on SENSE [1, 2], in part because the SENSE linear system maps in a natural way to cost-function minimization problems. System conditioning in GRAPPA [3] has received less attention, and this work seeks to improve methods used to train GRAPPA reconstruction coefficients for accelerated 2D EPI data. We examine both system normalization/preconditioning and simple Tikhonov regularization, and show that appropriate levels of regularization in EPI-based ASL can improve the measured perfusion images.

Methods: GRAPPA estimates a fully-sampled set of k-space data from an under-sampled acquisition by estimating missing data from a linear combination of neighboring data. This can be modeled as $Kg = t$, where t is the target k-space data, K is an array composed of neighboring k-space data, and g is a vector of GRAPPA coefficients that map a linear combination of K elements to the target data. The GRAPPA kernel itself extends by n_x points along the readout, n_y points along the phase encode dimension, and c coils. This gives the length of g equal to $(n_x \cdot n_y \cdot n_c)$. The number of rows in K is determined by the number times the kernel covers both source and target data points in the calibration data, and is often over-determined with many more rows than columns.

To improve the linear system condition when calibrating a GRAPPA kernel, one can apply system preconditioning [4] to normalize the signal level across rows of the system, via $\psi K g = \psi t$, where ψ is a diagonal matrix with elements equal to the inverse of the L_2 norm of the rows of the system matrix, $\psi_{ii} = 1/\sqrt{\sum_j |K_{ij}|^2}$. As most of the signal energy is concentrated in the center region of k-space, preconditioning can provide a better signal-energy balance across all rows of the system. After forming the normal equations to produce a smaller system matrix and reduce computational load, one can then apply Tikhonov regularization [4], which results in the system equation: $(K^H \psi^2 K + \lambda I) g = K^H \psi^2 t$.

In-plane accelerated ($R = 2$) PASL perfusion-weighted (3.4x3.4x4.0 mm, TR=3.2 sec, TE=13 ms, 64x64 matrix size, 24 slices, Q2TIPS labeling (TI=1800 ms, 700 ms bolus), 52 control/label pairs) EPI data were acquired in-vivo at 3T. Two blocks of pre-scan calibration data were acquired using conventional multi-shot EPI, with an opposite readout polarity for the second block for Dual-Polarity GRAPPA (DPG) [5] ghost correction. Missing data in the accelerated EPI images was also synthesized using DPG, to restrict conditioning effects to a single system inversion. The effect of the different system conditioning methods on the corresponding tSNR maps for each application data set was illustrated, along with the condition number, defined as the ratio of the smallest to largest singular value, $\sigma_{\min}/\sigma_{\max}$, of the modified linear system.

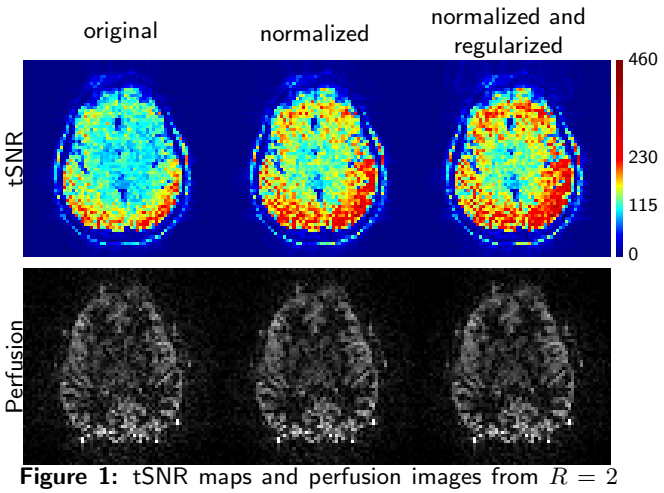

Figure 1: tSNR maps and perfusion images from $R = 2$ accelerated 3T PASL-based perfusion-weighted EPI data.

Results: Fig. 1 illustrates that PASL is an application where improved system conditioning can be critically important. Both tSNR and the associated perfusion-weighted images are shown. The top row shows a dramatic boost in tSNR after normalization and regularization are applied, which correspondingly reduces speckle noise in the low-perfusion regions in images on the second row.

Discussion and Conclusions: This study demonstrates that system conditioning approaches can have a positive impact on temporal SNR when reconstructing accelerated EPI data. While the effects of regularization have been previously investigated in the context of BOLD-weighted EPI [7], we have demonstrated here that perfusion applications can also benefit.

References: 1. King, Angelos, ISMRM 2001; 1771. 2. Lin, et al, MRM 2004;51(3):559–567. 3. Griswold, et al, MRM 2002; 47(6):1202–1210. 4. Björck Å. "Numerical methods for least squares problems," SIAM Press, 1996; 5. Hoge, Polimeni, MRM 2016; 76(1):32–44. 6. Triantafyllou, et al, Neuroimage 2011;55(2):597–606. 7. Polimeni, et al, MRM Med 2016;75(2):665–679.

Optimization of Velocity-Selective-Inversion Arterial Spin Labeling with 3D Acquisition

Dapeng Liu[1,2], Wenbo Li[1,2], Peter van Zijl[1,2], Doris D. Lin[1], Qin Qin[1,2]
1. Department of Radiology; Johns Hopkins University School of Medicine, Baltimore, Maryland, USA
2. F.M. Kirby Research Center for Functional Brain Imaging, Kennedy Krieger Institute, Baltimore, Maryland, USA

Introduction

Velocity-selective ASL (VSASL) [1] technique has the advantages over the conventional method of insensitivity to transit delay and no need of prescribing a labeling plane. However, it has mostly been demonstrated with 2D acquisition for conventional velocity-selective saturation (VSS) [1–6] and Fourier-transfer based velocity-selective inversion (VSI) [7]. Recently, VSI with low-flip-angle segmented 3D spiral acquisition was implemented for perfusion functional MRI [8]. The current work aims to optimize VSASL with 3D GRASE readout for baseline perfusion mapping. Comparisons with pseudo-continuous ASL (PCASL) [9] are also performed.

Methods

All experiments were performed on a Siemens 3T Prisma scanner. Multi-shot 3D GRASE readout was implemented to achieve high SNR efficiency. Parameters were taken from [1,7] for VSASL and [9,10,11] for PCASL.

We first optimized the post-labeling delay (PLD) for VSASL. Six PLDs (0.6, 0.9, 1.2, 1.5 and 1.8 sec) were compared for both VSS and VSI on two groups of subjects: 1) 20 ~ 35 yo, n = 5, 2 females and 2) 50 ~ 65 yo, n = 5, 3 females. Normalized perfusion signal, defined as difference between label and control divided by M_0, was calculated as the indicator of signal sensitivity.

VSS and VSI with the optimized PLD of 1.2 sec (see results) and PCASL with PLD of 2.0 sec were compared on the same two groups of subjects. In addition, they were also compared on a brain tumor patient (61 yo, male) with recurrent Glioblastoma (GBM).

Results

The normalized perfusion-weighted images of one middle slice from VSS and FT-VSI prepared ASL with 3D GRASE acquisition at different PLDs are demonstrated in Fig. 1a. Normalized perfusion signal in GM was plotted as a function of PLD from VSS and VSI (Fig. 1b, c). A PLD of 1.2 sec yielded maximal perfusion signal change among most of the subjects and was chosen for the subsequent VSASL scans.

The normalized perfusion-weighted images from the middle slice of the five older subjects are arrayed in Fig. 2. Note that the PCASL result of the first male subject shows markedly diminished perfusion signal in the occipital lobes (red arrowhead), as an example of the possible sensitivity to transit delay. In contrast, VSASL results do not display such an artifact.

The SNR in GM of FT-VSI based VSASL were 29.7% and 34.2% higher than PCASL and 27.6% and 29.5% higher than VSS-based VSASL, in the young and older groups, respectively (Fig. 3).

Fig. 4 shows an example of CBF mapping of whole brain coverage using PCASL and VSI ASL of a patient with recurrent left occipital GBM (red arrow). The hyperperfused tumor is well depicted by both methods but VSI shows slighter higher signal than PCASL.

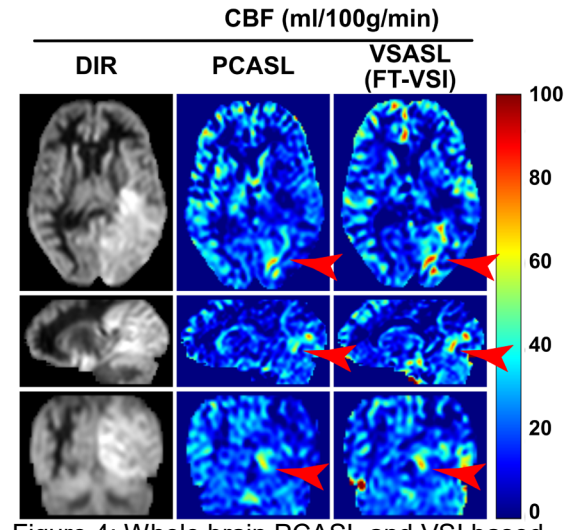

Figure 4: Whole brain PCASL and VSI based ASL of a patient with recurrent GBM.

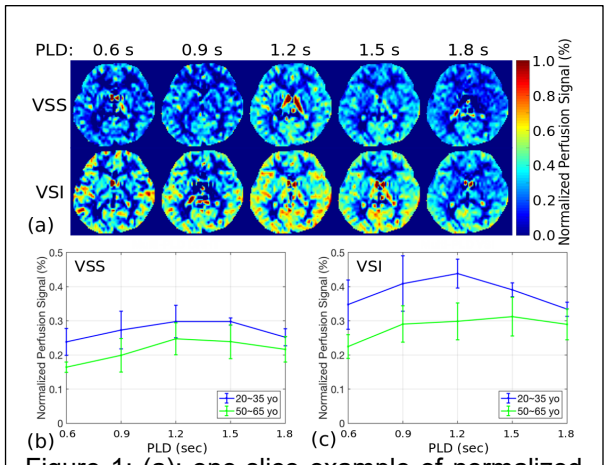

Figure 1: (a): one-slice example of normalized perfusion signal from one subject comparing VSS and VSI; (b): normalized perfusion signal in GM as a function of PLD; (c): normalized perfusion signal as a function of PLD.

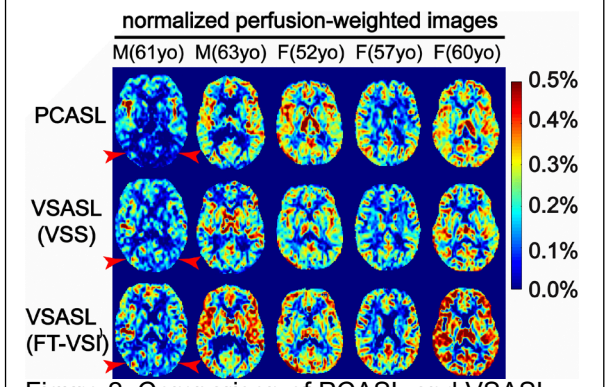

Figure 2: Comparison of PCASL and VSASL using VSS and VSI in group 2 (only one middle slice shown).

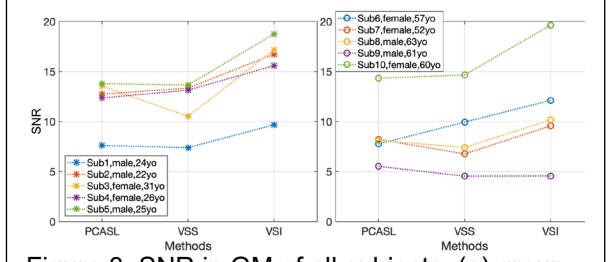

Figure 3: SNR in GM of all subjects: (a) group 1 and (b) group2.

Conclusion

FT-VSI with 3D-GRASE readout was successfully implemented. FT-VSI based VSASL showed higher sensitivity to perfusion signal than both PCASL and VSS based VSASL. The clinical prospect of VSASL with a 3D whole-brain coverage was demonstrated on a brain tumor patient.

References

[1] Wong, E, et al, MRM, 2006 55: p1334.
[2] Duhamel, G, et al. MRM, 2003 50: p145.
[3] Wu, C, et al. Neuroimage, 2006 32: p122.
[4] Qiu, D, et al. JMR, 2012 36: p110.
[5] Meakin, J, et al. MRM, 2013 69: p832.
[6] Guo, J, et al. MRM, 2015 73: p1084.
[7] Qin, Q, et al. MRM, 2016 76: p1136.
[8] Hernandez-Garcia, L, et al. MRM, 2019, DOI: 10.1002/mrm.27461.
[9] Dai, W, et al. MRM, 2008 60: p1488.
[10] Alsop, D, et al. MRM, 2015 73: p102.
[11] Zhao, L, et al. MRM, 2016 78: p1342.

Impact of calibration methods and processing options on CBF quantification using ASL

Joana Pinto[1], Michael A. Chappell[2,3], Thomas W. Okell[2], Melvin Mezue[2], Andrew R. Segerdahl[2], Irene Tracey[2,4], Pedro Vilela[5], Patrícia Figueiredo[1]

[1]Institute for Systems and Robotics and Department of Bioengineering, Instituto Superior Técnico, Universidade de Lisboa, Lisbon, Portugal; **[2]**Wellcome Centre for Integrative Neuroimaging, FMRIB, Nuffield Department of Clinical Neurosciences, University of Oxford, Oxford, UK; **[3]**Institute of Biomedical Engineering, Department of Engineering Science, University of Oxford, Oxford, UK; **[4]**Nuffield Division of Anaesthetics, Nuffield Department of Clinical Neuroscience, University of Oxford, Oxford, UK; **[5]**Imaging Department, Hospital da Luz, Lisbon, Portugal

Absolute perfusion quantification using ASL is highly dependent on a calibration procedure aiming at the normalization of the control-label difference images by the equilibrium magnetization of arterial blood. Although different calibration methods have been previously compared[1–3], the various processing options that need to be made in their practical implementation are frequently disregarded and left unreported, compromising the utility of absolute quantification.

In our work, we systematically compared different calibration methods and associated processing options in two multiple post-labeling-delay ASL datasets (PASL and pCASL). Only small differences were observed across the main calibration methods, based on a reference tissue (CSF, GM or WM) or on a voxelwise basis, when using specific carefully chosen options. However, when varying these options we found substantial discrepancies in CBF values. In particular, calibration methods based on CSF as a reference tissue were more sensitive to such options than the other methods. This is mostly due to the greater sensitivity of CSF measurements to RF field inhomogeneities, and also to T_1 corrections given the much larger T_1 value of CSF relative to GM and WM. Overall, the greatest sensitivity was found to correction for incomplete T_1 relaxation, RF field inhomogeneities and the value of presaturation efficiency. In contrast, the values of brain-blood water partition coefficient and the degree of spatial smoothing applied to the calibration images or the mask used for the reference tissue had moderate to negligible impact.

Our results support the use of a voxelwise calibration approach as proposed in the ASL white paper, due to its relatively low sensitivity to the various processing options. Nevertheless, regardless of the method chosen, our work highlights the need for the use of consistent calibration pipelines for CBF quantification, including a complete report of the associated processing options.

References

1. Cavuşoğlu M, Pfeuffer J, Uğurbil K, et al. Magn Reson Imaging 2009; 27: 1039–45.
2. Chen Y, Wang Z, Detre JA. *ISMRM 19* 2011; 300.
3. Fazlollahi A, Bourgeat P, Liang X, et al. *Neuroimage* 2015; 117: 191–201.

Accurate quantification of vascular territories using super-selective PCASL - Pitfalls and solutions

Jonas Schollenberger[1], C. Alberto Figueroa[1,2], Luis Hernandez-Garcia[1,3]
[1]Biomedical Engineering, [2]Surgery, and [3]FMRI Laboratory, University of Michigan, Ann Arbor, MI, USA

Introduction: Perfusion measurements of vascular territories in the brain offer critical clinical information on cerebrovascular function. In regions of mixed perfusion, measurements of the fractional contribution of individual arteries is of particular interest. For example, in the presence of cerebrovascular occlusive disease, territorial perfusion fraction maps can be used to identify and evaluate collateral flow pathways.

In super-selective pseudo-continuous ASL (SS-PCASL) [1], territorial perfusion images are acquired by creating a circular labeling spot which can be placed on individual arteries. However, when post-processing territorial perfusion images to calculate perfusion fractions maps, differences in labeling efficiency between labeled arteries can lead to significant inaccuracies. These differences can occur due to a mismatch between vessel and label spot (movement), off-resonance, or differences in blood velocities. In this work, we present a strategy to maximize labeling efficiency, account for differences between labeled arteries, and quantify territorial perfusion fractions.

Methods: Territorial perfusion fraction maps were acquired in two healthy subjects. A multi-phase pre-scan was collected to compensate for off-resonance in the label plane, which consisted of a non-selective PCASL with increasing RF-phase increments after each label/control pair. Cardiac-triggered SS-PCASL images of all four neck arteries were subsequently acquired, using a peripheral pulse oximeter to trigger the start of the saturation pulse before the label train [2]. In-between acquisitions, a 2D TOF of the label plane was collected to correct for vessel movement. Following, the labeling efficiency of each vessel was directly measured 2 cm above the label plane. Additionally, the blood velocity in the label plane was quantified with 2D PC-MRI. Vessel-averaged labeling efficiency was obtained by compensating for T1-decay during transit and calculating a velocity-weighted average across the vessel. Perfusion fraction maps were generated by scaling each vessel selective subtraction image by its corresponding label efficiency and dividing it by the sum of all the vessel selective subtraction images. Finally, a 3D TOF of the neck and brain was collected for reference.

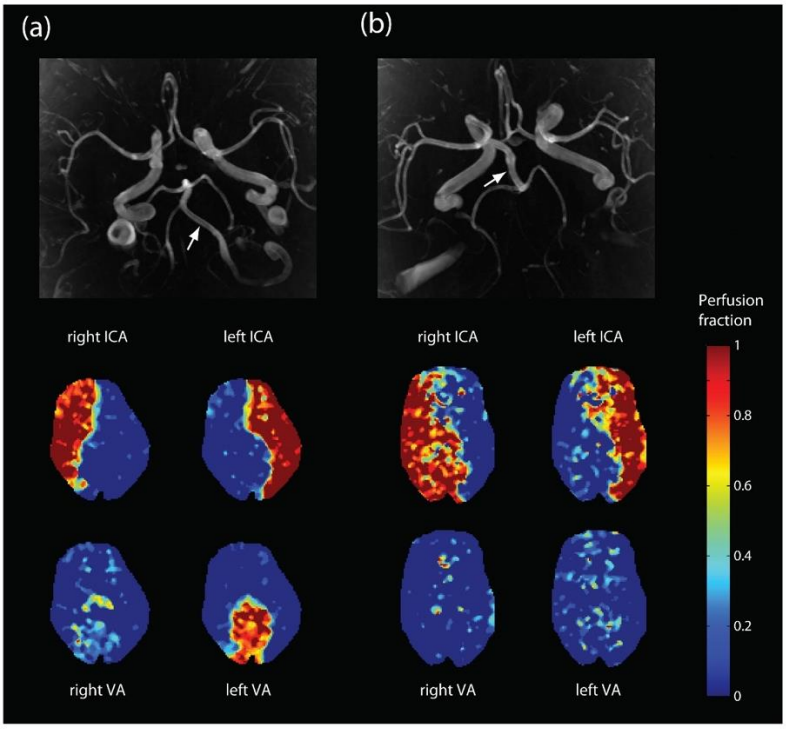

FIG. 1: Axial TOF and corresponding perfusion fractions of neck arteries of two subjects. (a) Subject with a posterior circulation dominantly perfused by left VA. TOF confirms increased caliber of left VA (arrow). (b) Subject with absent basilar artery. Posterior circulation is primarily perfused by right ICA (Arrow indicates the presence of the right posterior communicating artery with an increased caliber).

Results: Fig. 1 shows the resulting perfusion fraction maps for two subjects. Subject (a) revealed a posterior circulation dominated by the left vertebral artery. Subject (b) presented with a missing basilar artery. Blood flow to the posterior circulation was provided by the right internal carotid artery via the right posterior communicating artery. These findings are consistent with the 3D TOF images.

Discussion and conclusions: The scaled perfusion fraction maps based on our proposed strategy showed the perfusion territory of each vessel clearly. In mixed perfusion territories, such as the posterior circulation, perfusion fractions were in line with TOF images.

References: [1] Helle at al. 2010; [2] Li et al. 2018

Deep Learning-based Detection of DSC-Defined Penumbral Tissue on pCASL in Acute Ischemic Stroke

Kai Wang[1], Qinyang Shou[2], Samantha Ma[1], David Liebeskind[3], Xin Qiao[4], Fabien Scalzo[3], Jeffrey Saver[3], Noriko Salamon[4], Danny Wang[1]
[1]Lab of Functional MRI Technology, University of Southern California, Los Angeles, CA, [2]Shanghai Jiaotong University, Shanghai, China, [3]Neurology, University of California, Los Angeles, CA, [4]Radiology, University of California, Los Angeles, Los Angeles, CA

Introduction:

Acute ischemic stroke (AIS) patients with perfusion-diffusion lesion volume mismatch (i.e., penumbra) are more likely to benefit from endovascular thrombectomy [1]. Contrast-free arterial spin labeling (ASL) MRI techniques can provide cerebral blood flow (CBF) measures and show largely consistent results with dynamic susceptibility contrast-enhanced (DSC) perfusion in delineating hypoperfused brain regions in AIS. However, the precise hypoperfusion lesion and penumbra delineation in ASL images remains challenging due to low SNR and delayed arterial transit. In this study, we develop a deep learning-based model to identify the hypoperfusion lesions in ASL images, using the DSC-delineated perfusion lesions as the ground truth (GT), with the aim of aiding endovascular thrombectomy decision-making.

Methods:

157 AIS patients underwent 1-4 clinical stroke MRI on Siemens 1.5T Avanto or 3.0T TIM Trio systems using 12-channel head coils, providing 174 usable image datasets (1.5T: n=101; 3T: n=73). Pseudo-continuous arterial spin labeling (pCASL) with background suppressed 3D GRASE readout was used: TR/TE/label time/PLD=4000/22/ 1500/2000ms; FOV=22cm; matrix size=64×64, 26×5mm slices. Quantitative CBF maps were calculated from the pCASL images[2]. The Time-to-maximum (Tmax) map was generated from DSC and a threshold=6s delineated hypoperfusion regions. After thresholding, skull-stripping, CSF-masking, spatial smoothing, and clustering were applied, the final binary labels for perfusion lesions (Tmax$\geqslant$6s) were used for training.

HighRes3Dnet [3] with 20 layers and residual connections was used as the deep learning network. The network was trained on 2 Nvidia GeForce GTX 1080 Ti GPUs via NiftyNet [4]. ASL and DWI images were the input, and the DSC binary mask was the GT. 48*48*48 volumes (batch size=4) were randomly extracted from 3D preprocessed images for training. Volume level augmentation was employed including rotation and random spatial rescaling. The dice loss function and Adam optimization method were used (learning rate = 0.0001, $\beta1 = 0.9, \beta2 = 0.999$). The total iteration number was 30,000 to enable the training process to reach steady state.

For both subsets, 10-fold cross-validation was used. For voxel-level evaluation, Dice coefficient was calculated for each subject, and the group Dice was calculated as the average of all subjects. For subject-level evaluation, first hypoperfused volume was calculated and compared with ground truth, then following the diffusion/perfusion mismatch criterion for endovascular treatment [5] the suggestion was made based on both GT and the inference output, and the corresponding confusion matrices were calculated.

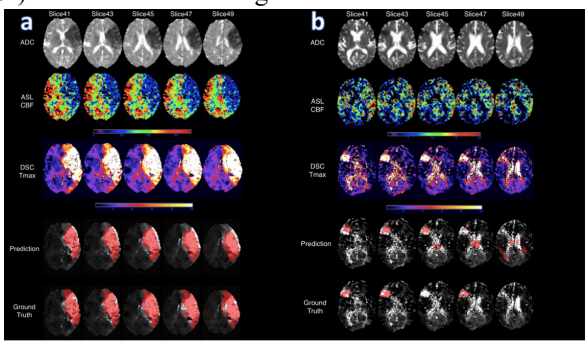

Fig.1 Prediction results from input images (ADC, ASL CBF), compared with ground truth. a) Successful case for the model. The prediction result matches well with the ground truth, although more spatially smoothed. b) Failed case for the model. The model captured hypoperfusion lesions as well as ventricle region. Since ventricle region also has low perfusion signal just like lesions, to some extent it makes sense that false positive was observed here; however, we expect the model to be able to differentiate lesions from ventricle regions by providing training data that's CSF masked. False positive was observed only for a few subjects, which suggests the model has the potential to do so. This problem should be solved by further

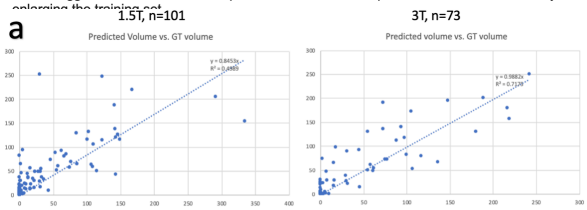

Fig.2 The correlation between predicted volume and ground truth (GT) by field strength, and the confusion matrices for endovascular thrombectomy decision making. a) For both 1.5T (left) and 3T (right) subsets, the predicted volume is highly correlated with GT, with a slew rate close to 1, especially for 3T. The 3T subset has a stronger correlation and a slew rate closer to 1 despite smaller dataset size, which may be the benefice of higher SNR of 3T scanner. **b)** Confusion matrix for 1.5T (left) and 3T (right). For 1.5T, the True Positive Rate (TPR) = 0.938, the True Negative Rate (TNR) = 0.812, and the total accuracy = 85%; for 3T, the TPR = 0.900, the TNR = 0.830, and the total accuracy = 85%.

Results and Discussion

Fig1 shows 2 representative cases of prediction results. For the first case, the prediction result matches well with the GT. For the second case, false positive results are seen in the ventricle, which also has a low perfusion value. The group average Dice is 0.303 and 0.381 for 1.5T and 3T, respectively, which is relatively low since many cases have only background (no lesion), so one false positive voxel would result in Dice=0. In Fig2a, a strong correlation was observed between the hypoperfusion lesion volumes from the model inference and DSC (for 1.5T, $y = 0.85x, r^2 = 0.50$; for 3T,$y = 0.99x, r^2 = 0.72$). In terms of endovascular thrombectomy decision making, accuracy of 85% was achieved on both subsets (Fig. 2b).

Conclusion

In general, our model was able to find the hypoperfused region from ASL images, though lesions in ASL and DSC do not match completely. Along with ADC images, this model provided an accuracy of 85% (using DSC as the reference) in terms of penumbral volume estimation. With increasing training dataset, we expect the accuracy will continue to improve.

Reference

[1] Albers GW, Marks MP, Kemp S, Christensen S, Tsai JP, Ortega-Gutierrez S, et al. Thrombectomy for stroke at 6 to 16 hours with selection by perfusion imaging. New England Journal of Medicine. 2018;378:708-718
[2] Straka M, Albers GW, Bammer R. Real-time diffusion-perfusion mismatch analysis in acute stroke. Journal of Magnetic Resonance Imaging. 2010;32:1024-1037
[3] Wang DJ, Alger JR, Qiao JX, Hao Q, Hou S, Fiaz R, et al. The value of arterial spin-labeled perfusion imaging in acute ischemic stroke: Comparison with dynamic susceptibility contrast-enhanced mri. Stroke. 2012;43:1018-1024
[4] Gibson, Eli, et al. "NiftyNet: a deep-learning platform for medical imaging." Computer methods and programs in biomedicine 158 (2018): 113-122.
[5] Li W, Wang G, Fidon L, et al. On the compactness, efficiency, and representation of 3D convolutional networks: brain parcellation as a pretext task[C]//International Conference on Information Processing in Medical Imaging. Springer, Cham, 2017: 348-360.
[6] Kingma, D., Ba, J.: Adam: A method for stochastic optimization (2014). arXiv:1412.6980

Accelerating Stack of Spirals 3D RARE Using Rotated Spirals and Compressed Sensing Reconstruction

Munsch F[1], Taso M[1], Zhao L[2], Lebel M[3], Guidon A[4], Alsop DC[1]

[1]Division of MRI research, Radiology, Beth Israel Deaconess Medical Center, Harvard Medical School, Boston, MA, United States, [2]Diagnostic Imaging and Radiology, Children's National Medical Center, Washington, DC, United States, [3]Global MR Applications and Workflow, GE Healthcare, Calgary, AB, Canada, [4]Global MR Applications and Workflow, GE Healthcare, Boston, MA, United States

Introduction:

Multi-shot interleaved 3D acquisitions with Stack of Spirals (SOS) RARE or GRASE acquisition are widely used for Arterial Spin Labeling (ASL) perfusion imaging because they enable whole-brain coverage, support excellent background suppression, and provide excellent sensitivity. But their use for applications and approaches demanding higher temporal resolution are not possible. Stimulated and resting state perfusion fluctuation studies could benefit from improved temporal resolution through single-shot acquisitions. Acceleration of 3D acquisitions to single-shot would ideally not compromise mean blood flow measurement. Here we report an approximate golden angle spiral rotation strategy compatible with single shot imaging by compressed sensing reconstruction but also standard regridding reconstruction of multi-shot interleaves. Application of the sequence to quantification of resting state network fluctuations is demonstrated.

Methods:

A standard interleaved SOS RARE acquisition sequence was modified in two ways. First the spiral trajectory was modified to variable density for full sampling of the center of k-space in each arm and then 8 fold undersampling of the outer region. Second, the rotation strategy was modified both across shots and slice encodes. Between shots and between increments of slice encoding, the spiral gradients were rotated by an approximate golden angle ($10\pi/13$, i.e. 138.46°, because the rotation repeats after 13 rotations) (Figure 1). This rotation spreads undersampling gaps between the slice and spiral directions to improve parallel imaging while also adding an irregular sampling pattern that may assist with compressed sensing reconstruction. Twelve healthy volunteers were scanned with a GE 3 Tesla MR750 scanner using a 32 channel head array coil from Nova Medical. ASL studies were performed with pseudocontinuous labeling (1.8s labeling, 1.8s postlabeling delay), background suppression, and 32 centric ordered 4mm thick slices. Spiral gradient waveforms were 6.14ms in duration with echo spacings of 12ms. Label and control images were alternated and then rotations of the spiral encode patterns were performed after each pair. 39 rotations were performed corresponding to 3 averages of 13 rotations for a total scan time of 8 minutes. Complex k-space subtraction was performed and fully sampled data were reconstructed by slice direction FFT followed by an in-plane non-uniform FFT (nuFFT). Coil sensitivities were estimated from this fully-sampled perfusion-weighted volume using ESPIRiT(1) (σ=0.01, threshold=0.8) followed by reconstruction of the 39 single-shot volumes using an L_1-wavelet Compressed-Sensing (CS) reconstruction (λ_1=0.005, 100 iterations) with the BART toolbox(2) under MATLAB. Single-shot time series were analyzed for resting state fluctuations(3) using a spatial Independent Component Analysis (ICA) using FASTICA.

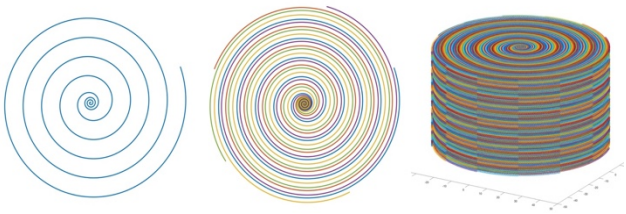

Figure 1 - Illustration of k-space trajectory for (left) a single spiral k-space trajectory (center) 5 overlayed interleaves to demonstrate angular rotation filling of k-space and (right) the 3D sampling pattern illustrating rotation across slice encodes

Results:

3D CS reconstruction of the 39 individual shots was readily achieved in 1100 seconds on an iMac Pro (6-core Intel Xeon W, 128Gb RAM) with a CPU-based parallelized implementation. Temporal averages of the single shot images (Figure 2-B) produced images with image quality close to the fully sampled acquisitions (Figure 2-A). ICA analysis of image time series extracted with good spatial resolution well-known brain networks, such as default mode, motor and visual networks (Figure 2-C).

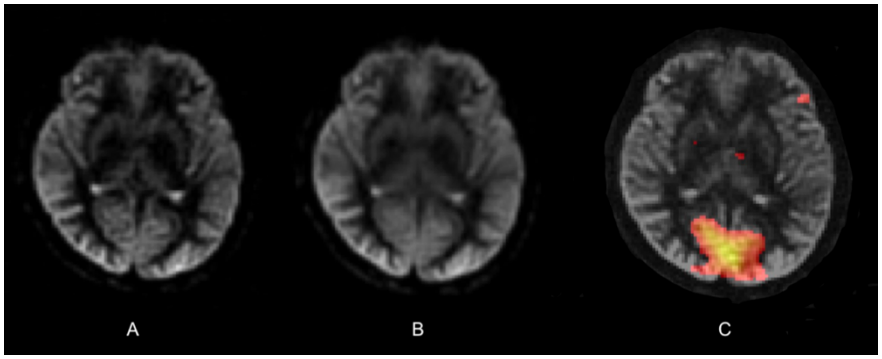

Figure 2 - A. Reconstructed average perfusion from the fully-sampled data; B. Temporal mean of the 39 single-shot; C. Resting-state visual median network identified from the single-shot time series and ICA.

Discussion and Conclusions:

Building upon prior work using spiral rotations for flexible scan prescription of ASL perfusion(4) and golden angle stack of stars for ASL angiography(5), our approximate golden angle rotation strategy enables uncompromised time average perfusion with the option for accelerated reconstruction up to single-shot with the same data. This should add flexibility for fast ASL, multiple contrast ASL acquisitions such as time-encoded ASL, and studies of perfusion fluctuations and modulation.

(1) Uecker M *et al. Magn. Reson. Med.* 2014
(2) Uecker M *et al. Proc. Intl. Soc. Mag. Reson. Med.* 2015
(3) Zhao L *et al. J Cereb Blood Flow Metab.* 2017
(4) Li Z *et al. Magn Reson Med.* 2016
(5) Zhou Z *et al. Magn Reson Med.* 2017

4D Vessel-Encoded pCASL Angiography in a Five-Minute Scan

S Sophie Schauman[1], Mark Chiew[1], Thomas W Okell[1]
[1]Wellcome Centre for Integrative Neuroimaging, FMRIB, NDCN, University of Oxford, UK

Introduction

Pseudo-continuous arterial spin labelling (pCASL) can be used for angiography [1] but is often limited by long acquisition times. Although some undersampled acquisition methods have been proposed [2], limited amounts of work have been done utilising sparse reconstruction methods [3].

Vessel-encoded (VE) ASL [4] is an extension to pCASL that provides additional information about cerebral haemodynamics by separating blood coming from different feeding arteries. However, it further increases scan time compared to standard pCASL. For example, to separate blood from three arteries, four images are required instead of the conventional two ('tag' and 'control'), doubling the scan time. To fully sample k-space of a 4D three-vessel VE-ASL angiogram as presented here, would take over five hours. By using sophisticated reconstruction methods, we show that we can reduce the scan time to five minutes and maintain image fidelity.

Methods

As an initial proof-of-principle, one healthy volunteer was scanned on a 3T Siemens Verio scanner. The vessel-encoding was a 4x4 Hadamard encoding scheme, encoding the right and left internal carotid arteries, and the basilar artery. Immediately following a 1 s ASL preparation module, a spoiled gradient echo sequence with a 3D golden angle radial trajectory [5] (TE/TR = 5.9/11.6ms, FA = 7º) was acquired. 108 radial spokes were acquired during each readout period (1.2 s). The continuously acquired spokes were split into 6 frames (temporal resolution 210 ms). This was repeated 33 times for each encoding (total scan time 5:16 min) to reach 594 spokes per frame (R = 97 at 1.1 mm isotropic resolution).

The raw data was reconstructed frame by frame in MATLAB in a compressed sensing (CS) framework. The modelled acquisition operator took into account three components of the imaging system: 1. The vessel encoding that was imposed on the blood magnetisation, 2. The coil sensitivity profiles of the 32-channel head coil (estimated from the data itself using the adaptive combine method [6]), and 3. The imaging trajectory and image-to-k-space transformation which was implemented using the non-uniform fast Fourier transform (NUFFT [7]). The CS optimisation was performed using a non-linear iterative algorithm (FISTA [8]).

Results

A 60% increase in SNR was observed for the CS reconstructed images compared with reconstruction using simple re-gridding and coil sensitivities only (Figure 1). Figure 2 shows the frame-by-frame CS reconstruction. Although the SNR is lower in the later frames the distal vessels can still be resolved.

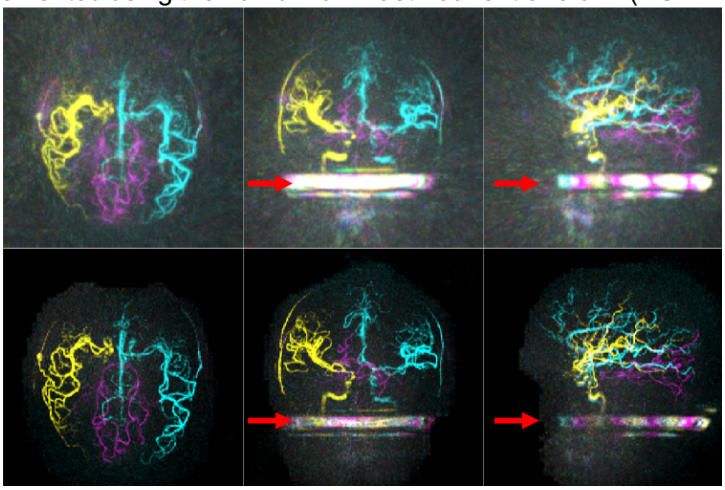

Figure 1 – Above: Simple re-gridding reconstruction (temporal average MIP). Below: CS Reconstruction. The red arrows indicate a labelling plane artifact.

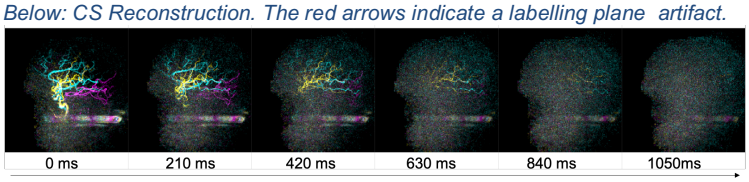

Figure 2 – Temporal dynamics of bolus of labelled blood through arterial tree

Discussion and Conclusion

As a proof-of-principle, the results are very promising with sharp delineation and well-separated vessels. Further development of the method will require optimisation of the reconstruction as the current reconstruction took >24h. A five-minute VE 4D scan is, however, a step towards making non-contrast-enhanced dynamic angiography clinically feasible.

References

1. Dixon W.T., et al., 1986. Projection angiograms of blood labeled by adiabatic fast passage.
2. Wu H., et al., 2013. Noncontrast-enhanced three-dimensional (3D) intracranial MR angiography using pseudocontinuous arterial spin labeling and accelerated 3D radial acquisition.
3. Zhou Z., et al., 2018. Accelerated noncontrast-enhanced 4-dimensional intracranial MR angiography using golden-angle stack-of-stars trajectory and compressed sensing with magnitude subtraction.
4. Wong E.C., 2007. Vessel-encoded arterial spin-labeling using pseudocontinuous tagging.
5. Okell T.W., 2018. Combined angiography and perfusion using radial imaging and arterial spin labelling.
6. Walsh D.O., et al., 2000, Adaptive reconstruction of phased array MR imagery.
7. Fessler J.A., et al., 2003, Nonuniform fast Fourier transforms using min-max interpolation.
8. Beck A., et al., 2009, A Fast Iterative Shrinkage-Thresholding Algorithm for Linear Inverse Problems.

A multi-site round robin assessment of ASL using a perfusion phantom

A. Oliver-Taylor[1], T. Hampshire[1], H.J. Mutsaerts[2,3,4], P. Clement[5], E. Warnert[6], J.P.A. Kuijer[2], K. Baas[3], J. Petr[7,8], J.C.W. Siero[4,9], J.P. Marques[10], S. Sunaert[11], R.J.H. Borra[12], M.J.P. van Osch[13], X. Golay[1,14], and E. Achten[5]

[1]Gold Standard Phantoms Limited, London, UK, [2]VUmc, Amsterdam, Netherlands, [3]AMC, Amsterdam, Netherlands, [4]UMCU, Utrecht, Netherlands, [5]Ghent University, Ghent, Belgium, [6]Erasmus MC, Rotterdam, Netherlands, [7]HZDR, Dresden, Germany, [8]RIT, Rochester NY, USA, [9]Spinoza Centre for Neuroimaging, Amsterdam, Netherlands, [10]Donders Institute, Nijmegen, Netherlands, [11]KULeuven, Leuven, Belgium, [12]MIC, UMCG, Groningen, Netherlands, [13]LUMC, Leiden, Netherlands, [14]ION, UCL, London, United Kingdom

Introduction: The measurement of Cerebral Blood Flow (CBF) using Arterial Spin Labelling (ASL) has seen a renewed interest following the publication of the Position Paper providing a set of clear guidelines on how to perform an ASL experiment[1]. In particular, it has been shown to be valid as a biomarker of neurological disease onset[2] and response to therapy[3]. Indeed, based on numerous reproducibility studies[4], the coefficient of variation of CBF has been well established, enabling its use as a biomarker in cross-sectional studies[5]. However, while the sources of potential physiological confounds are well established[6], it has so far not been possible to compare all ASL implementations depending uniquely on potential hardware differences.

In this study, we set out to assess the effective reproducibility of CBF estimates by ASL using a recently developed Perfusion phantom[7] at 11 different sites with a range of scanner manufacturers (total 17 systems). We present here the preliminary data from the first 5 scanners from 3 sites working on Philips 3T MRI scanners with the same software release (R5.3).

Imaging Parameter	Value
Label Duration	1800ms
Post Labelling Delay	1800ms
Label Plane Location	60mm from centre of FOV, parallel alignment.
No. dynamics	3
No. shots	4
SENSE factor	2.3
FOV	256x192x59mm
PE Direction	AP
Acquisition Matrix (per slice)	128x96
No Slices	12
Slice thickness/gap	4mm/1mm
TR	5000ms
TE	Min TE selected, given per MRI system 1-5: 11.271, 10.166, 11.283, 11.269, 10.16 ms
Background suppression	4 pulse product default

Figure 1: ASL sequence parameters.

Materials and Methods: A perfusion phantom was transported by car to 3T MRI imaging centres in the Netherlands over the course of a week and scanned on 5 Philips 3T MRI systems running software release R5.3 (3 Ingenia, 2 Achieva). ASL measurements were made using the product ASL sequence, comprising of pCASL labelling with a 4-shot 2D-EPI segmented acquisition (detailed in Figure 1.b), including an acquisition with a long-TR and without background suppression or labelling pulses for an M0 image, followed by 3 repetitions of control-label pairs. Measurements were made at two volume flow rates; 200ml/min and 350ml/min. At each site, care was taken to ensure the phantom was reproducibly placed on the patient couch (see Figure 2), and the FOV was centred at a landmark at the centre of the porous material and rotated into alignment with the phantom.

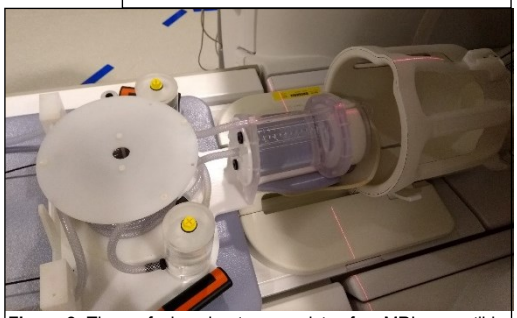

Figure 2: The perfusion phantom consists of an MRI compatible pump that delivers a liquid at a controlled flow rate to a perfusion chamber. The liquid is distributed in a 'vascular' network to a porous material cylinder that simulates the capillary bed of diameter 116mm and height 28.5mm.

Analysis was performed in Matlab R2016b (The Mathworks, Natick, MA, USA). Dicom images were converted to NIFTI using dicm2nii[8], and CBF maps calculated using the single subtraction equation for pCASL[1], with λ=0.32 corresponding to the phantom's porosity (void volume). The M0 image was registered to a structural atlas image of the phantom, from which an ROI mask of the entire porous material was generated. The mean CBF and standard deviation within this ROI were then calculated.

Results: Figure 3.a shows representative CBF maps of the fifth slice from each data set. Figures 3.b and c show the CBF value distributions within each mask for MRI System 5. The mean CBF values and standard deviations within each mask for each system and flow rate are shown in Figure 4.a and b. Across all systems, the mean CBF was 33.7±3.1 ml/100g/min at 200ml/min, and 76.7±9.0 ml/100g/min at 350ml/min.

Discussion: Across MRI systems, the coefficient of variance of the mean CBF was 9.2%/11.7% at 200/350 ml/min. As Figure 3.b and 3.c show, the actual voxel value distributions within the masked regions are complex and simple mean/standard deviation statistics do not capture this, leading to an underestimation in the perfusion signal CBF, and perhaps underestimation of the differences between MRI systems. At the higher flow rate the difference between systems in both the mean CBF and standard deviation of CBF is greater. In particular, System 2 shows a mean CBF and standard deviation that is noticeably higher than the other four systems. Possible reasons for this might be better labelling efficiency, or this could be a receive coil effect as this was the only system using an 8-channel head coil. No repeat measurements were made at each site, so there is no metric of intra-session variability which might also explain some of the variations observed between systems.

Conclusion: We have presented a multi-site assessment of 2D-EPI pCASL measurements on Philips 3T MRI systems running the same software version, using a perfusion phantom. In general, measurements made across all systems are in good agreement with each other; however, further analysis and measurements are required to determine a statistically significant difference between systems.

Acknowledgements: Anita Harteveld (UMCU, Utrecht, Netherlands) for time and assistance scanning. Pieter Vandemaele (Ghent University, Ghent, Belgium) for advice on standardised phantom positioning.

References: 1. Alsop DC, Detre JA, Golay X, Guenther M, et al. MRM 2015; 73: 102-116. **2.** Steketee, et al. Eur. Radiol. 26, 244–253, 2016. **3.** Wang, et al. J. Pharmacol. Exp. Ther. 337, 359–366, 2011. **4.** Mutsaerts, et al. Neuroimage 113, 2015. **5.** Sullivan, et al. Radiology. 2015 Dec;277(3):813-25. **6.** Clement, et al. JCBFM, 2018 Sep;38(9):1418-1437. **7.** Oliver-Taylor A et al. Proc. ISMRM, 2017, Abstract #0681. **8.** Version 20181102 https://github.com/xiangruili/dicm2nii

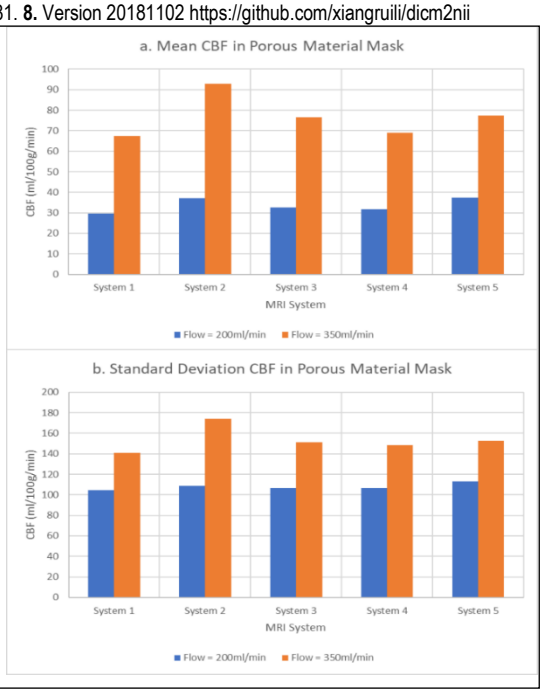

Figure 4: Mean CBF (a) and standard deviation of the CBF values (b) within the porous material masks. Trends in variation between the MRI systems visually correspond at flow rates, with variation at the higher flow rate more pronounced. In all cases, the mean CBF at 350ml/min is more than double what is measured at the 200ml/min, despite the flow rate ratio being 1.75. This is because at 200ml/min not all of the labelled bolus has reached the porous material at PLD=1800ms.

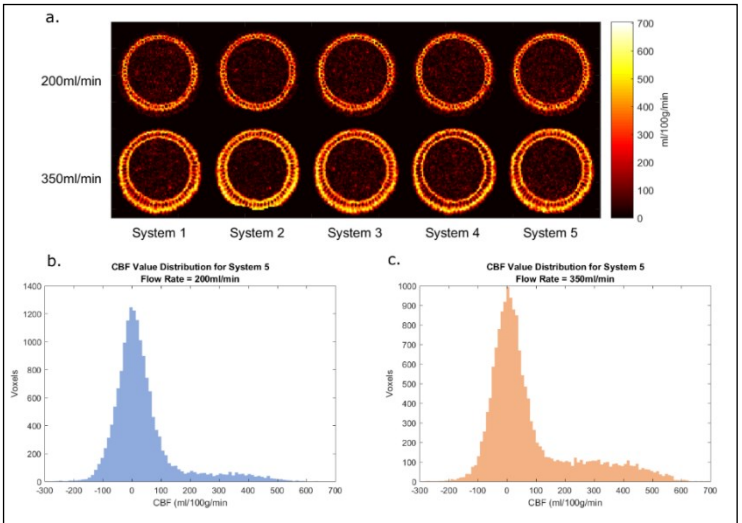

Figure 3: CBF maps of slice 5 at each flow rate in each data set from all systems (a). Histograms of the CBF value distributions within the mask at a flow rate of 200ml/min (b) and 350ml/min (c) for MRI System 5. There are two components: a Gaussian distribution centred around zero, due to noise in voxels where there is no perfusion signal; and a broader, nonzero centred Gaussian distribution of values from the perfusion signal.

Using deep learning to map cerebral blood flow from multiple post-label delay arterial spin-labeled images

Zahra Shirzadi[1,2,3], Daniel Djayakarsana[1], Nicholas J Luciw[1,2,3], Chinthaka C Heyn[3,4], Maged Goubran[2,3], Bradley J MacIntosh[1,2,3]

[1]Department of Medical Biophysics, University of Toronto; [2]Heart and Stroke Foundation Canadian Partnership for Stroke Recovery, Sunnybrook Research Institute, University of Toronto; [3]Hurvitz Brain Sciences, Sunnybrook Research Institute, University of Toronto; [4]Department of Medical Imaging, Sunnybrook Health Sciences Centre.

Introduction: Arterial spin labeling (ASL) is a powerful MRI technique with great clinical promise. There are, however, technical obstacles which have limited translation of ASL into clinical practice. Deep learning has tremendous potential for overcoming many of these such as outlier detection[1] and averaging[2] of ASL images, but there remain formidable challenges before this branch of artificial intelligence can have a clinical impact[3]. The purpose of this study is to establish the feasibility of using either a 3D or 2D convolutional neural network (CNN) to *predict* cerebral blood flow (CBF) maps from multiple *input* channels of difference images, each produced using a different post-label delay (PLD). Such a model would effectively *learn* features that reflect the ASL kinetic model and thereby produce CBF maps more rapidly and robustly which is critical in clinical applications.

Methods: Based on our previous work on multi-PLD ASL[4], we generated 98 in silico ASL datasets with 6 PLDs in which the ground-truth CBF images were generated a priori. For the 3D CNN model, data were split into training (n=66), validation (n=12) and test (n=20) datasets. Training data was augmented by flipping each image in the left/right direction. We implemented the CNN in Python 3.6 using the Keras and Talos libraries. As a proof of principle, this abstract focused on CBF maps only (ATT mapping results not shown). Optimal hyperparameters from the 3D CNN were used identically with the 2D CNN to facilitate model comparison. The CNN architecture included 4 convolutional layers using a 3x3(x3) kernel size producing 32 feature maps per layer, batch normalization, a leaky ReLU activation (alpha = 0.225), and a dropout layer (0.16). The final model layer consisted of a single feature map, which is the predicted CBF map from all the PLD images. Performance was evaluated using root mean square error (RMSE) and generalized Jaccard index.

Results: Figure 1A shows the test performance for the 2D and 3D CNN models. The 3D CNN outperformed the 2D model in both metrics. Figure 1B shows three predicted CBF maps with highest RMSE (poor cases) and Figure 1C shows the three predictions with lowest RMSE (best cases); in each pair of images, left is the ground-truth and right is the prediction. These figures highlight the high similarity between ground-truth and predicted CBF maps in our test datasets.

Discussion: We developed a CNN model to generate CBF maps from multi-PLD ASL difference images. Our model has two advantages: 1) CBF can be computed in less than one second (compared to minutes for kinetic model fitting), conducive to in-line processing on the scanner; and 2) a CNN model can be agnostic to the schedule of PLDs. Future developments will include multi-output predictions (i.e. CBF and ATT maps) and accommodate missing input ASL data.

References:

1. Kim KH, et al. Radiology. 2018 May;287(2):658-666.
2. Owen D, et al. Medical Image Computing and Computer Assisted Intervention – MICCAI 2018.
3. Zaharchuk G, et al. AJNR Am J Neuroradiol. 2018 Oct;39(10):1776-1784.
4. Buxton RB, et al. Magn Reson Med. 1998 Sep;40(3):383-96.
5. Shirzadi Z, et al. J Magn Reson Imaging. 2018 Mar;47(3):647-655.

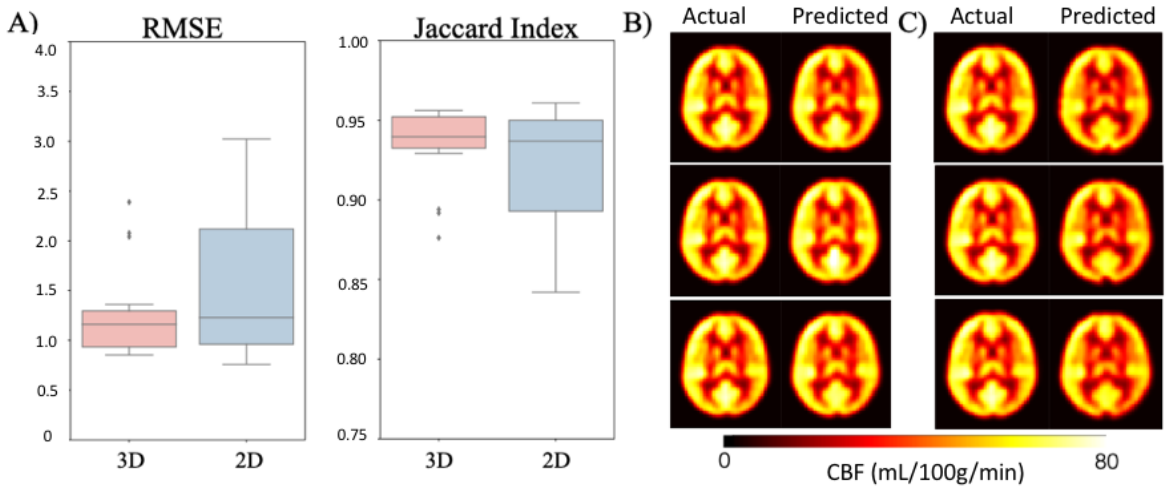

Figure 1: CNN model performance on test data computed using RMSE and Jaccard index (A). Comparison between ground-truth and predicted CBF images; B) three poor cases and C) three good cases. B and C obtained from 3D CNN.

Optimizing Arterial Spin Labeling MRI in Rat Spinal Cord Injury

Seongtaek Lee[1], Natasha Wilkins[2], Brian Schmit[1], Shekar Kurpad[2,3], Matthew Budde[2,3]
[1]Department of Biomedical Engineering, Marquette University & Medical College of Wisconsin, Milwaukee, WI, [2]Department of Neurosurgery, Medical College of Wisconsin, Milwaukee, WI, [3]Clement J. Zablocki Veterans Affairs Medical Center, Milwaukee, WI

Introduction: Reestablishing impaired blood flow to the injured spinal cord is a crucial target for acute clinical care. However, perfusion MRI methods for noninvasive monitoring of spinal cord blood flow are lacking despite their prominence for the brain. In part, the challenges of spinal cord MRI have complicated perfusion MRI in this organ [1-4]. The purpose of this study was to evaluate flow-sensitive alternating inversion recovery (FAIR) for quantifying spinal cord blood flow (SCBF) and its potential as a marker of injury severity.

Methods: Spinal cord contusion injury was induced at the T10 thoracic vertebral level in 38 female Sprague-Dawley rats: sham (n=8), mild (n=10), moderate (n=10), or severe (n=10), and imaging was carried out at 24 hrs post injury on a Bruker 9.4T MRI system. FAIR-images were acquired using a 4-shot EPI readout (TE=18 ms; Constant recovery=3000 ms; Slice thickness=2 mm; In-plane resolution=165 μm^2) with 10 inversion times (TI=50 ms to 7500 ms). A single-slice FAIR with axial inversion slab was used as the reference standard compared to prior studies [5,6], and multi-slice axial or coronal (orthogonal) inversions were also examined similar to OPTIMAL FAIR (Fig. 1) [7]. T_1 maps were generated for the selective (T_{1ss}) and non-selective inversions (T_{1ns}) and SCBF maps (mL/100 g/min) were obtained using the equation ($1/T_{1ss} = 1/T_{1ns} + f/\lambda$). The relationship between MRI metrics and behavioral assessments for locomotion (Basso, Beattie and Bresnahan score; BBB) were investigated using Person's correlations [8].

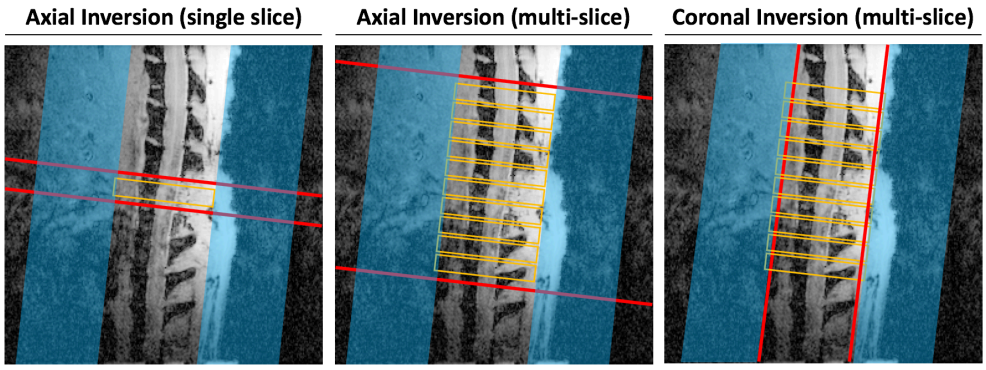

Figure 1. Axial and coronal inversion schemes on T_1 FLASH scans. For multi-slice FAIR images, the injury epicenter is located at 5th slice in this example (Red: Inversion planes; Yellow: Imaging slices; Blue: FOV saturation planes).

Results: With increasing severity of the injury, SCBF values were lower at the injury epicenter in both axial and coronal inversion schemes while T_{1ss} and T_{1ns} values increased (Fig. 2). Multi-slice results presented relatively lower SCBF regardless of inversion orientation and greater SCBF variability. While no significant correlation between SCBF and BBB score were observed, a strong positive correlation was shown between T_1 and BBB scores at 30 days after injury (R^2=0.66; p<0.0001).

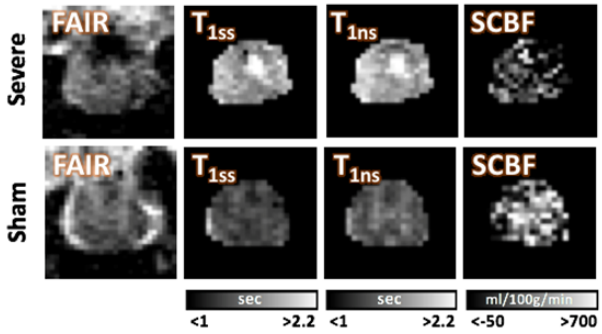

Figure 2. Single-slice axial inversion FAIR images (TI=250ms) at the injury site, as well as T_{1ss}, T_{1ns}, and SCBF maps of a severe and sham.

Conclusion: This study accessed the feasibility of spinal cord FAIR as a MR biomarker of spinal cord injury, showing that SCBF at the injury epicenter decreased with increasing injury severity. Likewise, single-slice axial FAIR has the largest SCBF and reliability. Interestingly, both T_{1ss} and T_{1ns} values at the acute stage of injury were strong predictors of outcome. The limitation of FAIR spinal cord imaging is the variability in SCBF estimation, partly due to motion artifacts since the acquisition was not respiratory gated, and the single-slice limitation. Other ASL techniques, including pseudo-continuous and velocity-selective tagging, are currently in development for the animal MRI system, compared to SCBF with single-slice imaging.

Acknowledgements: This work was supported in part by Merit Review Award I01 RX001497 from the US Department of Veterans Affairs Rehabilitation Research and Development Service and by the National Institutes of Neurological Disorders and Stroke R01 NS109090.

References: [1] Stroman PW et al., Neuroimage. 2014 Jan 1;84:1070-81. [2] Melissano G et al., J Cardiovasc Surg (Torino). 2015 Oct;56(5):699-706. [3] Amato ACM et al., J Vasc Bras. 2015 July-Sept.; 14(3):248-252. [4] Gillilan LA. J Comp Neurol. 1958 Aug;110(1):75-103. [5] Duhamel G et al., Magn Reson Med. 2009 Aug;62(2):430-9. [6] Duhamel G et al., Magn Reson Med. 2008 Apr;59(4):846-54. [7] Li X et al., NMR Biomed. 2013 Jun;26(6):613-21. [8] Basso DM et al., J Neurotrauma. 1995 Feb;12(1):1-21.

Cerebral perfusion covariance mapping to study differences between adolescents with and without bipolar disorder

Nicholas J. Luciw[a], Simina Toma[b,c], Benjamin I. Goldstein[b,c,d], Bradley J. MacIntosh[a,e,f]

[a]Department of Medical Biophysics, University of Toronto, Toronto, Canada, [b]Centre for Youth Bipolar Disorder, Sunnybrook Health Sciences Centre, Toronto, Canada, [c]Department of Psychiatry, University of Toronto, Toronto, Canada, [d]Department of Pharmacology, University of Toronto, Toronto, Canada, [e]Heart and Stroke Foundation Canadian Partnership for Stroke Recovery, Sunnybrook Research Institute, Toronto, Canada, [f]Physical Sciences, Sunnybrook Research Institute, Toronto, Canada

Introduction: Covariance mapping is one form of neuroimaging connectivity analysis. This approach exploits subject-to-subject differences, most commonly applied in anatomical MRI. Although much work has been done to characterize regional perfusion in clinical and healthy populations, use of perfusion covariance is limited. Cerebral perfusion is closely linked to both neuronal activity and metabolism, and can be quantitatively measured using arterial spin labelling (ASL) MRI. This study uses ASL to evaluate network-like perfusion patterns of inter-subject covariation. We compare these patterns between healthy controls and a cohort of adolescents with bipolar disorder (BD: a severe psychiatric condition associated with anomalous cerebral structure and perfusion). We assess seed-to-voxel perfusion covariance (as well as "paired" anatomical covariance) based on three regions of interest known to be affected in BD.

Methods: On a 3T MRI system using an 8-channel-receiver head coil, we collected perfusion images with pseudo-continuous arterial spin labeling in 72 adolescents with BD and 57 healthy controls. Anatomical T1-weighted (T1w) imaging was performed with a high-resolution fast field echo acquisition (TR/TE=9.5/2.3 ms, spatial resolution 0.9×0.7×1.2 mm, FOV 240×191×168 mm, scan duration 8 min 56 s). ASL MRI was performed with a single-shot two-dimensional echo planar imaging acquisition (TR/TE=4000/9.6 ms, spatial resolution 3×3×5 mm, FOV 192×192×90 mm), 1650 ms labeling duration, 1600 ms post-label delay, 35 control-label pairs, and a scan duration of 4 min 48 s. We used in-house preprocessing pipeline for motion correction, calculation of perfusion-weighted volumes, removal of corrupted volumes, and absolute perfusion quantification [1]. T1w images were aligned to a custom adolescent anatomical template with non-linear registration. Perfusion images were linearly registered to the subject-space T1w images and non-linearly warped to the template. To reduce the number of distinct perfusion brain regions, we used a parcellation technique that combined individual voxels through a hierarchical clustering. Then, with both perfusion and grey matter parcellated images, the following steps were taken for each of the three seeds: covariance maps were computed by calculating the seed-to-voxel correlation coefficient between the seed and every other region. BD and control covariance maps were generated separately. Correlation coefficients were transformed using Fisher's *r*-to-*z* transform. Significance of the *Z*-statistic for the difference between BD and controls was assessed using FDR correction and α=0.05. We evaluated the association between perfusion and structure by computing the correlation coefficient between whole-brain region-to-region covariance matrices.

Results: Relative to controls, the BD group exhibited both increased and decreased perfusion covariance with the subgenual ACC seed. The BD group also exhibited increased structural covariance with both the ACC and amygdala seeds. Figure shows regions where covariance was significantly different between BD and control groups. There were significantly ($p <$ 0.0001) stronger associations between structural and perfusion covariance in BD (r = 0.17) compared to controls (r = 0.13).

Discussion: ASL-based perfusion covariance can probe underlying physiology-based connectivity, akin to BOLD-based amplitude of low-frequency fluctuation and single-photon emission computed tomography studies [2,3]. A growing number of ASL studies now investigate perfusion covariance to capitalize on the potential between-group static neurovascular differences [4,5]. Relative to controls, perfusion in BD was found to covary more strongly between the subgenual ACC and temporal regions; the former is known to play a role in emotional regulation during depression and the latter in emotional processing. We also found a stronger structural covariation between the amygdala and the cuneus in the BD group; grey matter of both regions has been shown to differ in a comparison of BD subtypes characterized by level of episodic mood elevation. Future work will investigate differences across BD subtypes and symptomatic states. Overall, the regions implicated by this covariance method suggest a mood-related axis along which perfusion and structure are more tightly coupled between regions.

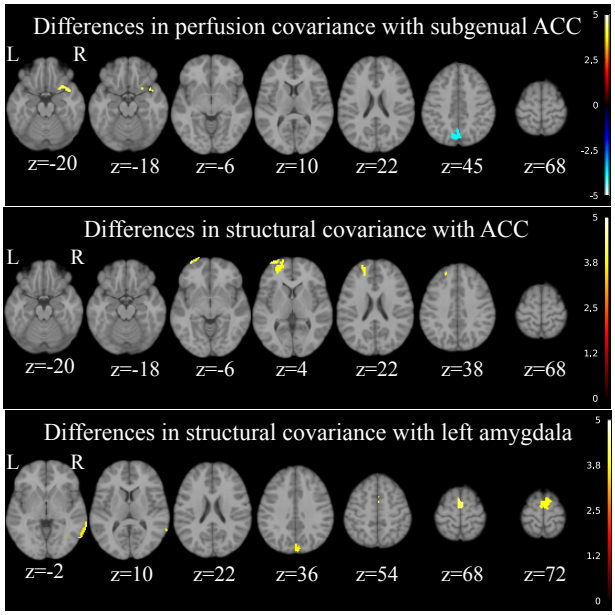

Figure: Significant regional *Z*-statistics for seed-to-voxel covariance difference between BD and controls. Warmer colours indicate greater covariance in BD, cooler colours indicate greater in controls.

References:

1. Shirzadi Z. et al. Enhancement of automated blood flow estimates (ENABLE) from arterial spin-labeled MRI: Enhanced Automated Blood Flow Estimates J. Magn. Reson. Imaging, 47(3):647-655, 2018.
2. Taylor P.A. et al. Functional Covariance Networks: Obtaining Resting-State Networks From Inter-Subject Variability. Brain Connectivity, 2(4):203-217, 2012.
3. Melie-García L. et al. Studying the topological organization of the cerebral blood flow fluctuations in resting state. NeuroImage, 64:173-184, 2013.
4. Zhu J. et al. Altered resting-state cerebral blood flow and its connectivity in schizophrenia. Journal of Psychiatric Research, 63:28-35, 2015.
5. Liu F. et al. Altered cerebral blood flow covariance network in schizophrenia. Frontiers in Neuroscience, 10:308, 2016.

Title: Fast substitution of ASL techniques by modularity of the dynamic platform-independent framework *gamma-star* (γ*)

Authors: Simon Konstandin[1], Cristoffer Cordes[1], and Matthias Günther[1,2]
[1]*MR Physics, Fraunhofer MEVIS, Bremen, Germany*
[2]*MR-Imaging and Spectroscopy, Faculty 01 (Physics/Electrical Engineering), University of Bremen, Bremen, Germany*

Introduction

MR sequence development is typically performed with vendor-specific software, which require calculations and preparations of different hardware events to be in a specific order to take account of the parameter dependencies. Self-written MR sequences cannot be ported easily to other scanner platforms (even to other software versions) and thus are difficult to be utilized for multi-center studies. Different solutions have been presented [1-5], however, protocols cannot be dynamically changed during measurements and/or further compilation steps are necessary. We are currently developing a platform-independent rapid prototyping environment for MR sequences to overcome this limitation [6-9]. A demo-tool [8] of our framework was presented that allows for quick preparation and visualization of protocols, which can be exported as the pulseq-sequence file format [4].
This abstract shows how sequence programming works by using the modularity of this framework concept. A pseudo-continuous arterial spin labeling (pCASL) sequence is created from a conventional pulsed ASL (PASL) sequence by adding/removing one submodule without worrying about other parameters such as time dependencies.

Methods

The sequence structures of the PASL and pCASL sequences are shown in Figure 1. The 3D-GRASE [10,11] readout is further composed of different submodules (fat saturation, spin echo, EPI readout, etc.), but will not be discussed here. The different modules need input data to be prepared (e.g. the saturation module requires start time, slice and gradient properties, number of rf pulses), but also provide some information/output (time interval after the last saturation pulse, which is necessary for the preparation of the background suppression).

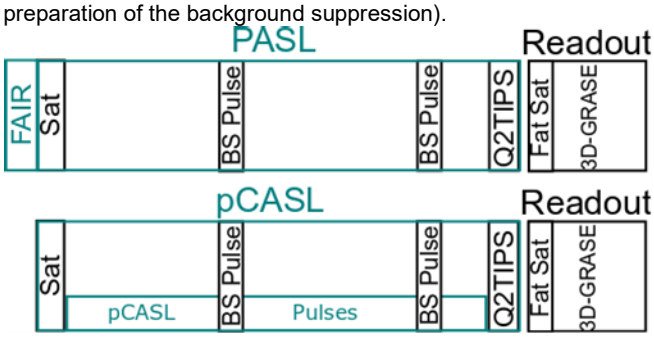

Figure 1: Sequence structure of a conventional PASL and pCASL sequence. The ASL preparation modules consist of further submodules, which can be easily exchanged. By adding the pCASL pulses and removing the FAIR module, a pCASL sequence can be quickly generated from a PASL sequence without changing other parameters.

PASL: The PASL preparation module consists of different submodules. After inversion with a FOCI [12] pulse (*FAIR*), the readout volume is saturated using three saturation pulses with subsequent spoilers. Two background suppression FOCI pulses are applied during the inversion time TI = 1.7 s to suppress signal coming from tissue with T1 = 700 ms and 1400 ms (*BS*). Q2TIPS pulses are applied for bolus saturation (*Q2TIPS*) before the readout.
pCASL: The pCASL preparation can be created from the *PASL* module by removing *FAIR* and adding the *pCASL Pulses* module.
Parameters of the 3D-GRASE readout are set as follows: TR = 4 s, TE = 50 ms, flip angles = 90° and 120° for spin echo pulses, readout bandwidth = 2000 Hz/px, field-of-view = 256×256×64 mm^3, matrix size = 64×64×16, EPI factor = 64, turbo factor = 8, which results in 2 segments for one image. Human brain measurements were performed on a whole-body MR scanner at 3 Tesla (MAGNETOM Skyra, Siemens Healthineers, Erlangen, Germany) with a 16-channels head coil.

Results & Discussion

Two exemplary slices of the PASL sequence are shown in Figure 2 acquired with one prescan and four averages resulting in a total measurement time of 68 seconds. The sequence preparation time was about 10 seconds. Future work will focus on accelerating the preparation and to implement further modules into *gamma-star* (γ*) so that the MR community can make use of it.

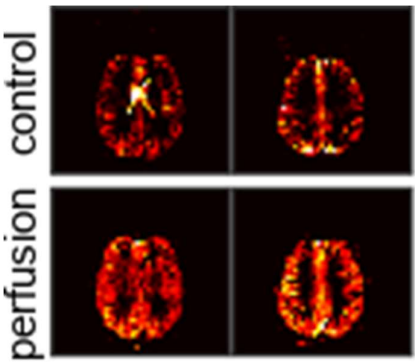

Figure 2: PASL measurement of the human brain with two exemplary control (upper row) and perfusion-weighted (lower row) images.

Acknowledgements

All funding for this study was provided by the internal *Attract* (600172) funding program of the German Fraunhofer-Gesellschaft.

References

1. Jochimsen TH & von Mengershausen M. J Magn Reson 2004;170(1):67-78.
2. Stöcker T, Vahedipour K, Pflugfelder D, Shah NJ. Magn Reson Med 2010;64(1):186-93.
3. Magland JF, Li C, Langham MC, Wehrli FW. Magn Reson Med 2016;75(1):257-65.
4. Layton KJ, Kroboth S, Jia F, Littin S, Yu H, Leupold J, Nielsen JF, Stöcker T, Zaitsev M. Magn Reson Med 2017;77(4):1544-52.
5. Nielsen JF & Noll DC. Magn Reson Med 2018;79(6):3128-34.
6. Cordes C, Honroth T, Hoinkiss D, Archipovas S, Porter DA, Günther M. Proc Intl Soc Mag Reson Med 2016;3198.
7. Cordes C, Konstandin S, Porter D, Günther M. Magn Reson Med (under review).
8. https://gamma-star.mevis.fraunhofer.de
9. Archipovas S, Honroth T, Cordes C, Günther M, Porter DA. Proc Intl Soc Mag Reson Med 2017;1510.
10. Oshio K, Feinberg DA. Magn Reson Med 1991;20(2):344-9.
11. Günther M, Oshio K, Feinberg DA. Magn Reson Med 2005;54(2):491-8.
12. Ordidge RJ, Wylezinska M, Hugg JW, Butterworth E, Franconi F. Magn Reson Med 1996;36(4):562-6.

Physiological underpinnings of variations in CBF measured by pCASL MRI

Dengrong Jiang[1], Yang Li[1], Zixuan Lin[1], Sandeepa Sur[1], Peiying Liu[1], Cuimei Xu[1], Kaisha Hazel[1], George Pottanat[1], Sevil Yasar[2], Paul Rosenberg[3], Marilyn Albert[4] and Hanzhang Lu[1]

[1]Department of Radiology, Johns Hopkins School of Medicine, Baltimore, MD, [2]Department of Medicine, Johns Hopkins School of Medicine, Baltimore, MD, [3]Department of Psychiatry and Behavioral Sciences, Johns Hopkins University School of Medicine, Baltimore, MD, [4]Department of Neurology, Johns Hopkins University School of Medicine, Baltimore, MD

INTRODUCTION: Cerebral blood flow (CBF) refers to the amount of blood supply to brain tissue and has been suggested to be a potential biomarker in various diseases such as Alzheimer's disease[1] and stroke.[2] With the emerging of arterial-spin-labeling (ASL) MRI, routine non-invasive measurement of CBF has been made feasible.[3] However, one remaining issue with the CBF measurement is the considerable inter-subject variations even in the healthy population, which have been reported to be 16-20%.[4] These variations may obscure the interpretation of CBF data and weaken the power of CBF as a biomarker. Therefore, it is essential to investigate the physiological sources underlying the inter-subject variations in CBF. In this work, we examined the extent to which end-tidal CO_2 ($EtCO_2$) can explain the inter-subject variations in CBF. In addition, we also studied the potential effects of other physiological parameters, including age, gender, hematocrit (Hct), arterial oxygenation (Y_a) and heart rate (HR), on CBF.

METHODS: *Participants:* Fifty-seven elderly subjects were recruited, of which 21 were cognitively normal, 32 had mild cognitive impairment (MCI) and 4 were mild dementia patients. The demographic characteristics of the subjects are shown in Table 1.

MRI experiments: All subjects were scanned on a Philips Achieva 3T scanner. The MRI protocol consisted of a magnetization-prepared rapid acquisition of gradient echo (MPRAGE) sequence, a 3D ASL sequence with pseudo-continuous labeling (pCASL) and background suppression, and a separate proton density (M_0) sequence. Scan parameters of MPRAGE were: voxel size=1×1×1mm^3, 160 sagittal slices, TR/TE/TI=8.1/3.7/1100ms, flip angle=12°, shot interval=2100ms, duration=4min. Sequence parameters of ASL included: field of view (FOV)=205×205×125mm^3, 39 axial slices, voxel size=3.2×3.2×3.2mm^3, TR/TE=6185/9.3ms, labeling duration=1800ms, post labeling delay=2200ms, scan duration=3.3min. The M_0 sequence used the same parameters except TR=10s and scan duration=50s. During the ASL scan, $EtCO_2$ was measured via a nasal cannula connected to a capnograph device. Y_a and HR were measured twice before the MRI scan and twice after the MRI scan. Hematocrit was measured through a blood draw.

Data processing: The ASL data were processed using a cloud-based tool, ASL-MRICloud.[5] Briefly, after motion correction, pairwise subtraction between the control and labeled images was conducted. The resulting difference images and the M_0 images were used to quantify the voxel-wise CBF values based on the model provided in the ASL white paper.[3] Whole brain CBF was calculated as the mean absolute CBF values inside a brain mask, which was obtained from the MPRAGE images using a T_1-based multi-atlas brain segmentation tool in the MRICloud platform.[6] The brain mask included white and gray matters as well as ventricles.

Statistical analysis: We firstly performed stepwise regression analyses on the whole group (N=57) in which whole brain CBF was the dependent variable and the candidate independent variables were Hct, $EtCO_2$, gender, Y_a and HR. Age was always included in the model. The independent variables were added to the model in a stepwise manner, starting from the most significant one until no more variables reached a $P<0.05$. Then, to examine if the obtained regression model reflected normal physiological or pathological effects on CBF variations, we repeated the same stepwise regression analysis on the subgroup of cognitively normal subjects (N=21).

RESULTS: The mean Hct, $EtCO_2$, Y_a and HR of the subjects are shown in Table 1, no significant difference was found among subgroups. We divided the subjects by quartiles of $EtCO_2$, and computed the mean absolute CBF maps of the subjects in each quartile. As shown in. Figure 1, subjects with higher $EtCO_2$ had overall higher CBF. Table 2 lists the results of stepwise regression on the whole group. Whole brain CBF is positively associated with $EtCO_2$ ($P=0.001$) and negatively associated with Hct ($P=4\times10^{-8}$). Age, Hct and $EtCO_2$ together can explain 47% of the inter-subject variations in CBF. Gender, Y_a and HR were unable to enter the stepwise model ($P>0.8$). Table 3 shows the stepwise regression analysis on the subgroup of cognitively normal subjects, resulting in the same model. Age, $EtCO_2$ and Hct together account for 44% of variations in CBF in cognitively normal subjects.

CONCLUSION: This study demonstrated that, across subjects, whole brain CBF measured by ASL is positively associated with $EtCO_2$. The dependence of CBF on $EtCO_2$ was significant whether evaluated on the whole group or on the cognitively normal subgroup. In addition, ASL CBF is also inversely associated with Hct, which may be through its effect on blood T_1 or a compensatory effect to maintain sufficient oxygen delivery.[7,8] Our results suggest that obtaining Hct and $EtCO_2$ information from the subjects can reduce the variance in CBF data by more than 40%, which is expected to significantly enhance the utility of CBF in scientific or clinical applications.

Table 1: Demographic information of the participants

	Total	Normal	MCI	Dementia
N	57	21	32	4
Age (years)	68.8±6.7	69.0±5.5	68.4±7.4	70.3±8.1
Gender	27M, 30F	6M, 15F	18M, 14F	3M, 1F
Hct (%)	41.3±3.3	41.2±2.9	41.4±3.7	40.3±3.6
$EtCO_2$ (mmHg)	37.2±4.5	36.2±5.1	37.5±4.2	39.4±4.0
Y_a (%)	96.5±1.5	96.9±1.1	96.3±1.6	96.3±1.9
HR (b.p.m.)	70.7±11.5	71.2±9.9	69.8±11.9	74.8±17.4

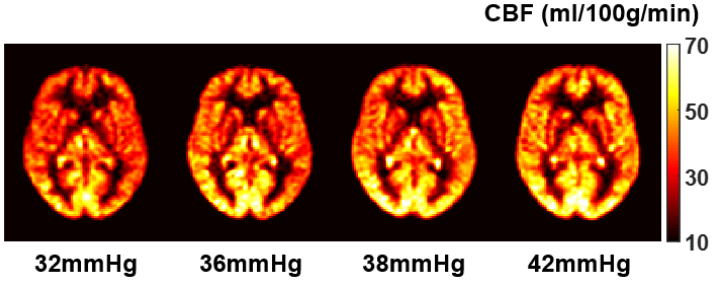

Figure 1. Mean absolute CBF maps (in MNI space) of subjects by quartiles of $EtCO_2$, along with mean $EtCO_2$ in each quartile.

Table 2: Stepwise linear regression on the whole group (N=57), $R^2=0.47$

Variables	β±SE	*P*-value
Age	-0.08±0.14	0.57
Hct	-1.81±0.28	4×10^{-8}
$EtCO_2$	0.69±0.20	0.001

Table 3: Stepwise linear regression on normal subjects (N=21), $R^2=0.44$

Variables	β±SE	*P*-value
Age	-0.15±0.28	0.61
Hct	-1.33±0.55	0.027
$EtCO_2$	0.91±0.30	0.007

REFERENCES: [1] Alsop et al. JAD 2010, 20:871–880. [2] Wang et al. Stroke 2012, 43:1018–1024. [3] Alsop et al. MRM 2015, 73:102–116. [4] Henriksen et al. JMRI 2012, 35:1290–1299. [5] Li et al. NMR Biomed 2019. [6] Mori et al. Comput Sci Eng. 2016, 18:21–35. [7] Xu et al. HBM 2018, 39:344–353 [8] Henriksen et al. JCBFM 2013, 33:787–792

Title: Automated subject-specific adaption of pCASL timing parameters in real time

Authors: Nora-Josefin Breutigam[1], Mareike Alicja Buck[1], Daniel Christopher Hoinkiss[1], Federico von Samson-Himmelstjerna[1], Matthias Günther[1,2]

[1]MR Physics, Fraunhofer MEVIS, Bremen, Germany, [2]MR-Imaging and Spectroscopy, Faculty 01 (Physics/Electrical Engineering), University of Bremen, Bremen, Germany

Introduction:

One of the major challenges of clinical Arterial Spin Labeling (ASL) is the high variability of arterial transit-times (ATT) causing the associated arterial transit-delay (ATD) artefacts [1]. This is especially relevant in patients with pathological changes like ischemic stroke or Moya-Moya. These artefacts occur when post-labeling delays (PLD) and bolus durations (BD) are not optimally adapted to the examined individual. This also affects the free-lunch (FL) approach [2] in Hadamard pseudo-continuous ASL (H-pCASL), where the first Hadamard-subbolus is used like a long conventional pCASL-bolus and the remaining subboli for time-encoding. Using Walsh-sorted time-encoded pCASL (WH-pCASL) with a dynamic feedback algorithm [3], it is possible to employ intermediate perfusion-weighted images (PWIs) for adjusting subbolus durations (SBD) during the measurement. The aim is to keep the free-lunch (FL) bolus long enough to maximize signal, but short enough to avoid ATD artefacts. To this end, the timepoint at which all tissue-voxels are filled with labelled blood is identified. The mentioned methodology was previously described in abstract form using offline calculations [3]. This abstract shows, for the first time, results of a complete integration of the technique into the WH-pCASL sequence utilizing a feedback cycle between image reconstruction and MRI sequence during the scan.

Methods:

Encoding:

An 8x8 Walsh-ordered Hadamard matrix is used which is mirrored left to right. Furthermore, the acquisition of the second row is repeated once after interchanging its label and control phases. This results in a 9x8 encoding matrix which enables the acquisition of two intermediate PWI after the first three acquisitions. A third intermediate PWI is calculated with the fourth acquisition.

Imaging:

Three healthy volunteers (27-52 years, 1 female) were scanned at 3T (MAGNETOM Skyra, SIEMENS Healthcare GmbH) with a 16-channel head coil. For background-suppression two FOCI pulses (2*T1) were used. The following parameters were used for the 3D-GRASE readout [4]: TR = 5 s, TE = 29.48 ms, readout bandwidth = 2298 Hz/px, field of view = 228x171x120 mm^3, matrix size = 64x48x24 (interpolated to 128x96x24), EPI factor = 48, turbo factor = 24, flip angle (refocusing pulses) = 120°; this resulted in a total measurement time of 0:45 min. The initial SBDs were: 650, 650, 650, 650, 300, 300, 300 [ms] resulting in an initial FL-Bolus of 2600 ms. The initial PLD was 100 ms.

Results & Discussion:

For all volunteers the initial FL-PLD was too short resulting in low signal in the FL-bolus and not optimal sampling of inflow times in measurement without dynamic adaption of the subolus durations (fig 1, bottom row). Consequently, the feedback algorithm reduced the duration of the FL-bolus stepwise (**final FL-bolus**, six subboli: **1757**, 300, 272, 271, 300, 300, 300 [ms]; **1743**, 300, 279, 278, 300, 300, 300 [ms]; **1831**, 300, 235, 234, 300, 300, 300 [ms]). The timing after adaptation resembles the proposed FL set-up for healthy volunteers (FL-bolus: 1800 ms, SBD 2 = 500 ms, SBD 3-7 = 240 ms, PLD = 100 ms) [2]. Finally, the eight resulting images were used to decode the corresponding seven subboli. Thus, the implemented online feedback successfully adapted the SBDs to an appropriate timing with high signal in the final FL-bolus and without visible ATD artefacts (fig. 1, upper row) during the measurement without increasing the scan time. Moreover, the calculation of new subbolus durations provides further optimization possibilities. For instance, analysis of image histograms could be used to identify arterial artefacts.

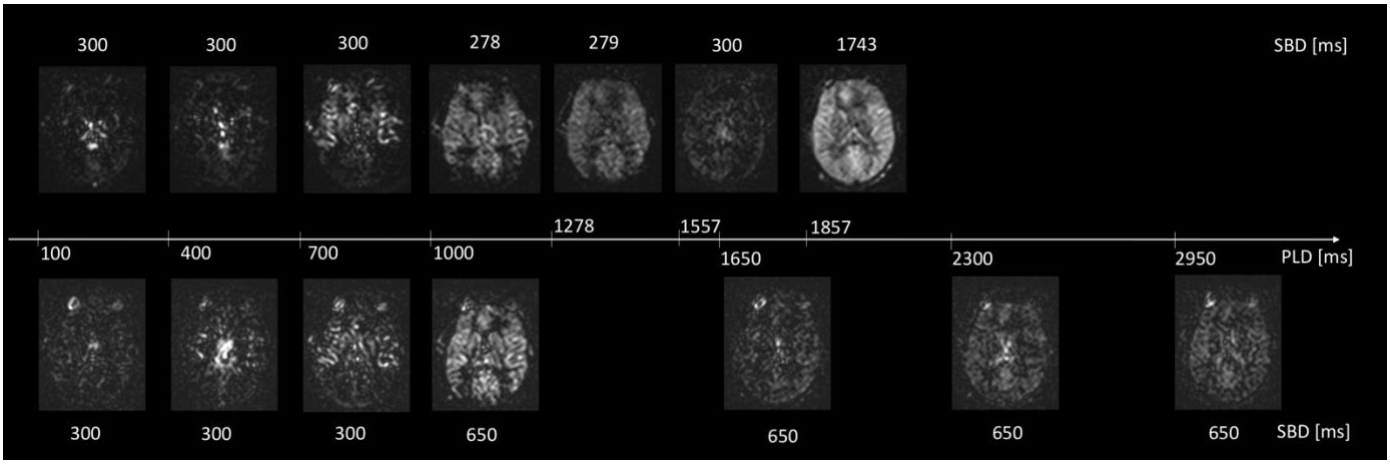

Figure 1: Comparison between not optimal timing (lower row) and the adapted optimized timing for one volunteer (upper row) with corresponding effective post labeling delays and subbolus durations. The short FL-bolus (650 ms) in combination with a long FL-PLD (2950 ms) results in major signal loss. The adapted timing shows high signal without ATD artefacts in the final FL-bolus.

References:

[1] Zaharchuk G. Transl. Stroke Res. 2012; 3:228–235. doi: 10.1007/s12975-012-0159-8.
[2] Teeuwisse et al. Magn. Reson. Med. 2014. doi: 10.1002/mrm.25083.
[3] Breutigam et al. Proceedings of the 24th Annual Meeting ISMRM 2016.
[4] Günther et al. Magn. Reson. Med. 2005; 54:491-498. doi: 10.1002/mrm.20580

Predicting obesity history from cross-sectional cerebral blood flow with machine learning: Arterial Spin Labeling data from the CARDIA study

Zahra Shirzadi[1,2,3], Maged Goubran[2,3], Lenore J Launer[4], R Nick Bryan[5], John Detre[6,7,8], Walter Swardfager[2,3,9] and Bradley J MacIntosh[1,2,3]

[1]Department of Medical Biophysics, University of Toronto; [2]Heart and Stroke Foundation, Canadian Partnership for Stroke Recovery, Sunnybrook Research Institute, University of Toronto; [3]Hurvitz Brain Sciences, Sunnybrook Research Institute, University of Toronto; [4]Laboratory of Epidemiology and Population Science, National Institute on Aging, Maryland; [5]Department of Diagnostic Medicine, University of Texas; [6]Department of Radiology, [7]Department of Neurology, [8]Center for Functional Neuroimaging, University of Pennsylvania; [9]Department of Pharmacology and Toxicology, University of Toronto

Introduction: Obesity prevalence tends to increase with age and contributes to cardiovascular and brain diseases. Obesity affects blood vessels in multiple organs of the body, but less is known about the brain. Here we report a *data-driven machine learning* analysis to explore relationships between a cerebral blood flow (CBF) image and obesity assessments over 25 years.

Methods: Data obtained from a multi-site bi-racial cohort participating in the community-based longitudinal Coronary Artery Risk Development in Young Adults (CARDIA) study. There were 378 participants with one MRI scan and 6 assessments of body mass index (BMI) and waist circumference (WC), that latter spanning 25 years. The 3T brain MRI at year 25 included T1-weighted (for brain region segmentation), and pseudo-continuous ASL with 2D echo planar imaging. CBF values were extracted for 96 brain regions. We used a convolutional neural network (CNN) to evaluate the association of a multivariate and highly collinear input (i.e., regional CBF) to longitudinal trajectories of BMI and WC. The CNN model was trained to effectively '*down-sample*' a matrix of regional CBF to predict the longitudinal BMI and WC estimates (Figure 1). After adjusting for age, sex, intracranial volume, years of education and study site, an 8 by 12 matrix of 96 CBF regions trained a CNN model to predict BMI and WC history (6x2; output was L2 normalized prior to CNN). 20% (n=76) of the sample was used for testing (i.e. "unseen" to the CNN model), 24% for model validation, and 56% for training. We used mean squared error for optimization. A range of models were tested to optimize CNN hyperparameters, i.e., filter sizes, learning rates, decay, dropout and optimization parameters.

Results: We identified a CNN model that produced the lowest mean squared error (i.e., normalized fractional difference between predicted and actual BMI and WC); 0.007 and 0.008 for validation and test data, respectively. We observed the model best prediction for BMI and WC corresponded to obesity data that was 10 and 15 years prior to the CBF scan.

Figures 2A and 2C show the predicted versus actual normalized BMI and WC, respectively (color denotes different visits). Figures 2B and 2D show the differences are centered around zero and variance is lowest for years 10 and 15.

Discussion: These results suggest there are linkages between obesity history and midlife CBF, identified using a data-driven CNN. Future research will focus on identifying brain regions that are most pertinent to obesity.

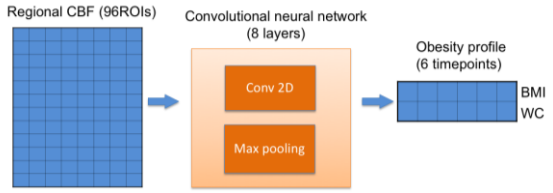

Figure 1: Study design to estimate obesity history from the ASL CBF

(BMI: body mass index, WC: waist circumference)

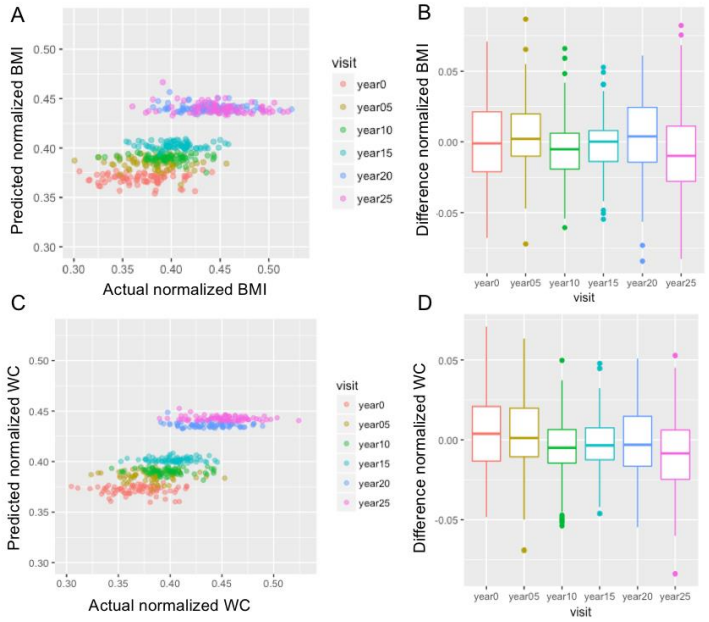

Figure 2: Results from *unseen* data by the CNN model. Predicted vs. actual values are shown for different visits (i.e. assessment year). Difference is defined as predicted minus actual.

(BMI: body mass index, WC: waist circumference)

Estimation of time-dependent labeling efficiency in Arterial Spin Labeling within 20 seconds

Matthias Günther[1,2,3]

[1]Fraunhofer MEVIS, Bremen, Germany, [2]University of Bremen, Germany, [3]mediri GmbH, Heidelberg, Germany

Introduction: In arterial spin labeling (ASL), the amount of blood magnetization getting tagged is of high relevance. While in pulsed ASL (PASL) this labeling efficiency is very close to 100%, the most often used continuous ASL variant, called pseudo-continuous ASL (pCASL) suffers from a somewhat lower labeling efficiency, which typically reaches 80% for in-vivo applications. Several techniques exist to measure labeling efficiency and use this value to normalize perfusion measurements. A technique often used was presented by Aslan et al. [1], where the amount of blood flowing into the brain is measured by direct flow measurements in feeding vessels and this amount is compared to the arterial spin labeled magnetization shown in the perfusion-weighted scans. A more recent approach employs a Look-Locker sequence shortly following a pCASL labeling block [2]. With this approach, the amount of labeled blood entering the imaging volume was imaged. However, the Look-Locker readout misses the early part of the labeled blood bolus and destroys the complete label during readout. Recently, a technique was presented [3], which allows data acquisition simultaneously with the labeling process (arterial spin labeled input function ASL-IF). This enables the acquisition of the input function of labeled blood, however, normalization to yield labeling efficiency was not included.

Here, we present a method to normalize the ASL-IF measurement, allowing to measure “realtime” labeling efficiency with a temporal resolution as high as 1.42ms.

Methods: ASL-IF extends the conventional pCASL labeling pulse train (‘ASL rf pulse’) by an additional RF excitation pulse (‘AIF rf pulse’) and a signal readout. Additional gradient switching might be necessary to provide extra spatial encoding. In pCASL, a non-zero mean gradient is applied along the flow direction (usually the z-direction) to enable flow-induced adiabatic inversion [REF]. This nonzero mean gradient leads to z-dependent phase accrual of transverse magnetization between two succeeding rf pulses. This is compensated for by considering this phase accrual in the phase of the incident rf pulses. In ASL-IF, the AIF rf pulse is applied at a location, where this phase accrual is exactly 90° larger than at the location of the ASL rf pulse. By this, the AIF signal will acquire exactly 180° phase over two rf periods, while the ASL pulse will always have 0° phase over two rf periods (this is the case for both, labeling and control state). By subtracting a time series from the same series shifted by two rf periods, only the AIF signal remains (adding the two will yield the ASL signal only). The resulting AIF pulse signal is the sum of blood and tissue magnetization. Subtracting data from label and control state of the ASL rf pulse cancels out the tissue signal and allows measurement of the labeled magnetization only, which travelled from the labeling slice to the AIF slice. However, this data is not normalized. For this, equilibrium magnetization of blood M0b is needed.

Normalization: M0b is estimated by an additional measurement upfront, where no ASL rf pulses are played but AIF pulses only. In addition to this, a FAIR-like preparation is performed, which consists of two separate acquisitions: one with a global inversion pulse and one without this pulse. The region of the AIF rf pulse is saturated right before application of the global inversion pulse. This produces tagged magnetization with a labeling efficiency of close to 100%. The inflow of this magnetization is acquired and used to estimate M0b in two different ways. If the labeled bolus is long enough to show T1 decay, an exponential fit is applied to yield T1 of blood along with M0b. If the bolus is too short for fitting, the maximum value is taken and corrected for T1 decay (assuming T1b=1650ms).

ASL-IF imaging parameters: variant uses the x-axis for frequency encoding. Due to additional rephrasing gradients the minimum TR was 1.42ms. No extra spatial encoding was needed. Spatial resolution was 9mm and temporal resolution of 1.42ms. A 4-cycle Hadamard encoding scheme was used for labeling.

Results & Discussion: Fig.1 shows the resulting labeling efficiency over time of a healthy human subject for three Hadamard-encoded labeling patterns (the pure control pattern was subtracted). A single measurement is shown (no averaging).

Conclusion: ASL-IF allows for measurement of the labeling efficiency during pCASL preparation. If calibrated correctly the labeled magnetization is disturbed by less than 5% by the ASL-IF pulse.

References

Aslan S, Xu F, Wang PL, Uh J, Yezhuvath US, van Osch M, Lu H. Estimation of labeling efficiency in pseudocontinuous arterial spin labeling. Magn Reson Med. 2010 Mar;63(3):765-71.

Chen Z, Zhao X, Zhang X, Guo R, Teeuwisse WM, Zhang B, Koken P, Smink J, Yuan C, van Osch MJP. Simultaneous measurement of brain perfusion and labeling efficiency in a single pseudo-continuous arterial spin labeling scan. Magn Reson Med. 2018 Apr;79(4):1922-1930.

Günther, M. Arterial Spin Labeled Input Function (ASLIF): signal acquisition during pseudo-continuous arterial spin. in Proc.ISMRM. 26 (2018), 0305

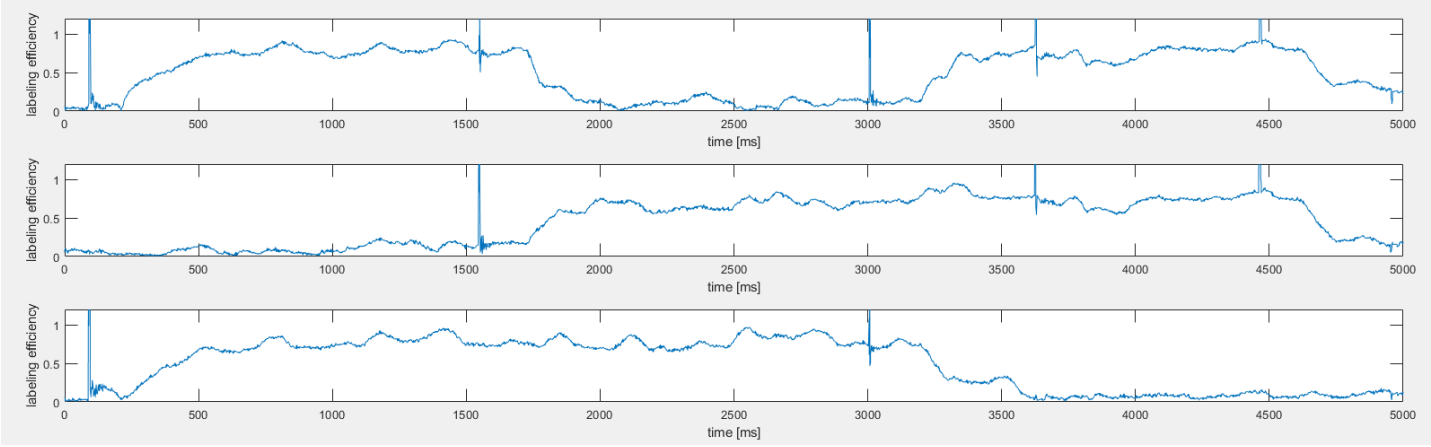

Figure 1: Single measurement labeling efficiency of a four phase Hadamard-encoded pCASL preparation. Temporal resolution was 1.42ms. Scan time (including normalization scan) was 20s.

Convolutional Neural Network based Automatic Planning for Pseudo-Continuous Arterial Spin Labeling

Karsten Sommer[1], Thomas Lindner[2], Kim van de Ven[3], and Michael Helle[1]

[1]Philips Research, Hamburg, Germany, [2]Department of Radiology and Neuroradiology, University Hospital Schleswig-Holstein Campus Kiel, Kiel, Germany, [3]Philips Healthcare, Best, The Netherlands

Introduction

In Pseudo-continuous arterial spin labeling (pCASL) careful planning of the labeling plane is required – ideally in regions where relevant feeding vessels are straight and cross the labeling plane perpendicularly, but operator-induced variability may alter the imaging results. Here, we demonstrate the feasibility of using a convolutional neural network (CNN) to automatically predict an appropriate labeling position based on given angiography images of the neck.

Methods

The training dataset consisted of 112 clinical angiography scans (time-of-flight: FOV 200x200x96mm^3, voxel size 1.5x1.5x1.5mm^3, 3D fast-field echo acquisition, 1:07 scan time) plus a separate test dataset of 5 additional scans all acquired on a 3T Achieva Scanner (Philips, Best, The Netherlands) under the general protocol for sequence development, approved by the local ethics committee. Only the coronal maximum intensity projections (MIPs) were selected for planning. Data augmentation was performed (stretching, shifting) to create a training dataset of 11.200 images in total. Appropriate locations for the labeling plane were manually selected by an experienced operator. Importantly, several possible labeling plane positions for a single image were allowed. A CNN was then trained to predict suitable labeling positions based on the angiographic coronal MIPs. Two convolutional layers (kernel size k=3, 32 channels) were employed, each followed by a max-pooling layer. This was followed by a fully connected layer with 500 neurons and a ReLU activation function. To account for the fact that multiple suitable labeling positions could be selected by the operator, a tailored loss function was employed that yielded the mean-squared error between the network output and the reference labeling position closest to the network's output.

Results

After training, mean/maximum deviations between network output and ground truth of 4.23/13.67px were obtained. No overfitting was observed. Figure 1 shows the network's performance on example images from the test dataset. For the first four images, the network's output is reasonably close to one of the reference labeling positions, indicating that the network successfully generalized from the training data. The bottom image presents one of the largest observed deviations (9.43px), where the network suggested a more proximal location. The results of the in vivo validation are shown in Figure 2. The network's suggested labeling plane was almost identical to the one chosen by the operator. The high quality of resulting ASL images underline the suitability of this selected labeling plane.

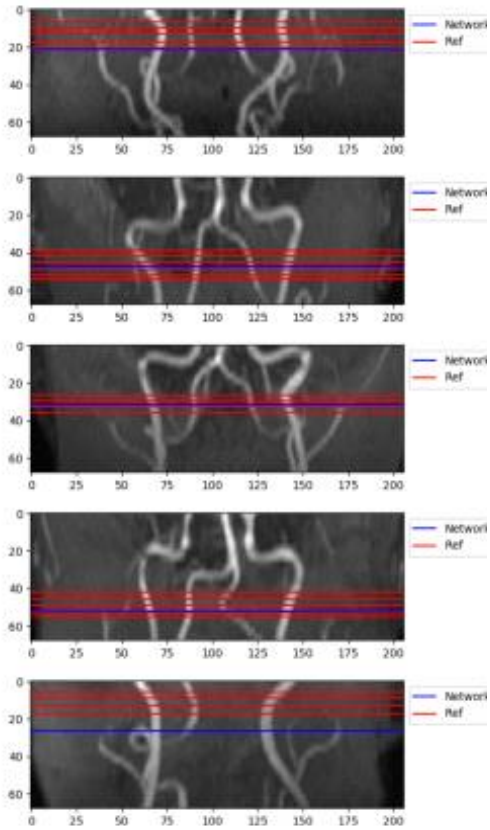

Fig. 1: Visualization of the network performance on the test dataset. The labeling positions provided by the network and the ground truth annotations (Ref) are displayed as blue and red horizontal lines, respectively. Largest deviation appears in the bottom image (9.43px).

Discussion

While the neural network suggested labeling positions that were close to the ground truth in most cases, relatively large deviations were observed in some cases. Careful inspection of this MIP (bottom image in Fig. 1), however, shows the inherent difficulty of the task, which is often a trade-off: while the labeling plane suggested by the network would lead to non-optimal labeling of the smaller vertebral arteries, it is almost ideal (i.e. perpendicular) for labeling of the carotid arteries. As seen in this example, large deviations from the ground truth may in some cases simply be caused by operator-specific preferences. Consequently, the presented method should be further evaluated on larger datasets with annotations from multiple operators. Moreover, clinical data collection would also include cases with vascular alterations and pathologies that might influence the positioning of the labeling plane.

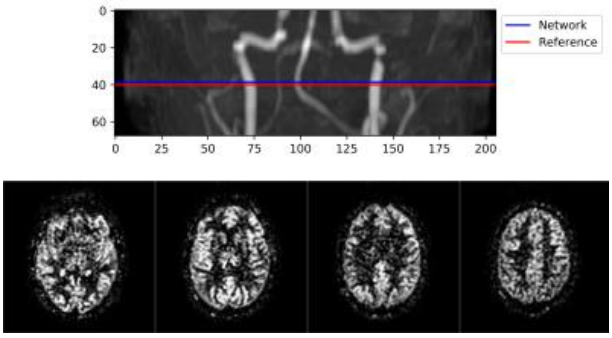

Fig. 2: In vivo validation of the network's performance. Top row: given the planning angiogram, the network suggests a labeling plane virtually identical to the operator. Bottom row: example slices of the ASL data acquired using the labeling plane suggested by the network.

Conclusion

In this study, we demonstrate the feasibility of a CNN based fully automatic planning approach of pCASL scans, which is the most frequently used ASL technique in clinical settings.

ASL spatial heterogeneity as a cognitive group classifier in Alzheimer's disease

Zahra Shirzadi, MESc[1,2], Bojana Stefanovic, PhD[1,2], Henri JMM Mutsaerts, MD, PhD[2,3], Mario Masellis, MD, PhD[2,4], Bradley J MacIntosh, PhD[1,2]; for the Alzheimer's Disease Neuroimaging Initiative

[1]Department of Medical Biophysics, University of Toronto; [2]Hurvitz Brain Sciences, Sunnybrook Research Institute, University of Toronto; [3]Department of Radiology, VU medical center, the Netherlands; [4]Department of Medicine (Neurology), Sunnybrook Health Sciences Centre, University of Toronto

Introduction: The spatial coefficient of variation (sCoV) in an arterial spin-labeled (ASL) MRI scan provides insight on arterial transit time. This metric reflects delayed blood delivery – seen as hyperintense ASL signal juxtaposed by hypointense regions. This study investigated the use of ASL sCoV in the classification of cognitively unimpaired (CU), mild cognitive impairment (MCI) and Alzheimer's disease (AD) cohorts.

Methods: ASL images from Alzheimer's disease neuroimaging initiative dataset in three groups of CU, MCI and AD (N=258) were used. Pulsed ASL (PICORE QT2) images were acquired on 3T Siemens systems (TE/TR=12/3400ms, TI1/2=700/1900ms). We calculated ASL-sCoV in temporal, parietal, occipital, and frontal lobes as well as global grey matter. The primary analysis was an analysis of covariance to investigate the effect of cognitive group (CU, MCI, AD) on sCoV. We also evaluated the repeatability of sCoV by calculating within-subject agreement in a subgroup of CU participants with a repeat ASL. The secondary analyses assessed ventricular volume, amyloid burden, glucose uptake, ASL-sCoV and regional CBF as cognitive group classifiers using logistic regression models and receiver operating characteristic analyses.

RESULTS: We found that global and temporal lobe sCoV differed between cognitive groups ($p<0.006$). Post hoc tests showed that temporal lobe sCoV was lower in CU than in MCI (Cohen's d=-0.36) or AD (Cohen's d=-1.36). We found that sCoV was moderately repeatable in CU (inter-session intraclass correlation=0.50; intra-session intraclass correlation=0.88). Subsequent logistic regression analyses revealed that temporal lobe sCoV and amyloid uptake classified CU *vs.* MCI (accuracy=78%). Temporal lobe sCoV, amyloid and glucose uptake classified CU *vs.* AD (accuracy=97%), and glucose uptake classified MCI *vs.* AD (accuracy=85%).

CONCLUSION: We showed that ASL spatial heterogeneity can be used alongside AD neuroimaging markers to distinguish cognitive groups, in particular, cognitively unimpaired from cognitively impaired individuals.

Figure 1: Examples of ASL CBF images that have low (left) and high (right) spatial heterogeneity.

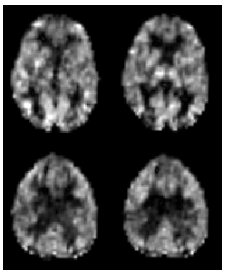

Cognitively unimpaired
74 years old Male
GM sCoV = 45%

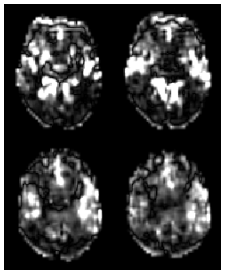

Alzheimer's dementia
76 years old Male
GM sCoV = 201%

Table 1: Results of between-group logistic regression models. Odds ratio (z values) are reported.

Neuroimaging marker	**CU *vs.* MCI**	**CU *vs.* AD**	**MCI *vs.* AD**
Ventricular volume (%ICV)	1.02 (1.7)	1.02(.56)	1.0 (1.5)
Amyloid burden (SUVR)	***1.35* (2.38)***	***5.6* (2.26)***	1.1 (1.1)
Meta-ROI Glucose uptake (SUVR)	1.15 (-.76)	***60.1* (-2.26)***	***2.7* (-3.8)***
Meta-ROI ASL CBF (mL/100g/min)	1.03 (.5)	1.02 (-.2)	1.1 (-1.5)
Temporal lobe ASL sCoV (%)	***1.16* (2.47)***	***1.8* (2.0)***	1.0 (.4)
Overall model accuracy	**78%**	**97%**	**85%**

*: significant p values at $p<0.05$. ICV: intracranial volume / SUVR: standardized uptake value ratio

Optimizing MRF-ASL Scan Design for Precise Quantification of Brain Hemodynamics

Anish Lahiri, Jeffrey A Fessler and Luis Hernandez-Garcia

Purpose: Multiparametric hemodynamic estimates obtained by combining ASL and MR Fingerprinting can be helpful in the comprehensive diagnosis and treatment planning of several cerebrovascular disorders [1,2]. However, this requires precise quantifiability over a wide parameter range. In this work, we: (i) extend our optimization towards precise quantification over a wide range of parameter values that includes a number of pathological conditions while maintaining constraints on total scan time, and (ii) use separate neural networks for regression based estimates of individual parameters.

Methods: Our scan optimization approach uses the Cramer-Rao Bound, which is the inverse of the Fisher information matrix defined as follows:

$$\boldsymbol{F}(\underline{\theta};\underline{\nu}) = \frac{1}{\sigma^2} \cdot [\nabla_{\underline{\theta}} \underline{\mathbf{s}}]^T [\nabla_{\underline{\theta}} \underline{\mathbf{s}}]. \tag{1}$$

where, $\underline{\mathbf{s}}(\cdot) \in \mathbb{R}^{N\times 1}$ is the signal generated from our model, $\underline{\theta} \in \mathbb{R}^{K\times 1}$ represents a single set of hemodynamic parameters, $\underline{\nu} \in \mathbb{R}^{P\times 1}$ are the scan parameter(s) and σ^2 is the i.i.d. Gaussian noise variance.

We optimize the scan parameters by considering a representative collection of true parameter values, $\boldsymbol{\Theta}$, uniformly spread over a comprehensive range by minimizing the following cost function:

$$\hat{\nu} = \underset{\nu\in\mathcal{V}}{\arg\min} \ \frac{1}{|\boldsymbol{\Theta}|} \sum_{\underline{\theta}\in\boldsymbol{\Theta}} \mathrm{Tr}\left(\boldsymbol{W} \cdot \frac{|\boldsymbol{F}^{-1}(\underline{\theta},\nu)|^{0.5}}{\boldsymbol{N}(\underline{\theta})} \cdot \boldsymbol{W} \right), \tag{2}$$

where $\boldsymbol{W}$ is a diagonal weighting matrix assigning priority to each hemodynamic parameter in the cost function and $\boldsymbol{N}(\underline{\theta}) = (\underline{\theta}^{0.5})(\underline{\theta}^{0.5})^T$ is a normalization matrix that is divided element-wise into the inverse Fisher information matrix.

Using exhaustive search to minimize the design cost function (2) ensures that our optimized scan yields precise estimates. The set of candidate labeling schedules is described using a linear interpolation of 5 equidistant points in the 'labeling space' (Fig 1).

We train individual neural networks [3,4,5] for estimating each parameter using training data generated by this optimized scan design applied to a simple two-compartment model. Using individual networks alleviates the need for relative weighing of targets during training. Moreover, we adopted a Mixture of Gaussian Prior on our training data to emphasize training on biologically feasible parameter ranges.

We the test our methods on data acquired from a healthy human subject, after it is 'de-trended' to strip scanner artifacts.

Results: Depicted in **Fig 1** is the optimized schedule for 700 frames and a 600s scan duration, as well as the predicted average normalized standard deviation of parameter estimates over a pathological range. It is clear that linear interpolation allows us to explore the 'label space' effectively.

Fig 2 shows that notwithstanding the need for de-trending, our methods indicate promising performances in healthy subjects.

Conclusion: Combining CRB based optimization with regression in MRF ASL enables fast, precise estimates of hemodynamic parameters and tissue properties in the presence of anomalies that are difficult to characterize. Our results on healthy subject data hint at realizing the clinical potential of MRF ASL.

Future work will involve in-vivo testing of our methods on patients with cerebrovascular disorders.

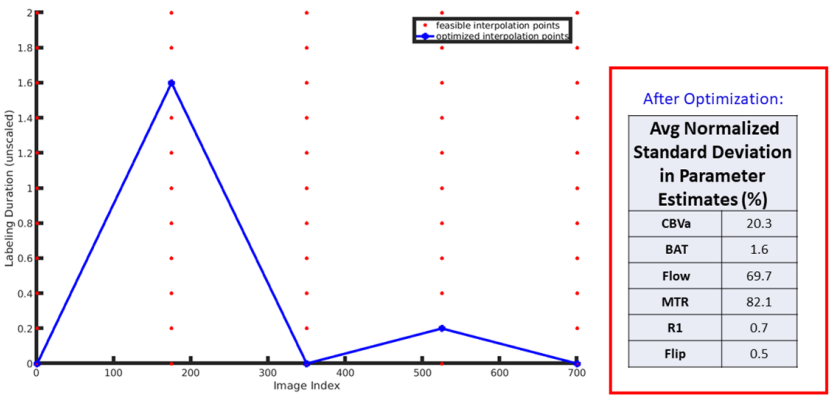

Figure 1

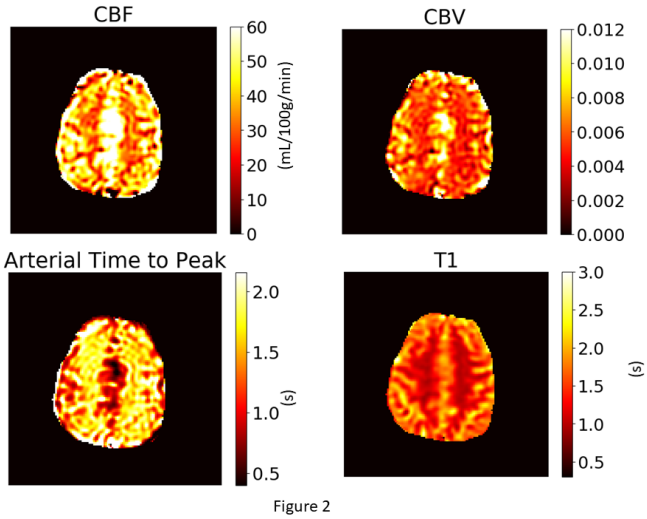

Figure 2

References:

1. K.L. Wright, Y. Jiang, D. Ma, D.C. Noll, M.A. Griswold, V. Gulani, and L. Hernandez-Garcia. 2018. “Estimation of Perfusion Properties with MR Fingerprinting Arterial Spin Labeling.” Magnetic Resonance Imaging 50. doi:10.1016/j.mri.2018.03.011.

2. Pan Su, Deng Mao, Peiying Liu, Yang Li, Marco C. Pinho, Babu G. Welch, and Hanzhang Lu. “Multiparametric estimation of brain hemodynamics with MR ngerprinting ASL”. Magnetic Resonance inMedicine, 00(November):1–12, 2016.

3. Anish Lahiri, Jerey Fessler, and Luis Hernandez-Garcia. 2018. “Optimized Scan Design for ASL Fingerprinting and Multiparametric Estimation Using Neural Network Regression.” In Proc Intl Soc Mag Reson Med, 309.

4. Cohen, O., Zhu, B., and Rosen, M. S. (2018). “MR ngerprinting Deep RecOnstruction NEtwork (DRONE). Magnetic Resonance in Medicine”, 80(3), 885–894. https://doi.org/10.1002/mrm.27198

5. Patrick Virtue, Stella X. Yu, Michael Lustig, “Better than Real: Complex-valued Neural Nets for MRI Fingerprintin”, Proc. IEEE International Conference on Image Processing (ICIP), 2017

Higher insular activation predicts treatment response to TMS for major depressive disorder

Tessa R. Abagis [a], Stephan F. Taylor [b], Luis Hernandez-Garcia [c,d]

a: Department of Psychology, University of Michigan
b: Department of Psychiatry, University of Michigan
c: Biomedical Engineering, University of Michigan
d: Functional MRI Laboratory, University of Michigan
Corresponding author email: tabagis@umich.edu

Transcranial magnetic stimulation (TMS) is a non-invasive form of brain stimulation which, when applied at a high frequency to the left dorsolateral prefrontal cortex (DLPFC), has been found to reduce depressive symptoms in patients with treatment resistant major depressive disorder (MDD). To investigate neural changes attributable to TMS treatment, we conducted a sham-controlled, double-blind, randomized trial with 32 patients with treatment resistant MDD. Patients underwent arterial spin labeling (ASL) scans while performing an n-back working memory task before and after blinded treatment in order to: 1) individually locate the left DLPFC in each patient for neuronavigated treatment and 2) investigate neural changes attributable to TMS. There were no significant changes in activation during the n-back task due to receiving TMS treatment. Fourteen of the patients who received sham TMS during the blinded treatment phase went on to receive TMS after the second scan. Task-based ASL data in responders (n = 27) to TMS treatment revealed that higher right insular activation in the scan immediately prior to receiving TMS was associated with a better treatment response, as measured by the Montgomery-Åsberg Depression Rating Scale (45, 2, 16; k=90; $p = 0.018\ FWE_{corr}$). This finding aligns with past literature which finds a relationship between reduced insular activity and higher levels of psychiatric disorders, including MDD.

This study was funded by NIH R21 MH098174 and Clinical Sciences Translational Award UL1TR000433. Research support was also provided by Neuronetics, which did not have a role in the design of the study.

A Non-Invasive Hybrid PET/MR Approach for Validation of ASL in Clinical Studies

Tracy Ssali[1,2], Lucas Narciso[1,2], Justin Hicks[1,2], Udunna Anazodo[1,2], Elizabeth Finger[1,2], Mike S Kovacs[1,2], Matthias Günther[3], Frank S Prato[1,2], and Keith St Lawrence[1,2]

[1]Lawson Health Research Institute, London, Canada, [2]Department of Medical Biophysics, Western Ontario, London, Canada, [3]Fraunhofer Institute for Medical Image Computing MEVIS, Bremen, Germany

Objectives

While PET with radiolabeled water (^{15}O-water) remains the gold standard for imaging CBF, widespread use is limited by the requirement of arterial sampling. Arterial spin labeling (ASL) MRI is non-invasive and quantitative; however, its sensitivity to the arterial transit time reduces its accuracy, making it challenging to image patients with cerebrovascular diseases (CVD). We previously proposed a non-invasive hybrid PET/MR approach that uses a measurement of global CBF (gCBF) by phase contrast (PC) MRI to convert PET activity into quantitative CBF images without the need for arterial sampling[1]. **This PET/MR approach has the potential to provide a method of measuring regional CBF that is accessible to patients whom arterial sampling is not advisable and more importantly, can be used as a reference to optimize ASL.** The technique was initially validated in a large animal model, and the next step is to adapt it to human studies. Although the PET imaging will be similar, the PC sequence needs to be optimized for measuring gCBF in humans. In this study, we assess the variability in gCBF due to slice location and gating, and as a proof of concept, we present the first CBF images from one participant obtained using this non-invasive hybrid PET/MR approach.

Methods

Data were acquired using the Siemens Biograph mMR in 6 healthy volunteers (age: 31±10, 2 females). PC images (4 averages, VENC: 70 cm/s, retrospective-gating) were acquired at the level of the first/second cervical vertebrae ($gCBF_{low}$) and basilar artery ($gCBF_{high}$). Global CBF_{low} was repeated using a non-gated sequence. In 3 volunteers, PC data were acquired on 2 occasions separated by 1-2 months. Global CBF was quantified by scaling the blood velocity by vessel area and brain volume. For hybrid PET/MR-CBF[1], 5 minutes of PET list-mode data were acquired after rapid intravenous bolus injection of ^{15}O-water (800 MBq). Raw PET data were reconstructed using an MR-based attenuation correction map. For comparison, ASL (PCASL-GRASE) data were acquired with PLD= 2s, LD= 1.8s.

Results

Global CBF was 53.9 ± 7.4 ($gCBF_{low}$) and 57.5 ± 12.6 ml/100g/min ($gCBF_{high}$) (ns). Repeat measurements were within 9.0% ($gCBF_{low}$) and 6.1% ($gCBF_{high}$) of each other. Non-gated gCBF was 24% lower than the gated sequence (ns). CBF images obtained by PET/MR and ASL are shown in Figure 1.

Conclusions

The gCBF estimates were similar[2] but lower than previous studies[3]. Differences could be attributed to increased noise resulting from a high VENC[4]. The 6.5% difference between $gCBF_{high}$ and $gCBF_{low}$, which may be significant with a larger sample size, could be related to partial volume errors due to contributions from stationary tissue [5,6]. PC-CBF measurements were reproducible, with <9% difference between measurements. Although gCBF generated by the two approaches were similar, the ratio of grey-to-white mater CBF appears to be higher in the ASL-CBF map (Figure 1). Future goals are to use this hybrid approach to image CBF in CVD patients to evaluate its ability to quantify perfusion abnormalities and subsequently, determine optimal parameters for imaging CBF in this population with ASL.

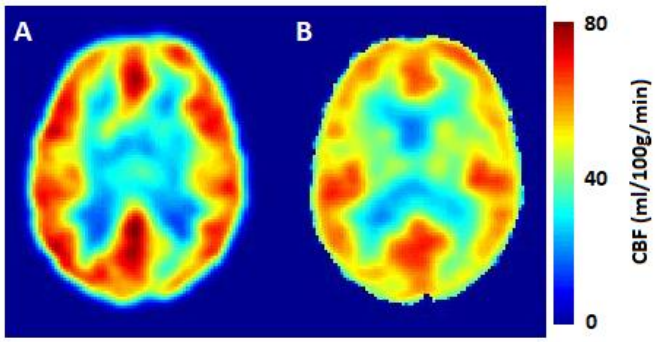

Figure 1: Cerebral perfusion maps measured by (A) ASL (CBF = 52.9ml/100g/min) and (B) PET/MR approach (CBF = 48.4 ml/100g/min).

References

1.Ssali, T. *et al*. *JNM*(2018). 2.Spilt, A. *et al. Radiology* (2005).3.Puig, O. *et al. JCBFM*(2018). 4.Lotz, J. *et al*. *JMRI*(2005). 5.Peng, S.-L. *et al. JMRI*(2015). 6. Tang, C. *et al*. *JMRI*(1993).

Does partial volume correction improve the repeatability of arterial spin labeling perfusion imaging?

F. Kennedy McConnell[1,2], A. Segerdahl[2], T. Okell[2], M. Mezue[2], I. Tracey[2], M. Chappell[1,2]

[1]Institute of Biomedical Engineering, University of Oxford, Oxford, United Kingdom, [2]Wellcome Centre for Integrative Neuroimaging, University of Oxford, Oxford, United Kingdom

Introduction: Partial volume effects (PVE) are important in arterial spin labelling (ASL) cerebral perfusion imaging, due to the low spatial resolution of ASL data and large differences in the perfusion properties of grey matter (GM) and white matter (WM). PVEs thereby present a barrier to the clinical application of ASL, particularly in disease contexts involving subtle, localized perfusion changes, such as dementia. Recent work [1] has shown that the two most commonly applied methods for PVE correction (PVEc) [2,3], improve the within-subject coefficients-of-variation of ASL perfusion measurements made on the same day, 1 week, and 1 month apart. The same work showed that the spatially regularised method (SR PVEc) [2] was better able to preserve spatial details within perfusion images, whereas the linear regression method (LR PVEc) [3] was less sensitive to noise in the data and errors in the PV estimates, which they concluded could be due to the greater smoothing introduced by the technique. In this work we further hypothesized that PVEc would improve the repeatability of ASL measurements in anatomically defined GM brain regions, by reducing apparent variability in perfusion due to PVE.

Methods: ASL data acquired by [4] from 7 seven subjects each scanned at rest up to 3 times over 2 sessions (1 week apart) was analysed retrospectively. A multiPLD pCASL acquisition with background suppression was used: labeling duration=1.40s, PLDs: 0.25, 0.50, 0.75, 1.00, 1.25, and 1.50s, TR=4s, TE=13ms, 24 slices each 4.95 mm. Each session included 96 alternating label-control volumes. A T1 weighted structural image, head and body coil calibration images and B0 field maps were also acquired. The ASL data were analysed using BASIL [5] within FSL. These tools were used to correct for EPI distortions, slice timing delays, and subject motion, as well as to perform label-control subtraction, averaging of repeats, and Bayesian inference of cerebral blood flow (CBF) and arterial transit time. Calibration used a CSF reference region. The analysis was performed in three ways: without PVEc (no PVEc), with SR PVEc [2], and with LR PVEc [3]. PV estimates were obtained from the T1 image. The effect of PVEc on within- and between-session differences in CBF were assessed using Bland-Altman analysis, and the within- and between- session agreement was assessed through correlation analysis.

Results/Discussion: Figure 1 shows results of Bland-Altman analysis. The within-session biases for all three approaches to PVEc were small (<5 %). The bias between the week-repeat acquisitions ranged from 9.4–11.1 % with LR PVEc showing the lowest bias and no PVEc showing the highest. Both no PVEc and the SR PVEc method had similar Bland-Altman confidence intervals, whereas LR PVEc showed reduced variability, likely due to the smoothing inherent to the LR PVEc technique. Correlation analysis showed reasonable and significant test-retest agreement (all R^2>0.57 and all p<0.001): lowest correlation was seen between-sessions and without PVEc (R^2=0.575), and highest was seen in the within-session experiment with LR PVEc (R^2=0.868). Correlation was always stronger within-sessions than between-sessions.

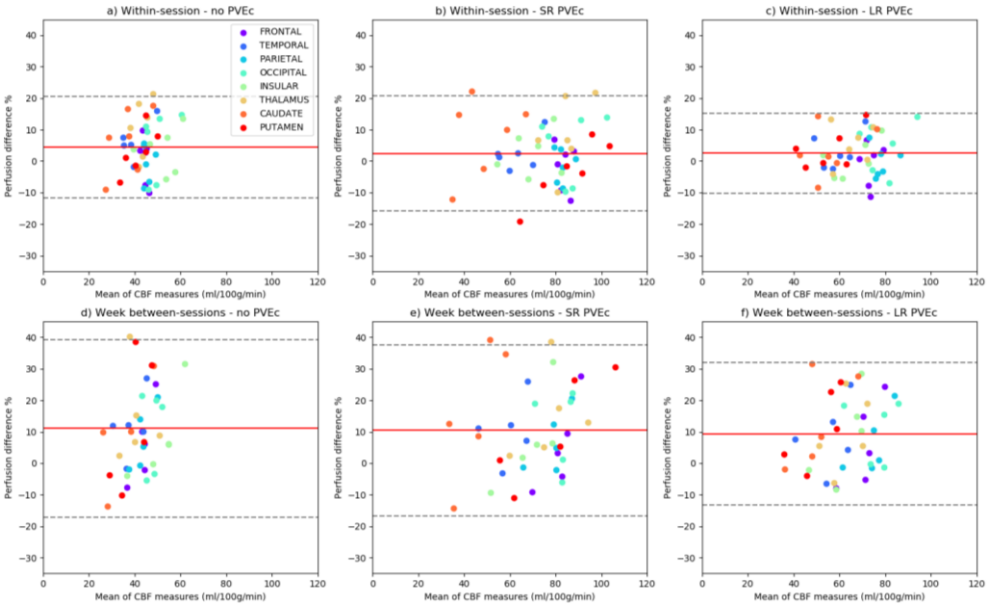

Figure 1 - Bland-Altman analysis showing repeatability of CBF measures in 8 brain regions. Vertical axis: difference between CBF measurements expressed as % of their mean. Red lines show bias and grey lines show 95% CIs (bias + 1.96*sd). Top row: within-session a) no PVEc: 4.4±16.1 %, b) SR PVEc: 2.5±18.4 %, c) LR PVEc: 2.5±12.7 %. Bottom row: week-repeat d) no PVEc: 11.1±28.26 %, e) SR PVEc: 10.5±27.1, f) LR PVEc: 9.4±22.6.

Conclusions: Building on the work of [1], these results show that PVEc improves test-retest agreement of ASL perfusion measures in GM brain regions and leads to similar (SR PVEc) or reduced (LR PVEc) heterogeneity in perfusion estimates. PVEc should therefore be considered for use in clinical applications of ASL.

References: [1] Zhao, Neuroimage, 2017; 162:384-397 [2] Chappell, Magn Reson Med, 2011; 65(4):1173-83 [3] Asllani, Magn Reson Med; 60(6):1362-71 [4] Mezue, J Cereb Blood Flow Metab, 2014; 34(12):1919–1927 [5] https://github.com/ibme-qubic/oxford_asl/releases

Neurovascular uncoupling in schizophrenia: A bimodal meta-analysis of brain perfusion and glucose metabolism

Niron Sukumar[1], Priyadharshini Sabesan[1], Udunna Anazodo[3], Lena Palaniyappan[1,2,3]

1 Department of Psychiatry, University of Western Ontario, London, Ontario, Canada.
2 Robarts Research Institute, University of Western Ontario, London, Ontario, Canada.
3 Lawson Health Research Institute, London, Ontario, Canada.

BACKGROUND: Since the time of Ernst von Feuchtersleben who coined the term psychosis (1845), psychotic disorders have been suspected to be associated with disturbances in cerebral blood supply. The use of modern neuroimaging approaches has uncovered abnormalities in the resting-state regional cerebral blood flow (rCBF) across various brain regions in schizophrenia. In a healthy brain, rCBF is tightly coupled to resting cerebral glucose metabolism (rCMRglu), which increases with synaptic activity. The coupling of rCBF (measured using arterial spin labeling, ASL) and rCMRglu (measured using ^{18}flurodeoxyglucose positron emission tomography, FDG-PET) depends on the integrity of the neurovascular unit. In schizophrenia, several lines of evidence point towards aberrant neurovascular coupling especially in the prefrontal regions, though no simultaneous ASL-PET studies identifying regions with concordance or discordance between metabolism and perfusion have been reported to our knowledge. To address this gap, we undertook a voxel-based bimodal meta-analysis to examine the relationship between rCBF and rCMRglu in schizophrenia. We hypothesized that several brain regions would show combined abnormalities of perfusion and metabolism, while uncoupling of these two parameters will be observed in prefrontal regions.

METHODS: We undertook a systematic literature search to include all available studies reporting voxelwise ASL or FDG-PET changes in schizophrenia using coordinates based multimodal meta-analysis implemented using Signed Differential Mapping (SDM) software. 21 studies met the inclusion criteria, comprised of data from 618 patients and 610 controls, available for meta-analysis. We used conjunction and moderator analyses to evaluate areas with concordant and discordant abnormalities in rCBF and rCMRglu respectively. We also undertook meta-regression analyses to study the effect of age, gender, duration of illness, anti-psychotic dosage, and illness severity on the illness related changes in rCBF and rCMRglu.

RESULTS: Among patients with schizophrenia, we observed a conjoint reduction in rCBF and rCMRglu in the right median cingulate / paracingulate gyri and left interior frontal gyrus. A conjoint increase in rCBF and rCMRglu was noted in the right cortico-spinal projections and right inferior temporal gyrus. Regional neurovascular uncoupling was notable in the superior frontal gyrus (reduced rCMRglu, normal rCBF) and cerebellum (increased rCMRglu, normal rCBF). Meta-regression analyses were unstable due to the low number of eligible studies.

CONCLUSION: Our results suggest that several key regions implicated in the pathophysiology of schizophrenia such as the frontoinsular cortex, dorsal ACC, putamen and temporal pole (constituting the Salience Network) show conjoint metabolic and perfusion abnormalities in patients. In contrast, discordance between metabolism and perfusion were seen in superior frontal gyrus and cerebellum, indicating that factors contributing to neurovascular uncoupling (e.g. inflammation, mitochondrial dysfunction, oxidative stress) are likely operates at these loci. Hybrid ASL-PET studies focussing on these regions could confirm our proposition.

Velocity Selective ASL in the Rat at 9.4T

Matthew Budde[1] Seongtaek Lee[2], Briana Meyer[3]
[1]Department of Neurosurgery, [3]Neuroscience Doctoral Program, Medical College of Wisconsin, Milwaukee, WI [2]Department of Biomedical Engineering, Marquette University & Medical College of Wisconsin, Milwaukee, WI

Introduction: Arterial spin labelling (ASL) has seen clear utility for the brain, yet similar applications to the spinal cord have remained limited. In addition to challenges of imaging the cord owing to its small size and motion and susceptibility artifacts, the blood supply is collateralized and segmental, and it does not lend itself to a single labelling plane as in pseudocontinuous ASL[1]. Velocity selective ASL (vsASL) has shown promise in tissues with similar features such as the heart[2] and placenta[3], but neither has vsASL been demonstrated on preclinical systems nor has it been used for the spinal cord. In this work, we lay the groundwork for preclinical spinal cord vsASL by first assessing the tagging performance in a flow phantom and rat thoracic aorta and kidney.

Methods: Two variants of the vsASL tagging module were implemented on a 9.4T MRI small animal system (Bruker Biospec). The BIR-8 scheme[4] consisted of adiabatic tanh/tan pulse[5] with κ=20, ζ=20, and ω_{max}=20 and a subpulse duration of 1ms for a total module time of 14 ms. Gradients of 53 mT/m with a 0.3 ms ramp, 0.5 ms plateau, and 0.34 ms delay achieved a velocity cutoff (V_c) of 2.0 cm/s. The velocity selective saturation (VSS) and inversion (VSI) tagging modules were implemented as described[6], with 9 hard pulses of 10 or 20° flip angles for saturation or inversion, respectively, 29 mT/m gradients, V_c of 4.0 cm/s, and a module time of 43 ms.

A flow phantom was used to asses the velocity tagging performance, with the mean flow rate approximating the rat aorta (~10cm/s). Tygon tubing connected to a parastaltic pump along with a static gel phantom were inserted into a 40 mm Litz cage coil (Doty Scientific, Inc). Flow-compensated gradient echo images were acquired (TR/TE=500/3 ms) with each of the tagging modules with a minimal (1 ms) post-label delay. Additionally, 10-14 week old Sprague Dawley rats were used for in vivo assessments. Rats were placed supine over a 4-channel surface coil in a 9 cm linear volume coil for excitation. A single axial slice included the aorta and kidney and gradient echo images were cardiac gated with varying R-wave delays. All studies were approved by the IACUC of the Milwaukee VA Medical Center and the Medical College of Wisconsin.

Results: The BIR-8 vsASL scheme demonstrated near complete suppression of signal in the flowing phantom with negligible changes in the static phantom. However, apparent flow artifacts were evident in the non-velocity encoded image, and these are attributed to the VS module since the same image obtained without it was devoid of artifacts. In the phantom, the VSS/VSI module also exhibited adequate suppression of flowing spins(not shown) but artifacts were also present in the non-velocity encoded images. In the rat aorta, similar performance was seen with clear suppression in the tagged condition, but also signal loss in the control condition, but full signal in the image without the preparation module. In the kidney, vsASL perfusion contrast was evident, but it was substantially reduced in SNR compared to the same measurement with pCASL.

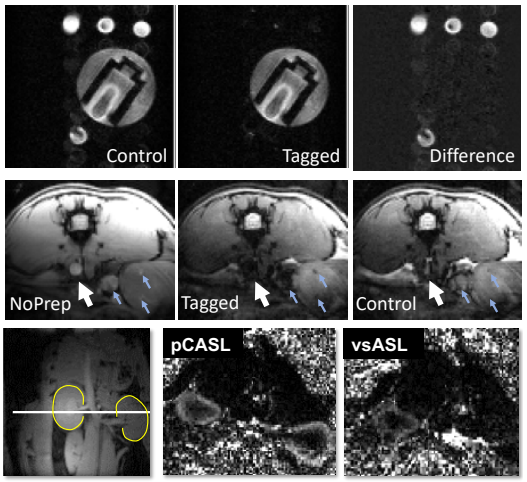

In the flow phantom (top), vsASL shows clear suppression of flowing signals, and negligible change in static signals using the BIR-8 scheme. In vivo (middle) signal suppression is evident in the aorta (white arrow) in the tagged condition, but also in the control condition while other vessels (blue arrows) show better tagged-control differences. In vivo in the rat kidney, pCASL shows better SNR in the kidney than vsASL.

Discussion: In these initial tests, the BIR-8 module provided better performance than the VSS/VSI modules. Optimizing the balance between pulse duration and off-resonance performance of the BIR-8 pulses will be investigated to minimize flow artifacts. In the thoracic rat spinal cord, the field deviates by approximately 400 Hz over our desired imaging volume. BIREF-1 pulses may be one alternative to minimize flow artifacts[7] but Bloch simulations indicate they may require higher power or pulse durations compared to BIR-8. Likewise, the VSS/VSI modules were not optimized for the large susceptibilties experienced at high field and require further investigation and simulation to improve their performance at 9.4T.

Acknowledgements: Supported in part by Merit Review Award I01 RX001497 from the US Department of Veterans Affairs Rehabilitation Research and Development Service and by the National Institutes of Neurological Disorders and Stroke R01 NS109090.

References: 1. D. C. Alsop, et al. Magn Reson Med 73, 102-16, (2015).2. T. R. Jao and K. S. Nayak. Magn Reson Med 80, 272-278, (2018). 3. Z. Zun and C. Limperopoulos. Magn Reson Med 80, 1036-1047, (2018). 4. J. Guo, et al. Magn Reson Med 73, 1085-94, (2015). 5. P. Kellman, et al. Magn Reson Med 71, 1428-34, (2014). 6. Q. Qin and P. C. van Zijl. Magn Reson Med 76, 1136-48, (2016). 7. E. R. Jenista, et al. Magn Reson Med 70, 1360-8, (2013).